A QUANTITATIVE STUDY OF COLLOIDAL FOULING IN MEMBRANE PROCESSES

GURDEV SINGH

NATIONAL UNIVERSITY OF SINGAPORE

2007

A QUANTITATIVE STUDY OF COLLOIDAL FOULING IN MEMBRANE PROCESSES

GURDEV SINGH

(*B.Eng, NUS*)

A THESIS SUBMITTED

FOR THE DEGREE OF DOCTOR OF PHILOSOPHY

DEPARTMENT OF CIVIL ENGINEERING

NATIONAL UNIVERSITY OF SINGAPORE

2007

Acknowledgements

First of all my, I would like to acknowledge my PhD Advisor, Associate Professor Song Lianfa with whom it has been both a pleasure and privilege to work with. Your outlook on life and research, which you have graciously shared, was both refreshing and inspirational.

I would also like to thank the members of my thesis committee, Associate Professor Hu Jiangyong and Assistant Professor Ng How Yong, for their invaluable suggestions and helpful comments of my work.

To the staff and colleagues in the Department of Civil Engineering, Division of Environmental Science & Engineering and Water & Science Technology Laboratory, a sincere thanks for all your help and company.

To my "extended thesis committee" consisting of family and friends your strong interest and constant volley of questions on my candidature kept me going in the final few weeks of thesis writing. I thoroughly enjoyed our endless conversations, outings and fun.

Finally to my parents, sister and fiancée, I cannot thank you enough for all the love, support and encouragement you have given me.

Table of Contents

Summary

Membrane processes have revolutionized water and wastewater treatment, making it possible to produce constantly high quality water at affordable prices from various water sources including unconventional ones, such as brackish water, seawater, and wastewater. This has short-circuited the hydrological/water cycle by allowing effluent from wastewater to be directly channeled to treatment for potable use, resulting in more efficient water management practices. However, membrane fouling, which is inherent in all membrane processes, persistently threatens the growth and development of this emerging technology. Membrane fouling reduces permeate quantity and quality and increases operation complexity. A significant portion of the total operation costs in membrane processes are associated with fouling prevention or mitigation, which seriously undermines the competitive edge of membrane technology over other processes. The development and implementation of an effective membrane fouling control strategy, which is critical to ensuring the integrity and efficient operation of a membrane separation system, hinges on the understanding of the fouling properties of the feed water. In other words, proper characterization and quantification of the fouling strength of feed water is the basis for the development of more effective fouling control or mitigation strategies and the success of membrane processes.

Colloidal particles are the most prevalent and biggest group of foulants encountered in membrane processes. Furthermore, with the emergence of engineered nanoparticles and their proliferation in water bodies, colloidal fouling will remain an important area of study. The last two decades has witnessed significant research emphasis on colloidal fouling, resulting in a better understanding of its dominating mechanisms. Colloidal fouling is strongly affected by colloidal interactions that are governed by the surface properties of the colloid and the chemistry of the liquid medium surrounding it. The hydraulic driving pressure, which exerts a permeation drag force on the colloidal particles, also plays a pivotal role in colloidal fouling.

However, studies focusing on the effects of feed water chemistry and its interplay with the operating hydrodynamic conditions on colloidal fouling are still very limited and only qualitative in nature. It is unknown to what extent these factors affect colloidal fouling.

The impact of water chemistry on colloidal fouling in membrane processes is systematically investigated in this thesis. Well-controlled experiments are designed to investigate the influence of critical physicochemical factors i.e. ionic strength, pH and driving pressure on colloidal fouling. Attempts are made to delineate the complex fouling phenomena by utilizing fundamental theories from colloidal interactions. Embryonic considerations in the thesis were directed to the development of a fouling-strength measure used to quantify the effects of feed water properties on membrane fouling. The suitability of the fouling potential as a benchmark for the appraisal of colloidal fouling was then evaluated and confirmed.

Feed water ionic strength, a fundamental parameter of water chemistry, was found to significantly exacerbate colloidal fouling. Experimental data conclusively indicated that the colloidal fouling potential increased linearly with the natural logarithm of ionic strength or 'double layer thickness' of the colloids and linearly with colloid concentration when all other conditions were kept constant. Experiments with different ions further revealed that while increasing ionic strength has a generic effect of worsening colloidal fouling, the valence and distinct counter-ion properties could further contribute to aggravating colloidal fouling. Nevertheless, the general relationship between the feed water ionic strength and fouling potential described above was conserved for all salts tested. This highlights the pertinence of the electrical double layer around the colloids to colloidal fouling.

The effect of feed water pH on the fouling potential was strongly dependent on the isoelectric point of the colloidal particles. The fouling potential increased significantly as the feed water pH approached the isoelectric point. A linear relationship between the fouling potential and the zeta potential, an electrokinetic parameter of the colloids, was observed for all the feed

waters tested. This suggested that zeta-potential could be a useful indicator of colloidal fouling in membrane processes. Comparison of feed water acidification using weak and strong acids revealed a notably higher fouling potential with the strong acids at low ionic strengths and negligible differences between the acids at high ionic strength.

The influence of driving pressure or, more aptly, permeation drag on colloidal fouling was elucidated by determining the compressibility of the colloidal cake. Cake compressibility was found to be independent of colloid concentration and membrane type, and strongly affected by the ionic strength and pH of the feed water. The colloidal cake compressibility decreased for increasing ionic strength and for pH values approaching the isoelectric point. For feed waters at solution chemistries of high ionic strength and pH near the colloid isoelectric point, the colloidal particles exhibited 'hard-sphere' like attributes with a very small cake compressibility. The strong dependence of cake compressibility on the feed solution chemistry is an important characteristic of colloidal foulants.

Having secured better insight to the intricacies of colloidal fouling from the empirical evaluation of the physicochemical factors, a numerical model to correlate the fouling potential with these physicochemical factors was developed. The fouling potential could be well reproduced with the model, which was based on classical theories of colloidal interactions and cake formation, when a correcting factor was introduced to account for the elevated liquid viscosity within the nano-sized pores of the cake. Interestingly the viscosity within the pores was found to be slightly over 7 times that of bulk liquid viscosity and unaffected by the different physicochemical conditions. Using this value, good fits were obtained between the predicted fouling potential and experimental fouling potentials. Through this study, it is shown that colloidal fouling in membrane processes can be well understood with the fundamental theories of colloidal interactions. The fouling potential developed here allows for the elucidation of the extent to which these colloidal phenomena and interactions affect colloidal fouling in membrane processes.

Nomenclature

a	=	Constant, dimensionless
a_p	=	Radius of particle (m)
A	=	Membrane surface area (m^2)
A_H	=	Hamaker Constant, dimensionless
A_S	=	Hydrodynamic correction factor, dimensionless
b	=	Constant, dimensionless
c	=	Salt concentration (mol/L)
$C.C.C$	=	Critical coagulation concentration (mol/L)
d_p	=	Pore size of membrane (m)
d	=	Distance of shear plane away from surface of particle (m)
D	=	Diffusion coefficient (m^2/s)
e	=	Electronic charge (1.6×10^{-19} J/K)
F	=	Interaction Force (N)
h	=	Distance between particle surfaces (m)
h_{cake}	=	Distance between particles in a cake (m)
I	=	Ionic strength of solution (mol/L)
k	=	Fouling potential of feed water ($Pa.s/m^2$)
k_s	=	Specific fouling potential of feed water (k/ c_b)
k_B	=	Boltzmann's Constant (1.38×10^{-23} J/K)
l_{AB}	=	Decay length for Acid-Base force (0.6 nm)
M_τ	=	Mass of permeate collected at time t (g)
N_A	=	Avogadro's constant (6.02×10^{23} mol^{-1})
N_{FC}	=	Critical filtration number
r_c	=	Specific cake resistance ($Pa.s/m^2$)
R_0, R_m	=	Intrinsic membrane resistance (Pa.s/m)
R_c	=	Resistance of cake layer (Pa.s/m)
R_t, $R(t)$	=	Total resistance measured at time t (Pa.s/m)
s	=	Distance away from center of particle (m)
t	=	Time (sec)
T	=	Temperature (K)
U	=	Interaction Energy (Nm)
v	=	Permeate flux (m/s)
V_t	=	Volume of permeate per unit area collected at time t (m^3/m^2)

z	=	Valence of ions

Greek symbols

α	=	Constant
β	=	Constant
$\delta_c(t)$	=	Thickness of cake layer at time t (m)
ΔP	=	Driving Pressure (Pa)
ΔP_C	=	Critical Pressure (Pa)
$\Delta \pi$	=	Transmembrane osmotic pressure (Pa)
ΔR_t	=	Increment in resistance due to cake formation at time t (Pa.s/m)
ε_o	=	Permittivity of free space (8.85×10^{-12} C V^{-1} m^{-1})
ε_r	=	Dielectric constant of water or relative permittivity
ϕ_b	=	Volume fraction of particles in feed water, dimensionless
ϕ_{cake}, ϕ_c,	=	Volume fraction of particles in cake layer, dimensionless
ϕ_g	=	Volume fraction of particles at gel concentration, dimensionless
ϕ_{max}	=	Maximum random packing of particles, dimensionless
γ	=	Ratio of particle radius to cell radius, dimensionless
κ	=	Debye-Huckel parameter (m^{-1})
μ	=	Dynamic viscosity (Pa.s)
μ_r	=	Relative viscosity, dimensionless
μ^*	=	Liquid viscosity within pores of Colloidal Cake (Pa.s)
λ	=	Characteristic wavelength (m)
ρ	=	Density of water (kg m^{-3})
π	=	Constant, dimensionless (3.14159)
ω	=	Cake compressibility coefficient, dimensionless
ψ	=	Surface potential (V)
ψ_0	=	Surface potential at colloid surface (V)
ξ	=	Kozeny constant, dimensionless
ζ	=	Zeta-potential (V)

List of Tables

List of Figures

Chapter 1

Introduction

1.1 Background and Motivation

The advancements in membrane technologies and their industrial applications have expanded considerably in the last two decades (Lonsdale, 1982; Belfort *et al.*, 1994). Water and wastewater treatment continue to exert the greatest demand on membrane usage, accounting for about half of the market share, with other leading applications including food and beverage processing, pharmaceutical and biomedical applications, chemical processing and gas separations (Wiesner and Chellam, 1999). Membrane processes such as ultrafiltration (UF), reverse osmosis (RO) and membrane bioreactors (MBR) are increasingly gaining preference over the conventional water and wastewater treatment processes. The demand for membrane applications is projected to grow further for water treatment as the need to secure alternative and/or augment existing drinking water supplies increases, such as through seawater desalination and wastewater reclamation. Membrane processes are valued as a significant contribution to a sustainable future in light of the growing world population (Howell, 2004). The heightened adoption of membrane technology in water and wastewater treatment has been fuelled by (a) more stringent regulatory pressure on potable and wastewater effluent standards, (b) efforts to minimize the addition of chemicals in treatment processes, (c) reuse and recycling strategies for wastewater, and (d) reducing costs of membrane technologies and the associated economies of scale. The amelioration in membrane operation processes and their successful implementation in full scale projects have also contributed to the increased reliance and confidence on membranes in achieving treatment objectives.

However, membrane processes are plagued by several limitations. The most serious and persistent problem in membrane processes is membrane fouling (Cheryan, 1986; Mulder,

1996). Membrane fouling refers to the phenomena or process of performance deterioration caused by the deposition and accumulation of foulants on the membrane surface and/or inside the membrane pores. As a result, membrane resistance increases with time and impedes permeate flow through the membrane, thereby curtailing the efficiency of the process. Fouling not only reduces the permeate production rate or increases the driving pressure, but increases the complexity of the process since the system has to be cleaned frequently to restore the flux. Depending on the nature and extent of fouling, restoring the flux may require powerful cleaning agents. This may affect the operating lifetimes of membranes (Vrijenhoek et al., 2001). Fouling can also compromise the permeate quality in extreme cases (Belfort *et al.*, 1994; Zhu and Elimelech, 1997). The additional costs associated with fouling are a pressing concern for the application of membrane processes, because it makes the separation process economically unfavorable. Furthermore, the amplification of membrane usage has magnified the issue of membrane fouling which now forms a central theme of much research and development efforts in membrane technology.

Over the years, membrane fouling has generally been recognized and accepted as an inevitable and inherent problem plaguing all membrane processes (Salam *et al.*, 1997; Teixeira and Rosa, 2003; Chen JC *et al.*, 2004; Mavredaki *et al.*, 2005; Yiantsios *et al.*, 2005). Therefore, fouling mitigation or control serves as the best strategy to minimizing the impact of membrane fouling, since it cannot be eliminated. The implementation of an effective strategy to combat membrane fouling requires an identification of the key factors which govern fouling, such as the operating conditions and feed water quality (Cheryan, 1986; McDonogh *et al.*, 1992; Belfort *et al.*, 1994). The feed water-fouling strength, which is dependent on the foulant properties, their concentrations in the feed water and their fouling characteristics or behaviour is an important consideration. This should preferably be known before membrane filtration so that fouling can be minimized either by pre-treatment or altering the operating conditions.

Colloidal particles are ubiquitous in aquatic environments due to their inherent presence in natural waters, industrial processes and wastewaters. Given their small sizes (1-1000 nm) and low settleability, these particles are easily transported from one water source to another. These properties also make their removal from water very difficult, which is now best achieved using membrane processes. Therefore colloidal particles are a group of persistently encountered foulants within membrane processes used in water and wastewater treatment trains. Membrane autopsies carried out on membrane systems from all over the world revealed that colloidal matter accounted for the majority of the total deposited foulants on the membranes (Darton and Fazell, 2001; Van Hoof et al., 2002; Darton *et al.*, 2004). With the emergence of nanotechnology and the proliferation of nanomaterials in water bodies (Guihen and Glennon, 2003; Lecoanet, 2004), the incidence of colloidal fouling is expected to increase significantly (Kilduff *et al.*, 2005; Kim *et al.*, 2006; Wisener *et al.*, 2006). The acuteness of colloidal fouling in membrane processes has stimulated vast research interests and activities on this topic and related issues.

Colloidal fouling is a complex and multifarious process which is affected by numerous factors, such as operating conditions, properties of the colloidal particles, and solution chemistry of the feed water (Cohen and Probstein, 1986; Belfort *et al.*, 1994; Bacchin *et al.*, 1995; Waite *et al*., 1999; Vrijenhoek *et al*., 2001). Among these factors, water chemistry is the primary controlling parameter for the colloidal interfacial properties and interactions (Snoeyink and Jenkins, 1980; Lyklema, 1991; Hunter, 2000). This fact has long been noted in the studies of colloidal suspensions but only recently was exploited for a better understanding of colloidal fouling (Chun *et al.*, 2001; Bowen *et al.*, 2003; Kim *et al.*, 2006). In fact, colloidal fouling in membrane processes cannot be fully delineated without properly incorporating the effects of water chemistry (Nirschl and Schafer, 2005).

Considerable progress in the study of water chemistry on colloidal fouling has been made in the last few years (Zhu and Elimelech, 1997; Faibish *et al.*, 1998; Wiesner and Chellam,

1999; Tarabara *et al.*, 2004; Van der Meeren *et al.*, 2004). Although currently the effects of individual water chemistry parameters, such as pH and ionic strength on the colloidal fouling strength can be qualitatively explained, the quantitative correlations between colloidal fouling and water properties are not yet studied or known. Colloidal fouling usually occurs as a result of the combined interactions between several physical and chemical factors (e.g. permeation drag, thermal motion (diffusion), and colloidal interactions) but the interplay between these physicochemical factors is inexplicit with a qualitative assessment. Additionally, there are innumerable types of colloidal particles which may respond differently to changes in water chemistry and therefore have different effects on colloidal fouling. A qualitative assessment of the effect of physicochemical factors on their fouling would be of limited use and benefit.

This thesis aims to further delineate the effects of water chemistry and operating pressure on colloidal fouling with well designed experimental investigations and theoretical developments. Quantitative analysis of the experimental results is emphasized throughout the study to elucidate the impact of these physicochemical factors individually and in combination on colloidal fouling. Attempts are made to link the fouling behavior quantitatively to the fundamental parameters of water chemistry that govern the interactions between the colloids.

1.2 Research Objectives and Scope

The objective of this study is to systematically investigate the role of water chemistry on colloidal fouling in membrane processes, with emphasis on quantitative correlation of colloidal fouling strength with the key water chemistry parameters and hydrodynamic drag force. This work is a step towards the ultimate goal of developing a theoretical framework for the fouling strength of colloidal particles in membrane processes that can be predicted from easily measurable water properties and operational conditions. To achieve this overall objective, the following specific tasks are undertaken in this thesis:

a. Development of a quantifiable parameter to assess the strength of colloidal fouling that correctly reflects the fouling property of colloids in the feed water.

b. Experimental investigation of the fouling strength of model silica colloidal particles under various water chemistries and hydraulic driving pressure.

c. Quantitative analysis of the colloidal fouling strength with feed water chemistry through fundamental colloidal interaction parameters.

d. Correlation of the colloidal fouling strength to easily measurable water and colloidal properties for known hydraulic driving pressure and other operating conditions.

The critical parameters for water chemistry discussed in this thesis and their influence on colloidal fouling are limited to ionic strength and solution pH. Besides the water ionic strength, different monovalent salts and divalent Calcium were also assessed for their specific effects on membrane fouling of the silica colloids. Both strong and weak acids were used in pH adjustment of the feed water and the impacts of different acid anions on colloidal fouling strength were compared. In this thesis, silica colloids were used as model foulants because their interaction properties are relatively well documented and they are ubiquitous in natural aquatic environments. The selection of such a control system allows for scientifically sound and accurate interpretation of physicochemical effects on colloidal fouling. In summary, the research in this thesis combines knowledge from three major areas: water chemistry, membrane science and colloid science. Fundamental concepts from these areas are used to explain and correlate experimental results. Through this multidisciplinary approach, it is hoped that a better understanding of the effects of water chemistry and operating conditions on colloidal fouling emerges.

1.3 Structure of Thesis

The rest of thesis is subdivided into 7 chapters briefly outlined below.

Chapter 2 – Literature Review

A review of the literature covering membrane processes, membrane fouling, as well as fundamental theories and principles of colloidal fouling and colloidal interactions are presented here. The scope covered, addresses only the background information that is necessary for subsequent appreciation of the material in this thesis.

Chapter 3 – The Fouling Potential of Feed Water

A parameter to quantify the strength of colloidal fouling, the fouling potential (k), is introduced in this chapter. The fouling potential can be easily determined with a lab-scale membrane device and can be used as a powerful tool to accurately study the fouling strength of colloids under various water chemistry and operating conditions. Experimental evaluation of the fouling potential and discussions of its advantages over other fouling parameters and indices are also presented.

Chapter 4 – Colloidal Fouling and Feed Water Ionic Strength

In this chapter the effect of solution ionic strength on the colloidal fouling potential is quantitatively evaluated. The influence of the various monovalent chloride salts of Na^+, Li^+, Cs^+, K^+ and divalent Ca^{2+} at different concentrations on the colloidal fouling potential are studied. An empirical bilinear model to correlate the effects of ionic strength and colloid concentration on the fouling potential below the critical coagulation concentration is presented. The fouling potential variation above the critical coagulation concentration is also discussed.

Chapter 5 – Colloidal Fouling and Feed Water pH

In this chapter the effect of solution pH on the colloidal fouling potential is quantitatively determined. A wide range of pH values are chosen, and the influence of ionic strength determined in Chapter 4 is further tested at the different pH values. Based on experimental data, relationships relating water properties to colloidal fouling potential are determined. Finally the effects of feed water acidification using strong and weak acids on the colloidal fouling potential are also assessed.

Chapter 6 – Colloidal Cake Compressibility and Water Chemistry

This chapter explores the effect of hydraulic driving pressure on the colloidal fouling potential under different solution chemistries. The changes in colloidal fouling potential with driving pressure are explained by the compressibility of the colloidal cake. The experimental evaluation of the effects of ionic strength and solution pH on cake compressibility and correlations of the parameters are presented in this chapter.

Chapter 7 – Predicting the Fouling Potential of Colloidal Feed Waters

A model to determine the fouling potential from water quality parameters and operational conditions is presented in this chapter. With the introduction of a relative viscosity term, the experimental fouling potentials of colloids under various conditions are well reproduced with the model based on the classic theories of colloidal interactions. Subsequently, the fouling potential is simulated for a range of physicochemical conditions.

Chapter 8 – Recommendations and Conclusion

The main findings of the thesis are summarized in this chapter. Recommendations for future studies and possible expansion of research scope are elaborated. Finally, the thesis is concluded with a summary of the main point.

Chapter 2

A Review of the Literature

2.1 Membranes and Membrane Fouling Phenomena

2.1.1 Introduction to Membranes and Membrane Processes

The classical definition of a membrane is a semi-permeable barrier separating two phases which allows the selective transport of matter through it (Mulder, 1996). However, this definition does not say much about the physical properties of the membrane or what causes the selective transport of matter through it. According to the International Union of Pure and Applied Chemistry (IUPAC), a membrane is defined as "*a structure, having lateral dimensions much greater than its thickness, through which transfer may occur under a variety of driving forces*" (IUPAC, 1996). A clearer understanding of a membrane emerges when the two definitions above are combined. Membrane processes can be distinguished by the driving forces. For example, microfiltration (MF), ultrafiltration (UF), nanofiltration (NF) and reverse osmosis (RO) are driven by pressure, forward osmosis (FO) and dialysis by concentration, membrane distillation by temperature, and electrodialysis by electrical potential. Membrane processes can also be characterized according to the membrane configurations e.g. flat sheet, tubular, hollow fiber, spiral wound, etc and/or their operation modes i.e. dead end and crossflow. The numerous classifications of membrane processes are testament to the growth of the membrane industry which has taken place in the last few decades.

A great milestone in membrane history which subsequently stimulated both commercial and academic interest in membranes and membrane processes is undoubtedly the production of the first high performance asymmetric integrally skinned cellulose acetate membrane by Loeb and Sourirajan in 1963 (Sourirajan, 1970; Sourirajan and Matsuura, 1985). The membrane industry has come a long way and today membranes are used in a vast array of fields.

Membrane usage ranges from water and wastewater treatment, food and beverage processing, automobile and petrochemical industries, to biomedical applications (Belfort *et al.*, 1994; Hong et al., 1997). It is believed that this growth is just the tip of the iceberg and membrane based applications are set to expand further in the future (Wiesner and Chellam, 1999).

2.1.2 Membrane Fouling

The present applications and continued growth of membrane processes are however greatly hindered by membrane fouling. Membrane fouling is defined as "*the process resulting in loss of performance of a membrane due to the deposition of suspended or dissolved substances on its external surfaces, at its pore openings, or within its pores*" (IUPAC, 1996). The central problem with membrane fouling is that it causes a loss of performance which can either be a decrease in permeate flux production rate, a deterioration of permeate quality or both. This not only affects the efficiency but also the economic viability of membrane processes (Baker, 2000). As membrane processes become increasingly widespread in different fields, membrane fouling has become a focal concern for industrialists and researchers (Zhu and Elimelech, 1997; Yiantsios and Karabelas, 1998; Howe and Clark, 2002).

However, a solution to completely eradicate membrane fouling still remains elusive. In fact it may not exist at all, given that fouling is considered to be inevitable in membrane process (Song, 1998a; Chen JC *et al.*, 2004; Yiantsios *et al.*, 2005). In the last decade, despite the quantum leaps achieved in membrane processes with technological advances, fouling remains as one of the biggest barriers stifling the development of membrane technology. Continuous efforts are constantly required to mitigate membrane fouling or to reduce its negative impact. These include modification of membranes (Belfer *et al.*, 2004; Taniguchi *et al.*, 2003; Kiduff *et al.*, 2005) and optimization of operational parameters or flow hydrodynamics (Belfort, 1989; Fane *et al.*, 1992; Chang *et al.*, 1995; Hong *et al.*, 1997; Tarabara *et al.*, 2004). Many of these fouling control strategies are employed on an *ad-hoc* basis and may only be applicable

to a particular membrane system or feed water. A universal fouling control strategy that works for all membrane processes and feed waters is not available yet. However, it is commonly accepted that colloidal particles are a group of major foulants to membranes. There is no doubt that a better understanding of the role of water chemistry on colloidal fouling and its interplay with hydraulic conditions will most likely provide a clue to the development of more effective fouling control strategies (Winfield, 1979; Cheryan, 1986; Vrijenhoek *et al.*, 2001).

2.1.3 Colloidal Fouling

Colloidal particles represent the most common group of foulants encountered in membrane processes (Belfort *et al.*, 1994; Bacchin *et al.*, 1995; Darton and Fazell, 2001; Darton *et al.*, 2004). Van Hoof *et al*. (2002) estimated that colloidal particles account for more than 70% of the deposits detected in membrane autopsies throughout the world. The properties of colloidal particles in suspension and their behaviors in membrane processes are strongly influenced by the water chemistry e.g. pH and ionic strength (Iler, 1979; Snoeyink and Jenkins, 1980; Hunter, 2000). For example, identical colloidal particles dispersed in sea water, rain water and distilled water would all behave differently and have significantly disparate consequences on colloidal fouling when filtered under the same conditions. Therefore, it is vital that a review of colloids and colloidal properties be initiated before embarking on colloidal fouling in membrane processes.

2.2 Fundamentals of Aquatic Colloids

2.2.1 Colloids in the Aquatic Environment and their Properties

Up to the middle of the 19th century, many scientists believed that there were only three states of matter into which any system could be characterized i.e. solid, liquid or gas. The physical and chemical properties exhibited by these systems would then adhere to the state of matter

they belonged to. In 1861, Thomas Graham (1805-1869) described a new class of matter called *colloids* which would not diffuse through a membrane. Colloids, sometimes referred to as the 4th state of matter, are systems where one state of matter (dispersed phase) of very small sizes are dispersed in another state of matter (continuous phase). In aquatic environments, the continuous phase is inevitably water, and the dispersed phase can either be solid, liquid or gas. Aquatic colloids or hydrosols usually refer to when the dispersed phase constitutes solid particles in the size range of 1 to 1000 nm (Lyklema, 1991; Hiemenz and Rajagopalan 1997). The general definition of a colloid is not strict but most colloids tend to remain suspended in the aquatic environments without settling for a long time and are able to scatter light in a phenomenon known as the Tyndall effect (Eve and Creasey, 1945). Colloidal particles are generally responsible for making waters murky or turbid.

There are many particles that fall within the so-called mesoscopic physical range of colloidal particles. These can be subdivided as inorganic and organic (Hunter, 2000). Nanoparticles are an increasingly important class of colloidal particles in aquatic environments. The American Standard Testing Methods (ASTM) only formed a committee (E56) to look into standardizing and providing guidance on nanotechnology and nanomaterials in 2005 which published its first standard E2456 on terminology for nanotechnology very recently. In this report, a nanoparticle is defined as *a sub-classification of ultrafine particle with lengths in two or three dimensions greater than 1 nm and smaller than about 100 nm which may or may not exhibit a size-related intensive property* (ASTM E 2456-06). Nanoparticles are seen as an important bridge between bulk materials and atomic or molecular structures. In the natural aquatic environment, examples of nanoparticles include macromolecules, inorganic metal oxides, dendrimers, liposomes, fullerenes, DNA, viruses, etc. The physical sizes of commonly encountered colloidal particles in aquatic environments are illustrated in Fig. 2.1.

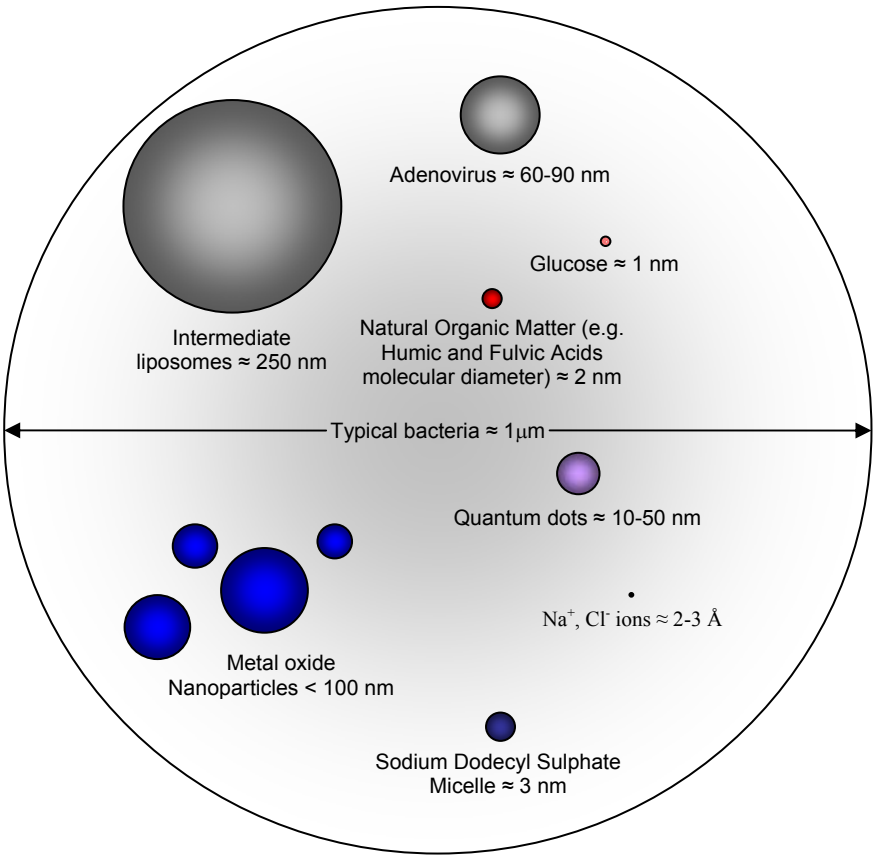

Fig. 2.1: Common colloidal particles found in aquatic environments and their typical sizes. The approximate physical size of typical bacteria and ions of sodium and chloride are shown for comparison.

The emergence of nanotechnology and nanobiotechnology looks set to increase the loading rate of a whole multitude of new and engineered colloidal particles in aquatic environments. Separation of colloidal particles from water is challenging given their small sizes (Guihen and Glennon, 2003; Eliseev *et al.*, 2004). At the same time, colloidal particles are among the most serious and persistent foulants to membrane processes in water and wastewater treatment. Common colloidal foulants include silica, iron oxide, aluminum oxide, humic and fulvic acids (Darton and Fazell 2001). Silica is one of the most common foulants found on membranes, possibly due to it being the main component of the earth's crust (Bergna and Roberts, 2006).

Colloidal particles, because of their small sizes, have large surface areas and exhibit distinctive interfacial phenomena (Hiemenz and Rajagopalan, 1997). Rather than the size of

the colloids, its interfacial properties control much of its behavior in water and when subjected to various conditions, e.g. applied pressure in membrane processes. A key underlying issue for colloidal particles is their stability which will be discussed in detail in the next section. Before embarking on this discussion, it is important to note that colloids in aqueous environments can be subdivided into hydrophilic (water-loving) and hydrophobic (water-hating) (Perrin, 1905) following the generalization by Freundlich and Neumann (1908). For hydrophilic colloids such as silica, polymers, polyelectrolytes, proteins, humic substances, starch and other water soluble macromolecules, water acts as a solvent so that the water-colloid system forms a solution. On the other hand, for hydrophobic colloids, water is not a natural solvent and sols are formed only when the colloids are stabilized. This implies that hydrophilic colloids are thermodynamically stable while hydrophobic colloids are not. Every system under standard temperature and pressure seeks to achieve a minimum free energy. In colloidal systems, smaller particles have much higher interfacial energy and there is a strong natural tendency for them to aggregate so that the free energy of the system is reduced (Hunter, 2000). Therefore, a stabilizing mechanism must be present to prevent the aggregation. In the case of hydrophobic colloids, kinetic stability is induced by the repulsive forces between the particles. Hydrophilic particles experience strong specific solvent effects in addition to all the forces experienced by the hydrophobic colloidal systems. These interfacial interactions are reviewed in the next section.

2.2.2 Introduction to Colloidal Interactions & DLVO Theory

Classically, literature introducing colloidal interactions would commence with an account of the interaction between molecules before addressing the interactions between colloidal systems, since colloids are made up of several molecules. However, historically the theoretical development of the two areas occurred concurrently with many important ideas applicable to both established from colloid science (Lyklema, 1991). The interface interaction potentials between colloidal particles can be characterized as attractive (i.e., they draw the

surfaces together) or repulsive (i.e., drive surfaces apart). The stability of colloidal systems depend on the balance of these interactions as described by the DLVO theory (first letter from the names of the two Russian and two Dutch researchers, as shown in the subsequent reference, who proposed it independently in the 1940s) (Derjaguin and Landau, 1941; Verwey and Overbeek, 1948). According to the theory, the two major long range interactions between colloidal particles are the van der Waals (VDW) attraction force and repulsive electrical double layer (EDL) force described below.

2.2.3 London-van der Waals Interaction

In 1873, van der Waals, as part of his doctoral thesis, postulated the existence of a long-range attractive force between molecules (van der Waals, 1873). However, the origin of this force was not forthcoming and it was subsequently shown that there are three possible sources for the attractive force: (a) *Orientation effect* (Keesom, 1920; 1921), (b) *Induction effect* (Debye, 1920; 1921), and (c) *Dispersion effect* (London, 1930). This allowed the quantitative evaluation of the attractive force between the molecules.

2.2.3.1 Hamaker's Approximation

Hamaker (1937) extended the definition of van der Waals attraction to macroscopic colloidal particles as the sum of all the van der Waals interactions between molecules in the two bodies. By this pairwise summation of forces, he was able to determine the interaction potential between two colloidal particles which was dependent on the radius of the particles (a_p), the separation distance (h) and a constant termed the Hamaker Constant (A_H). The interaction energy for close approach (i.e. $h << a_p$) between two equivalent colloidal spheres is represented in Eq. (2.1).

$$U(h) = -\frac{A_H a_p}{12h} \tag{2.1}$$

The Hamaker constant is closely related to the dielectric constants and the refractive indices of the colloidal particle and the suspending solution (Gregory, 1969). As an interesting side note, Hamaker also pointed out that it is possible for the van der Waals interaction between two different materials immersed in a liquid to be repulsive that was confirmed subsequently by several others (Derjaguin *et al.*, 1954; Fowkes, 1967; Visser, 1972; Neumann *et al.*, 1979).

2.2.3.2 Lifshitz Approach: Modern Dispersion Force Theory

The Hamaker method, however, tends to overestimate the interaction because of the assumption of complete additivity. This commonly results in an inaccuracy of 10-30% (Lyklema, 1991). In an alternative method, Lifshitz (1956) derived the interaction between macroscopic bodies by considering the electromagnetic properties of the medium. The quantitative analysis is based on quantum electrodynamics of continuous media summarized in two classical papers (Dzyaloshinskii *et al.*, 1960). However, given the complexity of the equations and unavailability of the dielectric range by the Liftshitz approach, the Hamaker approach is commonly preferred despite its shortcoming.

2.2.3.3 Retardation Effects

The decay length for the interaction between colloidal particles is h^{-2}, based on Hamaker's treatment for van der Waals interactions between colloidal particles. However, given the electromagnetic nature of dispersion forces this is only true for short separation distances (approximately $h < 10$ nm), due to retardation effects. Retardation comes about because of finite propagation time of electromagnetic waves (3×10^8 m/s in vacuum) resulting in delay in the response of an oscillation in a colloidal body to the spatial orientation of an oscillator in another colloidal body. As a result of the lag, the attraction is relatively weaker when compared to that at short distances, and the retardation decays more rapidly at h^{-3} for greater distances (Casimir and Polder, 1948). While retardation effects are accounted for in the Lifshitz's approach, for the Hamaker's analysis, retardation effects can be incorporated by

simple modifications to the Hamaker approach. Gregory (1981) accounted for the retardation effect and expressed the interaction energy between two colloidal spheres of equal size as

$$U(h) = -\frac{A_H a_p}{12h}\left(1 - \frac{bh}{\lambda}\ln\left[1 + \frac{\lambda}{bh}\right]\right) \tag{2.2}$$

Where, λ is the characteristic wavelength and *b* is a constant of value 5.32.

2.2.4 Electrical Double Layer Interactions

The second component of the DLVO theory comprises the repulsive potential between the colloidal particles as a result of the electrical double layer interactions. In this section, the reason for the occurrence of the electrical double layer, the factors affecting the strength of the double layer and the repulsive interaction energy between two equivalent spherical particles are discussed.

2.2.4.1 Surface Charge on Colloidal Particles

Ion movement due to charges is largely responsible for the development of electric charge on the surface of colloidal particles. When introduced into an aqueous environment, the ion transfer from the solid colloidal surface to liquid and vice versa is unequal, resulting in a difference in electrical potential at the solid/liquid interface. Generally surface charges on colloidal particles can be attained by the following methods (a) *surface dissociation or preferential dissolution of lattice ions,* (b) *ion adsorption from solution, and* (c) *crystal lattice defects* (Elimelech *et al.*, 1995; Hunter, 2000).

2.2.4.2 The Electrical Double Layer

The electric field developed due to the charges on the surface of the colloidal particles results in the accumulation of oppositely charged ions (counter-ions) and the reduction in ions with the same charge sign (co-ions) in a narrow region of liquid immediate to the colloid surface.

This non-uniform distribution of ions around the charged colloidal particle at the interfacial region is known as the *electrical double layer* which is shown in Fig 2.2 with the associated surface potential.

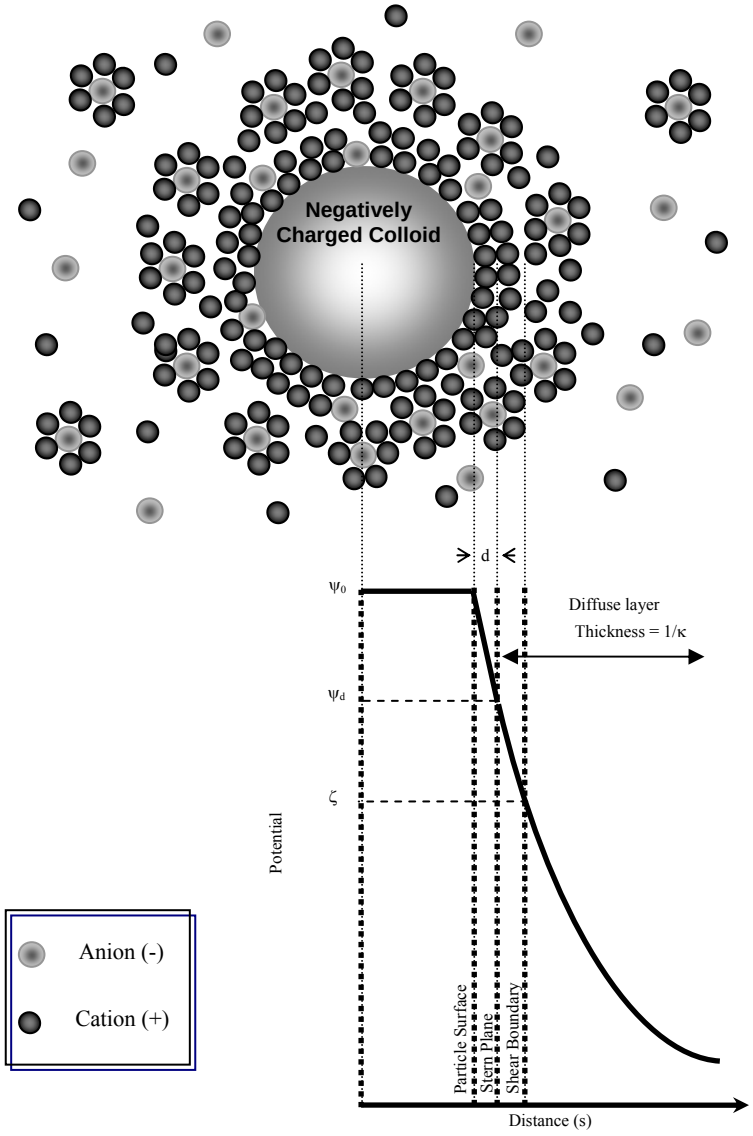

Fig 2.2 Distribution of ionic atmosphere around negatively charged colloidal particle. The variation of potential at distance, *s* away from the center of the particle is shown.

The distribution of ions near the surface has been proposed by several models. The simplest model available is the capacitor model as proposed by Helmhotz in 1879 (Bikerman, 1940). Here, the potential across the colloidal surface and the ion atmosphere is analogous to the

electrochemical potential across two parallel capacitor plates. However, the capacitor model does not provide information about the portion of the double layer that extends into the solution which is known as the diffuse layer.

The electrical double layer is better addressed by the model of Guoy-Chapman (Guoy, 1910; Chapman, 1913). However, the Guoy-Chapman theory suffers from some shortcomings. Firstly, the measured capacitance at certain interfaces can be much lower than that predicted by theory. Secondly, counterion concentration near charged interfaces is highly overestimated even for average values of surface potential. The reason for this discrepancy is because of the assumption of electrolytes as point charges. However, real ions have volumes which experience 'crowding' effects as they approach the colloidal surface. To account for the finite size and specific adsorption of ions, a boundary situated at a distance *d* which demarcates the aqueous part of the double layer from the adsorbed counterions and known as the stern layer is defined (IUPAC, 1972) as shown in Fig. 2.2. Grahame (1947) extended the theory by subdividing the stern layer into the inner Helmholtz plane (IHP) and outer Helmholtz plane (OHP). Beyond the OHP is the diffuse layer as described by the Guoy-Chapman theory. The surface of shear or shear plane in Fig. 2.2 is the boundary between the immobilized fluid and the mobilized fluid near the surface of the particle which moves with the same velocity as the particle. Although the actual location of the shear plane is unknown, it is presumed to be roughly near the stern layer, i.e., OHP. The potential at this shear plane is the zeta-potential (ζ), which is the most common electrokinetic parameter measured.

The potential drop across the diffuse double layer is described with the Poisson-Boltzmann equation using the Debye-Huckel approximation (i.e. $\psi < k_B T/ze$) and, for spherical particles, is expressed as

$$\psi = \psi_0 \left(\frac{a_p}{s} \right) \exp\left[-\kappa \left(s - a_p \right) \right] \tag{2.3}$$

Where s is the distance from the center of the particle as shown in Fig 2.2 and κ is the Debye-Huckel parameter (m^{-1}). The Debye-Huckel parameter is widely encountered throughout the discussions of double layer and its inverse is known as the 'thickness' of the double layer. Mathematically, it is the distance at which the potential drops by approximately 37% (100/e) of the surface potential (ψ_0). The Debye-Huckel parameter is dependent strictly on solution properties as described in Eq. (2.4)

$$\kappa = \sqrt{\frac{1000e^2 N_A \sum_i c_i z_i^2}{\varepsilon_0 \varepsilon_r k_B T}} \tag{2.4}$$

N_A is the Avogadro's constant (= 6.03×10^{23} mol^{-1}), e is the charge of the electron (= 1.6×10^{-19} C), c_i the molar concentration of ions i, z_i is the valence of the ion, ε_0 the dielectric permittivity of a vacuum (= 8.85×10^{-12} C V^{-1} m^{-1}), ε_r the relative dielectric permittivity in water (= 78). k_B is the Boltzmann's constant and T the absolute temperature in Kelvin. For monovalent ions in water at 25°C, the Debye-Huckel parameter can be simplified to

$$\kappa = 3.288\times10^9 \sqrt{I} \tag{2.5}$$

I is the ionic strength (mol/L) of the solution which is the summation of the molar concentrations of all ions multiplied by the square of their valence ($=\frac{1}{2}\sum c_i z_i^2$).

2.2.4.3 Overlap of Double Layers & Repulsive Forces

When two particles with their associated double layers approach each other, at some point, the double layers overlap. At the overlap region, there is a build-up of ion concentration which results in a repulsive osmotic pressure that pushes the particles apart as shown in Fig 2.3. It follows then that the repulsive force depends on the magnitude of the surface potential (i.e. zeta potential can be used as an approximation), the concentration and types of electrolyte (can be represented by the double layer thickness or ionic strength).

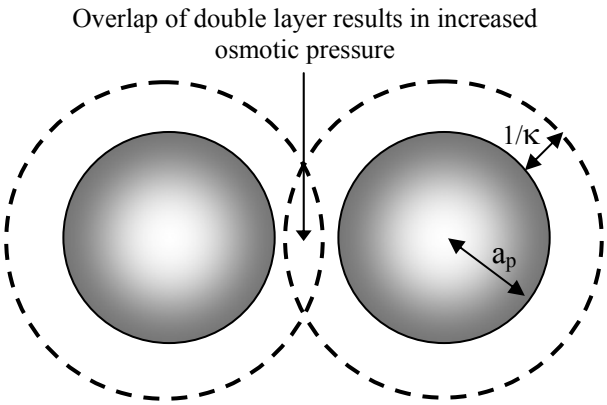

Fig 2.3: Double layer interactions between two approaching colloidal particles. The higher concentration of ions in the overlap region results in greater osmotic pressure pushing the particles apart.

The increased osmotic pressure in the overlap region forces the ions to move out and therefore affects the reorganization of the ions at the colloid surface. This naturally has an influence on the potential distribution and potential energy of interaction. For simplicity, it is common to assume that the surface ionic equilibrium is established quickly as the two colloidal particles approach.

The situation then condenses to one of constant surface charge or constant surface potential. This depends on the origin of the surface charge. For surface charges generated as a result of the adsorption of ions, the surface potential would remain constant as the double layers overlap. Alternatively, if the surface charges develop due to ionization the charge density would remain constant (Hiemenz and Rajagopalan, 1997).

For identical spherical particles at low surface potentials and thin double layers, Hogg *et al.* (1966) and Wiese and Healy (1970) derived the repulsive double layer interaction energy for constant surface potential (ψ) and constant surface charge (σ) respectively shown in Eq. (2.6) and Eq. (2.7)

$$U^{\psi}(h) = 2\pi\varepsilon_0\varepsilon_r a_p \psi_0^2 \ln\left[1+\exp(-\kappa h)\right] \tag{2.6}$$

$$U^{\sigma}(h) = 2\pi\varepsilon_0\varepsilon_r a_p \psi_0^2 \ln\left[1 - \exp(-\kappa h)\right] \tag{2.7}$$

The Derjaguin approximation (Derjaguin, 1934) is a commonly used integration method to extend the plate-to-plate double layer interaction to spherical particles. A limitation of this approach is that it breaks down at close approaches when the double layer is extensive or for $\kappa a_p < 5$. For such instances, Verwey and Overbeek (1948) developed an approximate procedure for low potentials as shown in Eq. (2.8) which is equivalent for constant surface charge and constant surface potential approximations

$$U^{\psi}(h) = U^{\sigma}(h) = 2\pi\varepsilon_0\varepsilon_r a_p \psi_0^2 \exp(-\kappa h) \tag{2.8}$$

It is common in practice to replace the surface potential value with the zeta potential value in Eqs. (2.6) to (2.8), since it can be determined.

2.3 Colloidal Silica and Interfacial Interactions

There are many excellent monographs that deal specifically with the properties and behavior of colloidal silica particles (Iler, 1955; Iler, 1979; Bergna and Roberts, 2006). It would be impossible to highlight all the properties of these amorphous, abundant and interesting colloidal particles. Only the pertinent aspects relevant to the purpose of the thesis will be highlighted. Despite the numerous industrial applications and advances made in understanding colloidal silica, many fundamental questions about the behavior of colloidal silica systems remain unanswered.

Silica is one of the most abundant minerals naturally occurring on earth (Iler, 1979; Sjoberg, 1996) and a major group of colloids and nanoparticles found in aquatic environments (Puls and Powell, 1992; Atteia *et al.*, 1998; Icopini *et al.*, 2005). It is one of the most complex metal oxides and a striking difference between silica and other metal oxides is its electrokinetic behavior. Silica colloidal particles show anomalously high stability at high ionic strength and at low pH values near its point of zero charge (Allen and Matijevic, 1969;

Depasse, 1999) in contrast to the predictions from the DLVO theory. Additionally, silica exhibits increasing sensitivity to electrolytes at higher pH values contrary to that ascribed by the electrical double layer theory (Iler, 1979).

The high stability of silica sols is attributed to a monotonic short range repulsion force between the colloidal particles (Peschel *et al.*, 1982; Chapel, 1994; Atkins and Ninham, 1997). Horn (1990) experimentally found that the interaction between amorphous silica surfaces was repulsive even up to a few angstroms of separation, suggesting that van der Waals attractive forces were not strong in the colloidal silica systems. However, the reason for the repulsion is the subject of much debate and has not been resolved yet (Raghavan *et al.*, 2000).

It was previously thought that the repulsion force was due to an immobilized layer of liquid on the surface of the colloidal particle brought by the ions attracted to the surface. The structuring of water induced a short range repulsive hydration force due to solvation between the silica surfaces (Rabinovich *et al.*, 1982; Ducker, 1991; Chapel, 1994). This repulsive surface force was found to be inversely related to the degree of hydration of the counterion (Chapel, 1994) for silica surfaces, which was opposite to that observed between mica surfaces (Pashley and Israelachvili, 1984). For many years, it was believed that hydration was the reason for the repulsive force observed between silica surfaces. However, after careful consideration of experimental and theoretical results, Israelachvili and Wennerstrom (1996) concluded that hydration forces are either attractive or oscillatory and the strong short range repulsion observed between surfaces may not have any origins from hydration. Nevertheless, it is still possible to find papers that attribute the short range repulsive forces to hydration.

Recently, through experimental investigations, the short range repulsive force for silica colloids was attributed to a gel layer or “silica hairs” approximately 1 nm thick that are formed on the silica surface on exposure to water. The hairy layer was believed to contain

both silicic and silanol groups that contribute to the steric-like repulsive force between silica particles (Vigil *et al.*, 1994; Kobayashi *et al.*, 2005). Experimental results from these studies further suggested that the change in the short range repulsion between silica is not highly sensitive to changes in the solution conditions such as pH and ionic strength. Interestingly, Grabbe and Horn (1993) who attributed the short range repulsion force for their experiments between two silica sheets to hydration, also concluded that this force was unaffected by the electrolyte concentration.

Although the existence of a non-DLVO short range force between the silica particles was known, its characterization, quantification and theoretical development was not forthcoming until the work of van Oss *et al.* (1986; 1987) who introduced them as Acid-Base Interactions.

2.3.1 Lewis Acid-Base Interactions

The Acid-Base interactions between surfaces are not of electrodynamic or electrostatic origin like the van der Waals and electrostatic interactions, as described from the DLVO theory. They are due to the interaction between electron acceptor and electron donor (Lewis Acid-Base) interactions in polar media such as water (van Oss *et al.*, 1988). As such they are also known as polar interactions.

These interactions can be attractive where they are described as hydrophobic interactions or repulsive as in the case of hydrophilic surfaces such as silica particles where it has been classified as hydration or structural force (Israelachvili, 1992). The Acid-Base interaction energies are strong and could be up to 2 decimal orders higher than the DLVO interaction energies (van Oss, 1994). However, as expected, these forces tend to have a much greater rate of decay with a decay length of approximately 1 nm for the repulsive hydration effect. This corresponds with the thickness of the gel layer proposed by Vigil *et al.* (1994).

2.3.2 Adsorption on Silica Colloids

In aquatic environments, silica particles are usually coated with adsorbed layers of other ions or molecules. These can include organics such as polymers, surfactants, dyes, small organic molecules, polysaccharides, proteins, etc, and inorganic or metallic ions (Persello, 2000). The adsorption of these species can significantly alter the surface characteristics of the colloidal particles and their subsequent interactions. In some cases, reversal of charge or completely new properties of the colloids emerge due to the adsorption. Adsorption also represents the basic mechanism by which fundamental feed water properties such as pH and specific ions affect the surface charges of the colloidal silica particles.

Adsorption on silica surfaces can take place via the following methods (a) *chemical bonding*; (b) *hydrogen bonding*; (c) *hydrophobic bonding*; or d) *van der Waals force.* Since the unique properties of silica particles are attributed to the thin 1 nm gel ('hairy') layer near its surface, adsorption of chemical species on the colloidal surface can mask this layer, thus controlling the special properties of the particles. Yoon and Vivek (1998) found that while a short range repulsive force at distances below 15 nm was present between silica particles in pure water, there was no such force when 15% methanol which adsorbed to the silica surface was added to the water. The groups on the silica surface also provide suitable adsorption sites for many ions and molecules in aquatic environments (Iler, 1979).

2.3.3 Stability of Silica Particles

The aggregation behavior of silica has been a constant topic of research in the last three decades. Much progress has been made in understanding the effect of pH and ionic strength on the coagulation of silica particles (Iler, 1975; Zerrouk *et al.*, 1990; Lee and Moon, 2003). It is however observed that there is usually little or no mention of the effect of colloid concentration on the critical salt concentration that triggers coagulation. Zeta potential and turbidity measurements are most frequently used to study the influence of salt addition on

aggregation behaviour of colloids. While zeta potential is a good indication of the likely stability or aggregation of colloids, it does not always prove to be so, particularly for silica particles. Allen and Matijevic (1969; 1970; 1971) in a series of papers examined the critical coagulation concentration for different salts on colloidal silica in the pH range of 6-11, and found that it did not correlate with changes in the electrophoretic mobility or zeta potential of the colloids.

2.4 Colloidal Fouling and Cake Formation in Membrane Processes

2.4.1 Filtration Theory

Membrane filtration of colloidal particles, results in two major phenomena on the membrane surface i.e. concentration polarization and cake formation. Water permeation through the membrane, exerts a drag force on the colloidal particles bringing them to the membrane surface. These colloidal particles, being larger than the pores of the membrane, are rejected and retain near the membrane surface. As water is removed through the membrane pores, colloidal accumulation leads to a higher colloidal concentration near the membrane surface as compared to the colloidal concentration in the bulk solution as shown in Fig 2.4.

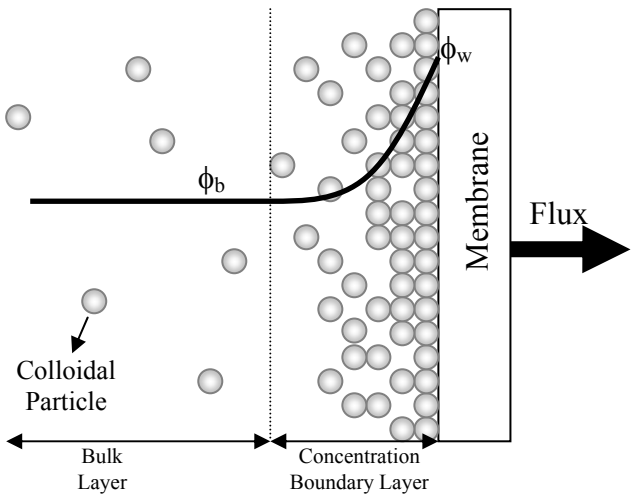

Fig 2.4: Colloid build-up on the membrane surface as a result of convective transport of permeate through the membrane. ϕ_b and ϕ_w are the solute concentration in the bulk and near the membrane surface respectively.

The concentration of colloidal particles near the membrane surface (ϕ_w) is the highest, and gradually decreases with distance away from the surface until it reaches a constant value in the bulk solution (ϕ_b). Brownian diffusion by the accumulated colloidal particles exerts a back transport towards the bulk, the strength of which is related to the size of the colloids.

The concentration profile in the boundary layer near the membrane surface is a fascinating and complex region. It affects the permeate transport mechanism through the membrane system. Depending on the pore size of the membrane used and the feed water constituents, solute or colloidal materials of different sizes are rejected and accumulate on the membrane surface. For Reverse Osmosis (RO) and Nanaofiltration (NF) processes, rejected feed water constituents tend to be smaller then a few nanometers e.g. ions, molecules, etc. As the diffusion coefficient of these species is high, they do not deposit on the membrane surface but exist as an elevated and mobile polarized layer on the membrane surface which is of higher concentration than in the bulk, known as the concentration polarization layer (Mulder, 1996). The permeate transport through this layer is dependent on the thermodynamic properties of the solute species in the concentration boundary layer and can be represented by the osmotic pressure model (Song and Elimelech, 1995) in Eq. (2.9).

$$v = \frac{\Delta P - \Delta \pi}{R_m} \tag{2.9}$$

ΔP, $\Delta \pi$, R_m are the pressure difference across the membrane, transmembrane osmotic pressure, and hydraulic membrane resistance respectively. Concentration polarization is temporary and disappears when filtration stops. This is because the feed water constituents do not deposit on the membrane and are mobile. Upon the removal of the hydraulic pressure or driving force, the accumulated materials quickly diffuse back into the bulk feed. Although concentration polarization can result in serious deterioration of permeate flux, it is not membrane fouling because no deposition takes place in or on the membrane.

In the simplest sense, the deposition of particles on the membrane surface depends on the balance between the hydraulic pressure and the back transport due to diffusion. Although deposition could take place by adsorption and precipitation of insoluble salts or scaling, this is not the concern here. For larger particles such as macromolecules or suspended solids, because their diffusivities are much smaller, they deposit on the membrane surface, forming a foulant layer known as the cake. This cake layer exerts a hydrodynamic resistance (R_c) to permeate flow and the permeate transport is represented by the filtration theory or cake filtration model in Eq. (2.10)

$$v = \frac{\Delta P}{R_m + R_c} \tag{2.10}$$

However, the strict application of these models to the different solutes has often not been adhered to (Wijmans et al., 1984). There is considerable debate surrounding the suitable theoretical framework to describe these mechanisms, since much of the theory is developed based on hypotheses of assumed behaviour (Chen JC et al., 2004). The applicability and suitability of the models is further complicated, when colloidal particles are involved, since they exhibit physical properties in between those of ions and macromolecules. Therefore the strict application of either model to colloidal particles could be questionable (Jonsson and Jonsson, 1996; Chen *et al.*, 1997; Bhattacharjee *et al.*, 1999; Bacchin *et al.*, 2002). Furthermore, feed waters can contain a wide range of particles and it is likely that both concentration polarization and cake formation could occur simultaneously and a unified consideration of these is necessary.

In recent years, more comprehensive descriptions of the membrane filtration process for colloidal particles have developed (Song and Elimelech, 1995; Bowen and Jenner, 1995c; Elimelech and Bhattacharjee, 1998; Bacchin *et al.*, 2002). These descriptions consider the transference from concentration polarization to cake formation, which occurs above a certain critical colloidal volume fraction in the boundary layer known as the gel concentration (ϕ_g)

(Michaels, 1968; Cheryan, 1986; Mulder, 1996). Interestingly, a similar concept is expressed with the perturbation theory in fluid mechanics which invokes an order-disorder transition phase of the fluid depending on the dispersed colloidal concentration (Barker and Henderson, 1967; Russel *et al.*, 1989). The colloids in the concentration polarization layer are mobile and flow along with the liquid. When the colloidal particles are compressed they lose their degrees of freedom and become an ordered, structured state known as the cake layer. Unlike the concentration polarization layer, the cake layer is theoretically assumed to be immobile and remains on the membrane surface even after filtration has stopped (Wijmans *et al.*, 1984; Petsev, 1993).

It follows from the descriptions above, that concentration polarization and cake formation are a change in phase of the boundary layer and the occurrence of cake formation from concentration polarization can be determined (Song and Elimelech, 1995; Bacchin *et al.*, 2002). The unified permeate transport equation given by

$$v = \frac{\Delta P - \Delta P_c}{R_m + R_c} \tag{2.11}$$

introduces the term ΔP_c, the critical pressure which is determined solely from the thermodynamic properties of the solution (Song, 1998a). This represents the maximum value of osmotic pressure at a given critical filtration number (N_{FC}) for non-interacting particles (rigid) which is described by

$$\Delta P_c = \frac{3k_B T}{4\pi a_p^3} N_{FC} \tag{2.12}$$

where k_b, T, a_p and N_{FC} are the Boltzmann's constant, absolute temperature, particle radius and critical filtration number respectively. Therefore, from the model, if the driving pressure was smaller than the critical pressure ($\Delta P < \Delta P_c$) the colloidal particles would not deposit and concentration polarization would be the dominating mechanism. On the other hand if the driving pressure were greater than the critical pressure, cake formation would occur and the

concentration polarization layer above it would be at maximal value ΔP_C as illustrated in Fig 2.5 for crossflow systems.

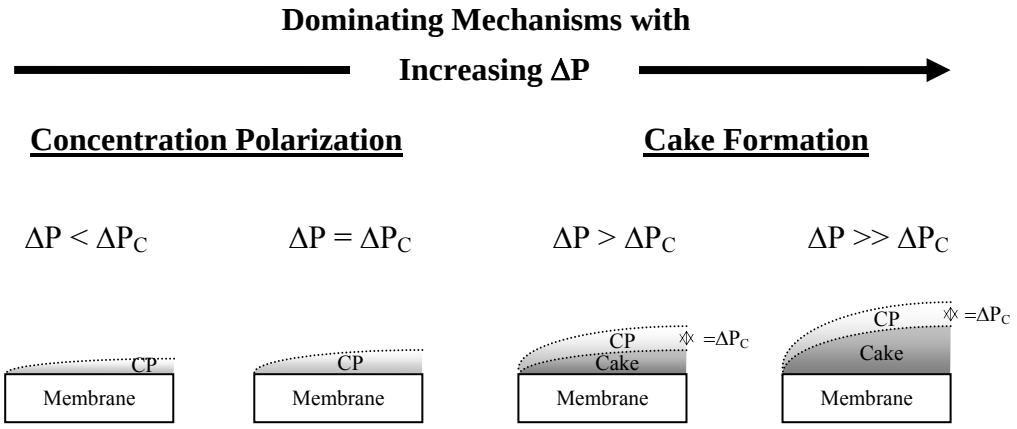

Fig 2.5: Illustration of concentration polarization (CP) and cake formation in a crossflow membrane system for increasing constant pressure (ΔP). Following the model of Song and Elimelech, 1995; CP occurs below the critical pressure (ΔP_C), and cake formation only takes place when the driving pressure is higher than ΔP_C beyond which point the pressure drop across the CP layer remains constant at ΔP_C.

As seen from Eq. (2.12) it is also observed that the critical pressure is inversely related to the cubic power of particle radius which explains why deposition of colloidal particles occurs instantaneously for particles larger than a few tens of nanometer in diameter for most membrane applications (Song and Elimelech, 1995; Song, 1998b). Past studies have revealed that concentration polarization for colloidal particles larger than approximately 10-20 nm diameter is negligible in membrane filtration (Wiesner *et al.*, 1989; Hong *et al.*, 1997; Elimelech and Bhattacharjee, 1998; Kim *et al.*, 2006). As the particles used in this study are larger than this, cake formation is the dominant mechanism and will be the focus here subsequently.

2.4.2 Characterization of Colloidal Fouling

Colloidal fouling can be characterized by the manner in which the colloidal foulants deposit on the membrane surface. Depending on the relative physical properties of the colloidal

particles, membrane surface and pores in the membrane, the deposition behavior of colloidal foulants can be classified as the following (Hermans and Bredee, 1936; Hermia, 1982);

a) *Complete blocking*, where the colloidal particles completely obstruct the membrane pore, preventing or reducing water flow through it
b) *Standard blocking*, where the colloidal particles are small enough to penetrate the pores, reducing the pore volume amenable to filtration
c) *Intermediate blocking*, where the colloidal particles in addition to complete blocking form a surface deposit on the membrane
d) *Cake filtration*, where colloidal particles form a surface cake deposit on the membrane surface

The deposition behavior described in a) to c) are commonly observed in Microfiltration (MF) and for loose Ultrafiltration (UF) membrane applications. Deposition behaviour d), also referred to as cake formation, is prevalent in colloidal fouling observed in the smaller pore-sized UF, NF and RO membrane applications. As discussed previously, cake formation is the dominant form of fouling for colloidal particles observed in most membrane processes (Peavy *et al.*, 1985; Fane *et al.*, 1992). In addition to the deposition behavior described above it is also possible for certain colloidal foulants to be adsorbed or precipitated on the membrane surface, as is common in biofouling, organic fouling and scaling, but these will not be discussed in this thesis.

Hermans and Bredee (1936) and subsequent reanalysis by Hermia (1982) summarized the deposition behavior to conform to the following equation where the exponent *n* of values 0, 1, 1.5 and 2 correspond to complete, standard, intermediate blocking and cake filtration respectively.

$$\frac{d^2t}{dV^2} = A_o\left[\frac{dt}{dV}\right]^n \tag{2.13}$$

t, V are the time of filtration, filtration volume and A_o, *n* are filtration constants. The assumptions made in developing the model were homogeneous feed water containing spherical colloidal particles, Poiseuille's Law through cylindrical parallel homogenous pores and that the particles are either trapped in the pores or on the membrane surface. By curve fitting of experimental data to each of the different conditions, it is possible to determine which filtration equation or so-called filtration law was obeyed.

However, this method has received its fair share of criticism. It is possible that more than one filtration equation can be fitted to the experimental data. As such there is considerable controversy regarding the fouling mechanisms and subsequent fouling control strategies. For example, experimental work conducted on the same colloidal material (Bovine Serum Albumin) using similar membranes, Bowen and Gan (1991) found their data to fit best with the complete blocking law, while Hlavacek and Bouchet (1993) found that the intermediate blocking law provided the best fit to their experimental data, and Kelly and Zydney (1995) found that neither of the filtration laws fitted to their experimental data and instead proposed a modified form of the pore blockage model (standard blocking). In some cases, the fitted filtration laws obtained for experimental data did not correspond with the experimental conditions. As highlighted by Aimar (2003), it is possible for the cake filtration law to be fitted to experimental data even when the membrane pore size is ten times larger than the size of the colloidal particles. There is also suggestion that the filtration laws are too simplified and several mechanisms may be concurrently contributing to fouling. Interestingly in many cases, experimental data have been shown to fit Eq. (2.10) for exponent values (*n*) that are much higher than 2 and smaller than zero (Iritani *et al.*, 1995; Ho and Zydney, 2000; Yuan *et al.*, 2002). Membrane surface morphology and heterogeneities have been suggested to play a critical role other than the pore size of the membrane on the fouling rate of colloidal particles (Bacchin *et al.*, 1995; Fratila-Apachitei *et al.*, 2001; Vrijenhoek *et al.*, 2001). These aspects are unfortunately not considered in the filtration laws. A better characterization of colloidal fouling is therefore required, and this will be addressed in Chapter 3.

2.4.3 Colloidal Cake Structures

A colloidal cake is an assemblage of colloidal particles on the membrane surface. It forms due to the 'solidification' of the colloidal particles under the coupling of hydrodynamic and surface interaction forces of the particles. The colloidal cake layer is a porous structure surrounded by liquid which flows through the voidage. The cake layer for charged colloidal particles is significantly different from that for an uncharged (rigid colloidal particles) one as shown in Fig 2.6. In the uncharged colloidal cake, particles pack at or near the maximal packing solids volume fraction, whereas for charged particles the solids volume fraction is lower than the maximal packing.

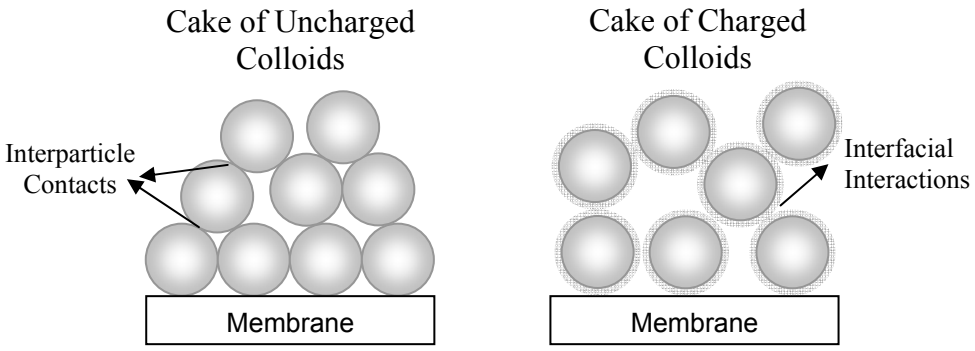

Fig. 2.6: The difference in the cake layer for uncharged (rigid) colloidal particles and charged colloidal particles. Rigid colloidal particles are supported by interparticle contacts, however these are not possible in charged colloidal systems because of strong interfacial interactions between them. The colloidal cake for the charged system is in an immobile fluidized state.

Unlike the packing of colloids in uncharged colloidal cakes, interparticle contacts do not support individual particles in the charged colloidal cake. Instead, individual particles behave almost like in a 'fluidized' system and the particles are fixed in position by the balance of the hydrodynamic and particle interaction forces (Chen JC *et al.*, 2004; Kim and Hoek, 2002). To investigate the structural characteristics of porous bodies, the following experimental techniques are commonly employed (de Boer and Linsen, 1970; Feder, 1988; Churaev, 2000)

a) Capillary condensation

b) Adsorption and gas flow

c) Liquid flow

d) Radiotracer technique

In membrane systems, the determination of structural characteristics of colloidal cakes is achieved in the most effective, non-invasive and convenient method by liquid flow. The pressure drop resulting from the passage of fluid through a dense bed of particles can be estimated with considerable precision by various models. The two main models are the Carmen-Kozeny and the Happel Cell models, which were developed for monodispersed, smooth, rigid particles, but widely used to explicate flow through colloidal cakes in membrane processes.

2.4.4 Carmen-Kozeny Model

Liquid flow through a packed bed of particles is expected to be anfractuous, because the water molecules would have to traverse through the voids formed by the particles. The flow pattern is often referred to as tortuous (Kim and Yuan, 2005). The average length of the flow (L_τ) would be greater than the length or thickness of the assemblage of the particles (L). The principal consideration in the Carmen-Kozeny derivation is that the pore space is equivalent to a number of parallel capillaries of equivalent cross sectional radius and shape (Kozeny, 1953). With this, the pressure drop across the assemblage of particles can then be expressed as

$$\frac{\Delta P}{L} = \frac{\xi_o \mu S^2}{(1-\phi)^3} \frac{L_\tau}{L} V \tag{2.14}$$

Where V is the liquid flow velocity through the assemblage, ϕ is the volume fraction of the particles in the assemblage, μ the liquid viscosity and S is known as the specific surface (particle surface area per unit volume of bed). For spheres of radius a_p the specific surface is $S = 3\phi/a_p$ (Carman, 1939). The ratio (L_τ/L) is known as the tortuosity factor and ξ_o is a shape correction factor for the assumed capillary in the colloidal cake. The product of the tortuosity and shape correction factors is referred to as the Kozeny constant (ξ). For spherical particles a

fixed cake structure with, $\xi \approx 5$ is commonly assumed. Therefore Eq. (2.14) can be expressed as

$$\frac{\Delta P}{L} = \frac{45\mu\phi^2}{a_p^2(1-\phi)^3}V \tag{2.15}$$

Since the resistance (R) offered by an assemblage of particles to fluid motion is defined as $R = \Delta P/V$, the specific resistance (r_c) of the assemblage is then determined as the resistance per unit length of the assemblage (L) in Eq. (2.16)

$$r_c = \frac{45\mu\phi^2}{a_p^2(1-\phi)^3} \tag{2.16}$$

2.4.5 Happel Cell Model

For concentrated systems, Happel developed a sphere in cell drag model expressing the pressure drop (ΔP) across an assemblage of particles of length (L) due to the passage of fluid passing at velocity (V) through it (Happel, 1958; Happel and Brenner, 1991) as shown below.

$$\frac{\Delta P}{L} = \frac{9\mu\gamma^3 V}{2a_p^2}\left(\frac{3+2\gamma^5}{3-\left(9/2\right)\gamma+\left(9/2\right)\gamma^5-3\gamma^6}\right) \tag{2.17}$$

γ is the ratio of the particle radius to the cell radius and is related to the volume fraction of the colloids in the assemblage ($\gamma = \phi^{1/3}$). The term outside the bracket represents the pressure drop per unit length obtained by adding the resistances due to individual spheres on the assumption of no interaction between them. The term in the square brackets represents the correction factor for multi-body effects of particles in concentrated assemblage of particles. Similar to the Carmen-Kozeny equation, the Happel model can be expressed in terms of specific resistance and volume fraction of the colloids as in Eq (2.18)

$$r_c = \frac{9\mu\gamma^3}{2a_p^2}\left(\frac{3+2\gamma^5}{3-\left(9/2\right)\gamma+\left(9/2\right)\gamma^5-3\gamma^6}\right) \tag{2.18}$$

A comparison of the specific resistance at different volume fractions obtained from the Carmen-Kozeny equation (for different ξ values) and Happel Cell model are shown in Fig 2.7.

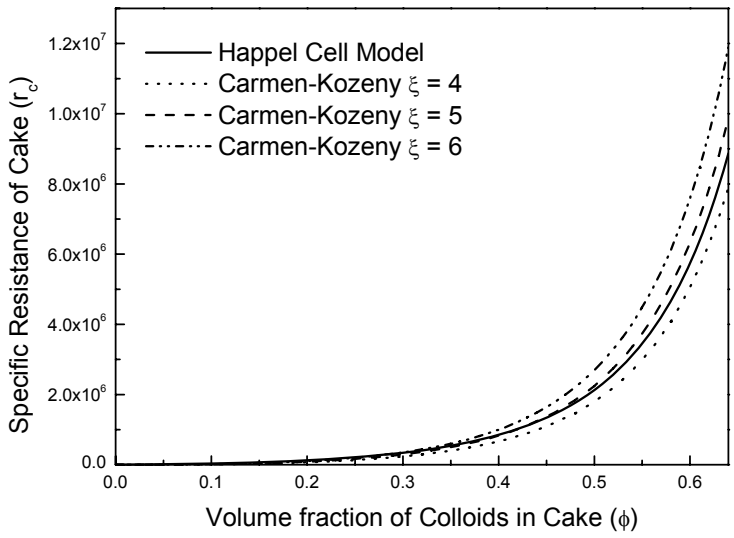

Fig 2.7: Comparison between the specific resistance from the Carmen-Kozeny equation for Kozeny constant 4, 5 and 6 and the Happel Cell model at different volume fraction of particles. A Kozeny constant of 5 provides the best fit between the Carmen-Kozeny equation and the Happel Cell model.

The Carmen-Kozeny model with a Kozeny constant of 5 provides the closest match to the Happel cell model as shown in Fig 2.7. Mathematically, the best match to the Happel cell model is achieved when a Kozeny constant of 4.8 is used.

However, both models do not consider the effects of interfacial interactions between the particles in the cake layer in their derivations. Additionally, the microscopic effects such as dilational components of the original fluid motion on the liquid properties within the pores of the cake layer (e.g. viscosity) are not accounted for (Happel and Brenner, 1991). Nevertheless, the models are still widely used with the inadequacies addressed by the inclusion of correction factors. It is evident from the models and previous discussions on porous cakes that the volume fraction of the particles is a fundamental parameter, and its

determination is pivotal to any information about these cakes. However, this proves to be quite difficult, because very often assumptions of the way particles pack are required to make a calculated guess on the volume fraction of the colloidal cake layer. Also the volume fraction may change within the cake layer so that the assumption of an average volume fraction makes the analysis more macroscopic than microscopic (Hong *et al.*, 1997). Over the years, several theoretical maximal packing structures for rigid, monodispersed particles under various assumed geometrical arrangements have been determined and are summarized in Table 2.1 (Birdi, 1997). These provide a suitable reference and guide for possible particle volume fractions in colloidal cakes. For membrane filtration applications, a maximal volume fraction of 0.64 corresponding to maximum random close packing is commonly assumed (Song 1998b).

Table 2.1: Theoretical maximum volume fractions for various particle arrangement configurations (Birdi, 1997)

Assumed Particle Arrangement	Maximum volume fraction (ϕ_{max})
Simple Cubic/Loosely packed	0.520
Minimum thermodynamically stable configuration	0.548
Hexagonally packed just touching	0.605
Random close packing	0.637
Body-centered cubic packing	0.680
Face centered cubic/Hexagonal close packing	0.740

2.4.6. Solution Chemistry and Cake Formation

Solution chemistry has a strong effect on the electrokinetic properties of the colloidal particles and hence cake formation. The feed water chemistry affects both the deposition kinetics of the colloidal particles in the membrane system and the hydraulic resistance of the deposit (Bacchin et al., 1995). It is accepted that the productivity and efficiency of membrane filtration for colloidal particles is dependent on the physico-chemical properties of the

suspension, such as its salinity and pH (Cohen and Probstein, 1986; Belfort *et al.*, 1994). These factors have a strong effect on the electrostatic double layer force, which is the dominating interparticle force in the cake layer for colloidal particles with diameters smaller than 100 nm (McDonogh *et al.*, 1992). Tadros and Mayes (1980) found that the specific resistance of the colloidal cake increased when the electrolyte concentration increased. They attributed their findings to the decreasing effective size of the colloidal particles as salt concentration increased. Similar findings were reported by Faibish *et al.* (1998) who found high cake layer porosities of up to 0.7 at low ionic strengths which decreased as feed water ionic strength increased in their filtration experiments. Colloidal fouling is also affected by the charge on the colloidal surface which can be adjusted by feed water pH (Bowen and Jenner, 1995a; Bowen and Jenner, 1995c). McDonogh *et al.* (1992) found that permeate flux from the filtration of colloidal particles increased as the surface charge on the colloidal particles increased. Studies on the effects of water chemistry on colloidal fouling have so far been qualitative. Commonly, the permeate flux, cake layer porosity or specific resistance from filtration experiments is compared under different feed water chemistry conditions. These parameters change with filtration time and usually normalization with the initial value is used for comparison between different conditions. However, such normalization methods do not reveal the extent to which feed water chemistry affects colloidal fouling and could possibly be biased (detailed in Section 3.2.2). Therefore a better normalization method, which allows quantitative evaluation of the effect of solution chemistry on colloidal fouling, is urgently required.

2.4.7 Electroviscous Phenomena in Porous Media

The electrokinetic phenomenon which arises due to the motion of liquid near a charged surface with an electrostatic double layer has important implications on the liquid flow through porous media such as colloidal cakes and membranes. When liquid is forced through a pore by applied pressure, the counter-ions in the mobile portion (diffuse layer) of the EDL

are sheared off and move together with the liquid out of the pore. This downstream movement of counter-ions through the porous body results in the build-up of potential across the porous body and is known as streaming potential. The potential difference across the porous structure induces an electrical current (due to back movement of ions) known as the conduction current in the direction opposite to the applied pressure. Since the back movement of ions will also result in the liquid molecules being pulled along, flow in the direction opposite to pressure driven flow develops. The net effect is reduced flow rate of liquid through the pores in the applied pressure direction as compared to liquid flow through the pores derived from conventional fluid mechanics without considering the presence of the EDL. It would then seem that the liquid has an apparently higher viscosity and is known as the electroviscous effect (Hunter, 2000). From the description, it is clear that electroviscous effects would depend on the ratio of the pore radius to the electrical double layer thickness. Theoretically, the electroviscous effects have been found to be pronounced only when the ratio of the pore radius (r_p) to the double layer thickness ($1/\kappa$) is in the range 1 to 3 (Bowen and Jenner, 1995b; Churaev, 2000). For larger and smaller pore radii, the electroviscous effects are negligible.

2.4.8 Compressibility of Colloidal Cakes

The compressibility of colloidal cakes is caused by the collapsing, rearrangement or compaction of particulate structures under the influence of pressure. Cake compressibility depends on the intrinsic property of the colloidal particles present in the water. It is well documented that compressibility is dependent on the colloid particle size (Tiller *et al.*, 1987; Chen *et al.*, 2002; Kim and Hoek, 2002), shape (Sharma and Lei, 1991; Cho *et al.*, 2006) and degree of aggregation (Choi and Dempsey, 2004; Park *et al.*, 2006). The material properties of the colloidal particles also significantly influences the compressibility of the cakes. Deformable particles (soft colloids) commonly exhibit high compressibility coefficient values (Hamachi and Mietton-Peuchot, 1999; Matsumoto *et al.*, 1999; Meeten, 2000). On the other hand, the rigid colloidal particles such as mineral oxides do not deform much under pressure.

Compressibility for rigid colloidal particles refers rather to closer packing and rearrangement of the colloidal particles in the cake layer under pressure. Although compactability might be more appropriate to describe the behavior for rigid colloidal particles under pressure, (Leu *et al.*, 1993) compressibility will continue to be used given its widespread acceptance.

The impact of solution chemistry on cake compressibility of colloidal particles is one area that has not been previously investigated. The structure of the colloidal cake under the coupling of the hydraulic driving pressure and the inter-particle interactions can be significantly altered by the water chemistry.

2.5 The Key Issues

Colloidal fouling is the most important form of membrane fouling and therefore its control or mitigation is critical to membrane processes. A review of the literature in this chapter showed that the properties of colloidal particles have been a subject of rigorous study for a long time and subsequently been used to understand and explain complex colloidal phenomenon. However, these fundamental principles and theories have not been widely applied in the study of colloidal fouling in membrane processes. Most of the studies on colloidal fouling or colloidal fouling framework was developed based on rigid spheres, where the colloidal interactions between the particles were almost completely neglected. As seen in this chapter, colloidal interactions can play a critical role in every facet of colloidal fouling and through correlations of these fundamental factors, a better understanding of colloidal fouling would emerge.

Approximately a decade ago, Belfort *et al.* (1994) published a definitive paper on colloidal fouling, in which they highlighted the need for quantitative understanding of interactions between particles and other colloidal materials which can be present in process streams on fouling. However, this aspect has not been fully addressed and there is still some way to go in

achieving this objective. In the meantime, there has been heightened interest with many studies focusing on the effects that solution properties can have on colloidal fouling but there is still no work which has quantitatively linked these effects to colloidal fouling (Zhu and Elimelech, 1997; Faibish *et al.*, 1998; Hwang *et al.*, 1998).

Colloidal fouling is a multifarious process where different physical and chemical phenomena partake. It is generally accepted that colloidal fouling is controlled by the interplay between permeation drag and the electrical double layer repulsion (Zhu and Elimelech, 1997; Kim and Hoek, 2002; Tarabara *et al.*, 2004). However a systematic investigation to determine how the inter-relationships or coupling between the different physicochemical conditions affect colloidal fouling has not been attempted.

It is one of the main objectives of this thesis to further apply the fundamental principles of colloidal interactions to the study of colloidal fouling in membrane processes. Special effort will be placed on the development of quantitative correlations between colloidal fouling and the key water chemistry parameters and hydraulic conditions. A better understanding of colloidal fouling in membrane processes is expected with the help of the fundamental principles and theories of colloidal interactions.

Chapter 3

The Fouling Potential of Feed Water

3.1 Introduction

Membrane fouling is recognized as the biggest obstacle in the widespread implementation of membrane processes. Unfortunately, it is a problem which cannot be totally eradicated and can only be controlled to within tolerable limits. The key issue lies with the quality of the water that is being filtered. Waters high in solute concentration, organics, nanoparticles, bacteria, proteins, etc, have a high fouling strength indicating their tendency to foul the membrane.

Quantification of fouling ensures accurate prediction of flux decline and enables the implementation of any necessary feed water pretreatment steps to optimize system performance. This will allow for cost estimations of pretreatment and membrane cleaning or replacement to be factored into process design so that efficient decisions can be made. In research, the influence of various feed water parameters on fouling can be elucidated from the determination of feed water fouling strength. This will facilitate better understanding of the fouling mechanisms so that control strategies can be designed and implemented. Two key considerations for a fouling indicator are that (1) it should be a representative gauge of fouling in the membrane, and (2) it should be universally applicable to all membrane processes. There are presently no fouling indicators that satisfy both criteria.

In this chapter, the limitations of current fouling indices, the Silt Density Index (SDI), Modified Fouling Index (MFI) and common normalization techniques to compare membrane fouling are highlighted. To address these shortcomings and satisfy the two criteria for a fouling indicator mentioned above, the *fouling potential* and the methods used to determine it

from experimental data are introduced. The effects of colloid concentration, pressure, membranes and filtration systems on the fouling potential are presented.

3.2 Background Information

3.2.1 Presently Used Fouling Indices & Limitations

Attempts to quantify the fouling tendency have received attention over the years, with the two most notable methods being the Silt Density Index (SDI) first introduced by the Du Pont company, and the Modified Fouling Index (MFI) which is an improved version developed subsequently (Schippers *et al.*, 1980). Both methods make use of standardized apparatus and procedures to obtain the fouling index of the feed water in dead end mode.

The SDI is a static test, with measurements taken at the beginning and the end of the test. It is not based on any theory and uses time as the basis for comparison. In the SDI test, a membrane of pore size 0.45μm is used. As this does not capture the majority of the foulants in aquatic environments, the extrapolation of data to UF, NF and RO membrane processes is questionable. Also there is no linear relationship between the SDI and foulant concentration in the feed water (Kremen and Tanner 1998). Interestingly, despite these fundamental problems, the SDI remains a popular method for fouling prediction in all membranes.

As the understanding of membrane fouling increased it became clear that the resistance of the foulant being deposited on the membrane surface was a function of permeate volume rather than time which was the premise of the SDI. The MFI was then developed to address this and other shortcomings of the SDI method. It was proposed that measurements be made every 30 seconds as opposed to static measurements and was derived based on cake filtration theory. However, as it was derived from the SDI, the same apparatus and operating conditions were used. To improve on this, it was recently proposed that instead of a 0.45μm pore size membrane, a UF membrane of Molecular Weight Cut-Off of 13kDa be used (Boerlage et. al

2003). The determination of the MFI and its derivatives i.e. MFI-UF, MFI-NF (Khirani *et al.*, 2006) and, possibly in the future, MFI-RO suffer from the same limitations detailed below.

Firstly, the fouling index is determined only in dead end mode. Increasingly many membrane systems are being operated in crossflow modes and the fouling index may not accurately depict the fouling in these systems which are influenced by crossflow shear-induced fouling mechanisms.

Secondly, the assumption of cake filtration as the major mechanism of colloidal fouling is an oversimplification as there might be pore constriction, adsorption and other fouling mechanisms which may dominate or coexist with cake filtration (Yiantsios *et al.*, 2005). With nanoparticles, these might get lodged in the pores of the membrane or penetrate the top matrix of the membrane. Moreover, with the development of new membranes such as asymmetric membranes there is higher chance for the more porous portion of the membrane to be filled with colloids, thereby affecting fouling determination.

Thirdly, the cake filtration theory developed as one of the filtration laws discussed in Chapter 2 assumes ideal rigid particles with no interaction forces between them. In complex water streams where different charged colloidal particles are present, their interactions might result in different membrane fouling phenomena than that observed simply due to cake filtration, such as strong interaction forces between membrane surfaces and colloidal particles. These colloidal interactions, coupled with crossflow velocity, may cause changes to colloidal cake morphology during the filtration process due to aggregation, rearrangement or binding of cake layer due to fines which cannot be accounted for by the theory (Kim and Yuan 2005). As described in Chapter 2, cake filtration is only one of many possible filtration theories and its universal application to all waters is questionable (see section 2.7.1).

Finally, both the SDI and MFI advocate the use of standardized equipment to determine the fouling index and then propose that this value be used as an indicator of fouling on other equipment with different configurations and conditions. However, membrane processes are operated using a multitude of membranes (MF, UF, NF, RO) in different configurations (flat sheet, tubular, hollow fiber, spiral wound) and modes (dead end, crossflow) and this could have strong effects on the foulant layer and fouling in the membrane process. Therefore ideally the fouling index should be determinable in any membrane process. However, the effects of the membrane configuration and mode should be discounted so that they play as limited a role as possible. Hence the fouling index should also be a normalized parameter to accurately quantify the fouling potential of feed water, irregardless of the system or mode of operation.

3.2.2 Current Normalization Techniques & Limitations

Currently the most commonly utilized normalization method is the division of permeate flux at any instant (v) with the initial or clean membrane flux (v_0). This intuitive normalization method is not based on any theoretical or well understood fouling kinetics. It can be shown that the normalization method is in fact biased towards operational conditions with the illustration below. Consider two membranes (referred to as subscript 1 and 2) of different resistance, R_0, which are used to filter exactly the same feed water at the same net driving pressure ($\Delta P = \Delta p - \Delta \pi$) where Δp and $\Delta \pi$ are the driving pressure and the osmotic pressure, respectively as shown in Fig 3.1. The increment in resistance (ΔR) due to fouling depends on the permeate flux or permeation drag exerted on the foulants, since the foulant concentration in the feed waters are identical (Belfort, 1989). Therefore the increment in resistance for membrane system 2 is higher than the increment in resistance for membrane system 1, ($\Delta R_2 > \Delta R_1$), at any time or volume of permeate generated. Based on this it follows that the ratio of

increment in resistance to membrane resistance $\left(\frac{\Delta R}{R_0}\right)$ is higher for membrane system 2 as compared to system 1 as shown in the graph of Fig 3.1.

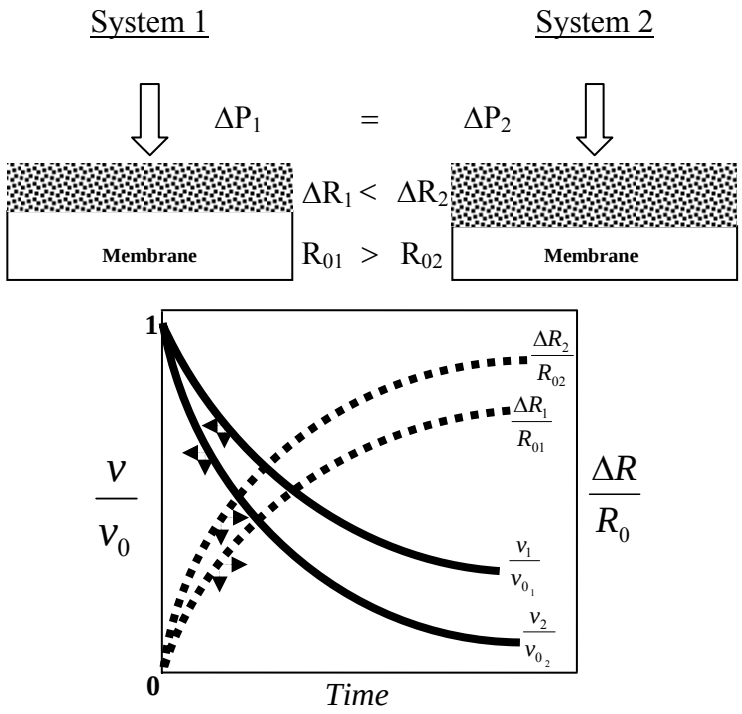

Fig 3.1: Two membranes of different resistance such that $R_{01} > R_{02}$ are operated at the same net driving pressure (ΔP) using identical feed water. The increment in resistance is higher in system 2 than in system 1 ($\Delta R_2 > \Delta R_1$) since the permeation drag on the foulants is smaller in the latter. However, the normalization by initial permeate flux will consistently show that the system containing the membrane with the higher resistance has less fouling than the other system. This is not true since the feed water is the same to both systems with the same applied pressure.

It can then be shown mathematically that the normalization method by permeate flux will constantly favour the membrane system with higher initial membrane resistance, i.e. $\left(\frac{v_1}{v_{0_1}}\right) > \left(\frac{v_2}{v_{0_2}}\right)$. This gives the impression that the fouling tendency of the feed water used on membrane system 2 is higher than that used in membrane system 1, which is not true since the feed waters are identical. This is a serious problem with the current set of normalization

methods, which requires an urgent addressing so that a better normalized indicator of fouling is developed and used.

3.3 Theoretical Development of the Fouling Potential

3.3.1 Fouling Potential as a Normalization Technique

The increment in membrane resistance due to fouling is attributed to two major factors (Song, 1998a; Song *et al.*, 2004)

(1) *permeate flux* – which encapsulates all the operational conditions such as net driving pressure, membrane resistance and crossflow velocity.

(2) *fouling potential* – properties of the feed water and the interaction of foulants in the fouling layer.

The total resistance ($R(t)$) at any time t in a membrane process can be represented mathematically in Eq. (3.1) as the summation of the membrane resistance (R_0) with the product of the fouling potential (k) and the volume of permeate generated per unit membrane area $\left(\int_0^t v.dt \right)$ where v is the permeate flux.

$$R(t) = R_0 + k\int_0^t v.dt \tag{3.1}$$

Rearranging Eq. (3.1), the fouling potential is mathematically defined in Eq. (3.2)

$$k = \frac{R(t) - R_0}{\int_0^t v.dt} \tag{3.2}$$

The fouling potential as shown in Eq. (3.2), is the increment in membrane resistance ($\Delta R = R(t) - R_0$) due to fouling per unit volume of permeate generated for a unit area of membrane surface. The method to determine the fouling potential from experimental data will be elaborated later. At this point it will be more useful to describe further how the normalization method works. Differentiating Eq. (3.1) with respect to time, the expression

$$\frac{dR(t)}{dt} = kv(t) \tag{3.3}$$

is obtained. The permeate flux can be related to the net driving pressure and total resistance from membrane transport theory as

$$v(t) = \frac{\Delta P}{R(t)} \tag{3.4}$$

Differentiating Eq. (3.4) with respect to time results in

$$\frac{dv(t)}{dt} = -\frac{\Delta P}{R^2(t)}\frac{dR(t)}{dt} \tag{3.5}$$

Substituting Eq.(3.3) into Eq.(3.5) and rearranging,

$$k = -\left(\frac{R(t)^3}{\Delta P^2}\right)\frac{dv(t)}{dt} = -\left(\frac{\Delta P}{v(t)^3}\right)\frac{dv(t)}{dt} \tag{3.6}$$

The fouling potential is therefore the rate of permeate flux decline normalized by the cubic power of permeate flux and the net driving pressure $\left(\frac{v(t)^3}{\Delta P}\right)$. This implies that the fouling potential is independent of the operating conditions such as pressure and membrane resistance.

To illustrate the effectiveness of the normalization method, we consider two membrane systems (referred to as subscript 1 and 2) filtering identical feed water but with different membrane resistance and net driving pressure. From particle transport theory, it is well known that the increment in resistance at a particular time is directly related to the foulant deposition rate when a constant specific resistance is assumed (Song, 1998a; Hoek and Elimelech, 2003). The foulant deposition rate is expressed as the product of the permeate flux (v) and the foulant concentration in the bulk (ϕ_0) as shown below

$$\frac{\Delta R_1}{\Delta R_2} = \frac{v_1\phi_{01}}{v_2\phi_{02}} \tag{3.7}$$

Since the feed water used in both systems is identical, i.e. $\phi_{01} = \phi_{02}$, Eq.(3.7) simplifies to

$$\frac{\Delta R_1}{\Delta R_2} = \frac{v_1}{v_2} = \frac{R_2 \Delta P_1}{R_1 \Delta P_2} \tag{3.8}$$

Rearranging Eq. (3.8) further simplifies to

$$(\Delta R_1) R_1 \Delta P_2 = (\Delta R_2) R_2 \Delta P_1 \tag{3.9}$$

Substituting Eq. (3.5) into Eq. (3.6), the normalized method can be expressed as,

$$k = \frac{R(\Delta R)}{\Delta P} \tag{3.10}$$

Therefore taking the ratio of the fouling potential of the feed water obtained in system 1 (k_1) to the fouling potential of the same feed water obtained in system 2 (k_2) results in

$$\frac{k_1}{k_2} = \frac{R_1 (\Delta R_1) \Delta P_2}{R_2 (\Delta R_2) \Delta P_1} \tag{3.11}$$

Taking into consideration Eq. (3.9), it is evident that the ratio of the fouling potentials is unity, indicating they are identical. This is expected since the feed water is identical and the effect of membrane resistance and net driving pressure, i.e. operational conditions, does not influence the fouling potential measurement. Therefore their effects have been normalized so that the fouling potential is dependent strictly on the feed water properties.

Besides being a normalization method, the fouling potential has additional advantages over the other fouling indicators. Unlike other fouling indicators which require the use of specific membranes or apparatus and operational conditions to determine the fouling index, the fouling potential as shown theoretically does not. Any membrane or operating conditions can be used assuming the foulant properties in the feed water do not change under those operational conditions or due to foulant interaction with the membrane. If such changes do occur, then they would be reflected through the fouling potential measure. Their effects should be included in the fouling potential measure, since the changes are due to the properties of the feed water.

Another important benefit of the fouling potential method is that it can be directly incorporated into a developed model to predict full scale RO membrane process performance (Chen KL *et al.*, 2004; Tay and Song, 2005) without the need for pilot tests. Given the progress made in understanding and modeling flow hydrodynamics in the full scale membrane process, any system performance from MF to RO in any mode or configuration can be determined if the fouling potential of the feed is known. This can be easily obtained by performing a lab scale membrane filtration test using the same membrane and feed water as in the actual full scale process.

A major advantage of the fouling potential is that it is not concerned with the type of fouling that takes place on the membrane surface. Whether it be scaling, organic adsorption, cake filtration or pore blocking etc, there will be an increase in resistance with the volume of permeate generated. This is the true definition of fouling and therefore would be a better indicator of fouling.

3.3.2 Determination of the Fouling Potential

The amount of permeate generated at any time is the most critical parameter in determining the fouling potential of feed water. Song *et al.* (2004) proposed a trial and error approach to determine the fouling potential from the filtration data. They suggested that the fouling potential could be obtained by best fitting a modified cake filtration equation incorporating the fouling potential with the experimental data. However, this approach limits the fouling potential to only cases where the cake filtration model holds. Also it requires optimizing the fouling potential by non-linear regression which is complicated. In this thesis a simpler graphical approach is recommended from which the fouling potential is obtained.

Permeate production with time from filtration experiments are mostly determined by measuring the mass of permeate generated using a mass balance at each time interval. The

mass measurements at each time interval (M_t) can be converted into volume measurement (V_t) per unit membrane area by dividing with the density of permeate (ρ) (assumed to be the density of water) and the membrane surface area (A) as shown below.

$$V_t = \frac{M_t}{\rho A} \tag{3.12}$$

The permeate flux (v) at each time interval is then determined from,

$$v = \frac{\Delta V}{\Delta t} = \frac{\Delta M}{\rho A \Delta t} \tag{3.13}$$

From the permeate flux and net driving pressure (ΔP), the total resistance (R_t) at each time interval can be obtained using Eq. (3.4). Following the definition in Eq. (3.2), the fouling potential can then be determined graphically as the slope of the line when the increment in resistance ($\Delta R_t = R_t - R_0$) at each time interval is plotted against the corresponding volume of permeate generated per unit membrane area shown in Eq. (3.12).

3.4 Experimental Section

3.4.1 Membrane Systems

The fouling potential can be determined in any simple bench scale membrane system. To investigate its effects in different membrane systems, one dead end and three crossflow membrane systems were used. The membrane systems are described below.

3.4.1.1 Crossflow Membrane Systems

A general schematic of the crossflow membrane units used are shown in Fig. 3.2. The three different crossflow systems are named 1) tubular, 2) low pressure flat sheet and 3) high pressure flat sheet for simplicity. There are minor differences in the membrane modules and pumps used in the different crossflow membrane systems which are highlighted below.

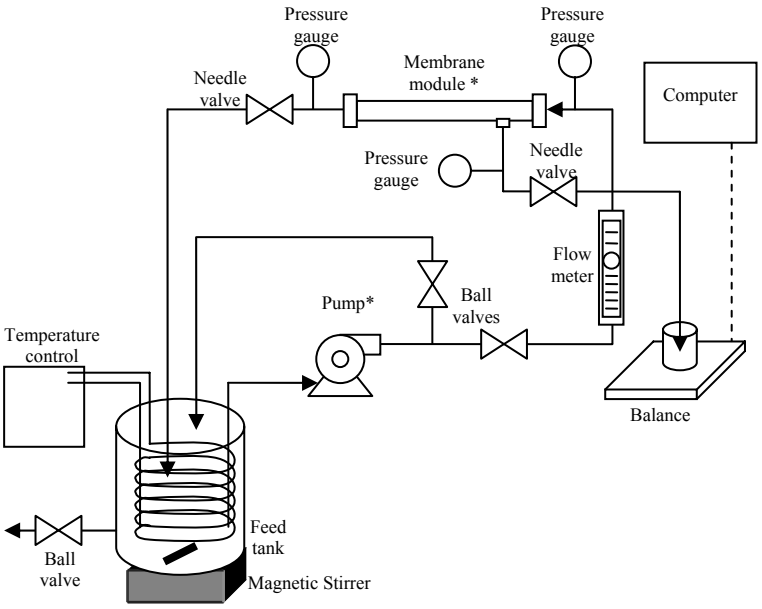

Fig 3.2: Schematic of crossflow filtration system. There are differences in the pumps and membrane modules indicated with the asterisk in the figure for the different crossflow systems as detailed in the text.

In all three systems, feed water was stored in a 50L stainless steel tank which was stirred using a magnetic stirrer. The temperature of the feed water was controlled between 24-25°C by the insertion of a stainless steel coil in the feed tank which was connected to a chiller. Feed water was circulated through the membrane module by a pump. The pumps and membranes used in the tubular, low pressure flat sheet and high pressure flat sheet systems are described in (a), (b) and (c), respectively,

(a) A centrifugal pump (CN1-13, Grundfos Pumps Corp, Olathe, KS) was used to drive feed water through a tubular ceramic membranes housed in a cylindrical stainless steel casing (USFilter Corp., Warrendale, PA). Three different ceramic membranes of varying pore sizes were used (1) zirconia 50 nm pore size membrane (T1-70-25Z, USFilter Corp., Warrendale, PA), (2) zirconia 20 nm pore size membrane (1T1-70-25Z, USFilter Corp., Warrendale, PA), and (3) titania 5000 Dalton pore size membrane (T1-70-25, USFilter Corp., Warrendale, PA). The membranes are 250 mm long and 7 mm in inner diameter and have an effective surface area of 55.0 cm^2.

Pressure and temperature limits specified by manufacturers for all the membranes are 784kPa (112psi) and 95°C, respectively.

(b) The feed water was circulated by a stainless steel rotary vane pump head (PO 3501, Fluid-o-Tech., Milano, Italy) to a stainless steel flat sheet membrane module with channel height 0.7mm which can house any suitable circular flat sheet membrane of diameter 10.5cm with an effective surface area of 86.59 cm^2. The maximum pressure that can be delivered by the pump system is 230psi.

(c) A high pressure diaphragm pump (Hydra-cell M-03, Wanner Engineering Inc., Minneapolis, MN, USA) capable of supplying up to 1000 psi was used to circulate feed water through a flat sheet membrane module identical to that described in (b).

The feed flow rate and pressures at the inlet and outlet of the membrane modules were measured with the F440 flow meter (Blue White Industries, Huntington Beach, CA) and Ametek pressure gauges (U.S. Gauge, Feasterville, PA), respectively. Permeate was collected in a glass beaker and measured by digital mass balances (PG4002-S, PG8001-S, Mettler Toledo, Greifensee, Switzerland). The data from the balance was transmitted to and stored in a computer in real time.

3.4.1.2 Dead End Membrane System

The dead end system, as shown in Fig. 3.3, consisted of a Millipore unstirred cell unit (Model No 8400, Bedford, USA) where the flat sheet membrane was housed. The effective membrane surface area is 41.8 cm^2 and the maximum pressure that can be applied to the cell is 517 kPa (75 psi). The unstirred cell unit was connected to a reservoir of volume 800 mL. Pressure was supplied by Nitrogen (N_2) gas and controlled by a pressure regulator. The pressure was monitored by Ametek pressure gauges (U.S. Gauge, Feasterville, PA). Permeate was collected in a beaker placed on a mass balance (PG8001-S, Mettler Toledo, Greifensee, Switzerland) which was directly connected to a computer that logged the mass of permeate per unit time.

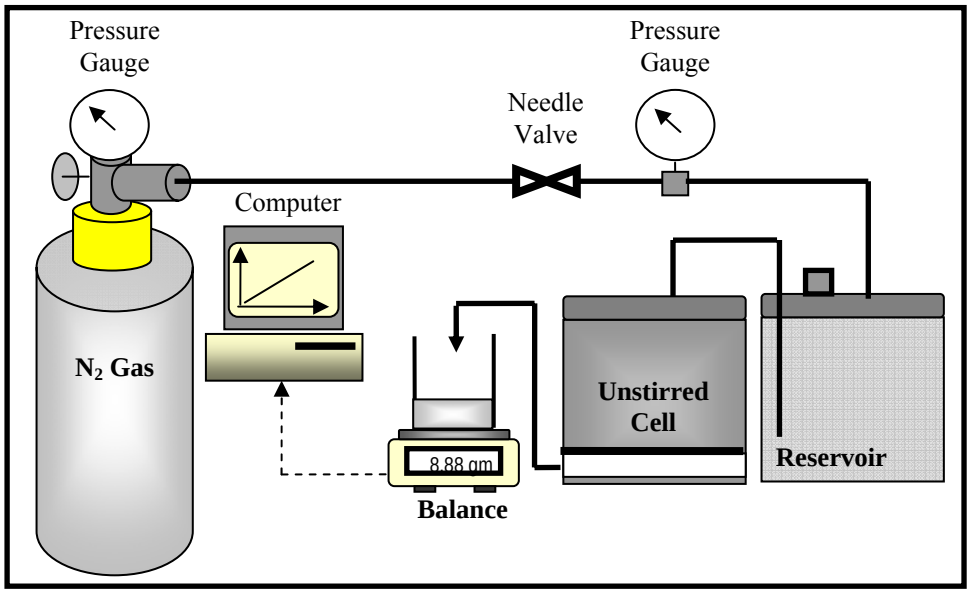

Fig 3.3 Unstirred Cell Setup for operation in Dead End Mode

3.4.2 Feed Water

Commercially available colloidal silica Snowtex 20L (ST20L), Snowtex ZL (STZL) and Snowtex 50 (ST50) (Nissan Chemical Industries, Ltd., Tokyo, Japan) were used in this study as model foulants. The colloidal particles were delivered in liquid form and used as received. The diameter of the particles as measured with 90 Plus Particle Size Analyzer (Brookhaven Instruments Corp., Holtsville, NY) was found to be 83 nm, 130 nm and 30 nm respectively. Colloidal feed water of the required concentration was prepared by dispersing the commercial colloidal suspension in deionized water of conductivity less than 1 µS/cm. The ionic strength of the feed water was adjusted using sodium chloride (Sigma-Aldrich, Gmbh, Germany).

3.5 Results and Discussion

3.5.1 Fouling Potential in Dead End and Crossflow Mode

The most common configurations of membrane filtration are the dead end and crossflow modes as shown in Fig 3.4a. As observed, the critical difference between the two modes is the

fluid flow relative to the membrane with dead end being normal to the membrane surface and crossflow, tangential to it. This difference has a characteristic effect on the foulant deposition rate in the latter stages of filtration and therefore the profile of the flux decline is as shown in Fig 3.4b. In crossflow systems, due to the shear flow by the feed, reentrainment of polarized and deposited solutes by wall shear stresses occur. Over time, equilibrium is reached between the amount of solute deposited on the membrane surface due to permeate flux and the amount being removed by the crossflow velocity. When this occurs the system reaches a steady state and the flux remains constant. In dead end mode foulant build-up continues infinitely, therefore the permeate flux continues to decline with time. The relationship between the increment in membrane resistance and the volume of permeate generated at any time is shown in Fig 3.4c. For dead end systems, the plot of increment in resistance against the volume of permeate generated per unit membrane area increases throughout the filtration time. However, for crossflow systems, the increment in membrane resistance eventually reaches a plateau.

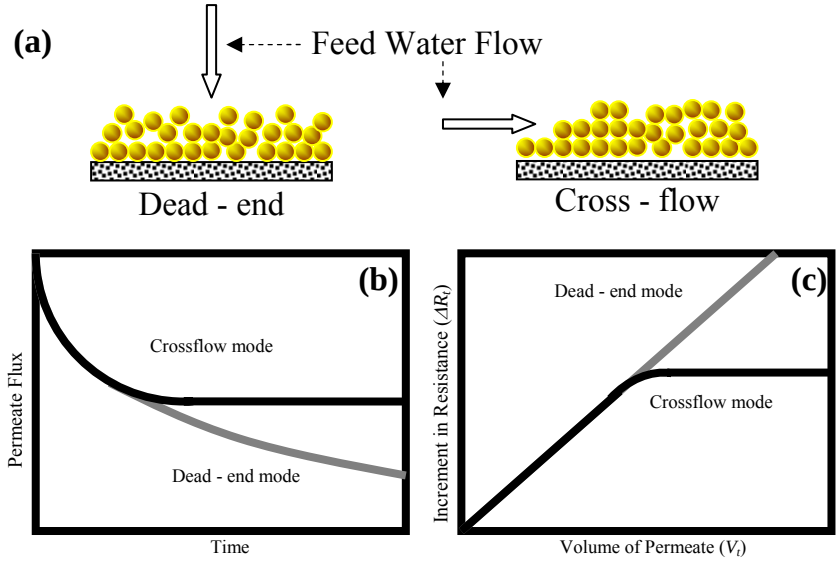

Fig. 3.4 General comparison of fouling kinetics in dead end versus crossflow filtration modes (a) schematic of dead end and crossflow modes, (b) permeate flux decline trends in both modes, and (c) relationship between increment in resistance and volume of permeate generated for both modes.

This is further illustrated with actual filtration data conducted on feed water containing ST20L colloids at concentration of 4.18×10^{-4} v/v as shown in Fig 3.5. The feed water was

filtered using the low pressure flat sheet and dead end membrane systems with a Polysulfone membrane (Osmonics, ER) of pore size 30kDa in both systems. Both experiments were conducted at the same operating pressure of 276kPa (40psi).

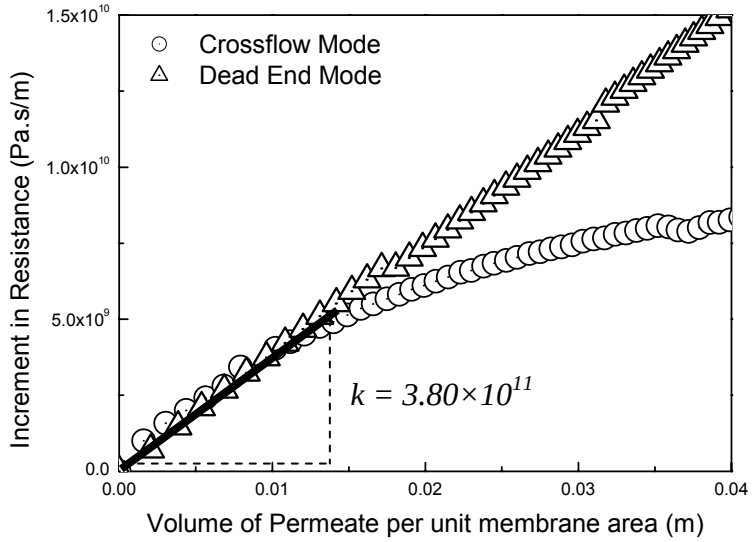

Fig. 3.5: Plot of increment in resistance per unit volume of permeate generated for equivalent feed water filtered through the same membrane in crossflow and dead end modes under the same driving pressure.

As seen from the graph, the relationship between the increment in resistance and volume of permeate per unit membrane area remains constant and almost identical for both the dead end and crossflow modes at small volumes of permeate collected. At higher volumes the relationship remains linear for the dead end mode, but decreases non-linearly reaching a plateau at higher volumes for the crossflow mode. As described in Section 3.3.2, the fouling potential obtained in both dead end and crossflow modes was 3.8×10^{11} Pa.s/m^2 determined at the initial linear portion of the graph. The mechanisms involved in the trend observed for crossflow mode are further elaborated below.

The relationship between the increment in resistance and the volume of permeate generated per unit membrane area for ST20L colloids of concentration 5.13×10^{-4} v/v, with salt concentration of 0.01M sodium chloride, filtered through a tubular zirconia membrane of pore

size 20 nm at driving pressure 276kPa (40psi) and crossflow velocity of 164cm/s as shown in Fig 3.6 is used to illustrate the dominating mechanisms in crossflow mode. The solid line in Fig. 3.6 indicates the shape of the general trend observed and the dots the experimental data.

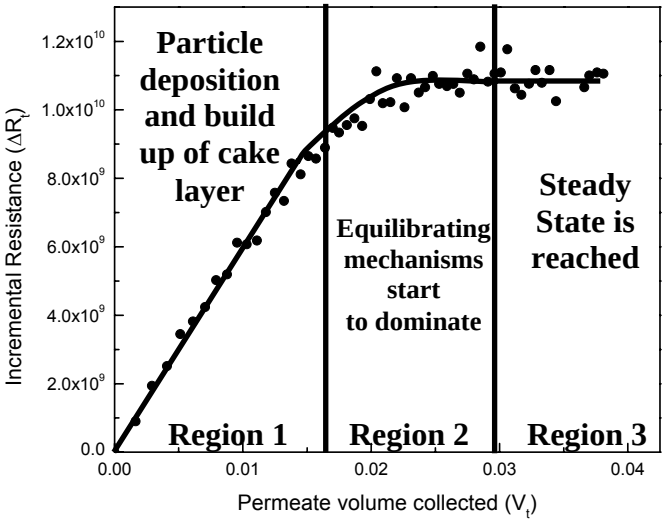

Fig 3.6: Demarcation of the dominating mechanisms in crossflow filtration of colloidal particles. Points represent the experimental data and solid line represents the general trend observed (Singh and Song, 2004).

It is noticed that the trend can be demarcated into 3 regions. The first region is the linear portion of the graph; this represents the initial deposition of the colloidal particles on the membrane surface and the build-up of the cake layer. Region 2 indicates the non linear region of the graph, where the increment in resistance per unit volume of permeate generated decreases. This corresponds to the region where equilibrating mechanisms due tangential flow begin to dominate, suggesting the transference of membrane fouling from non-equilibrium to equilibrium state (Song 1998a). Examples of such mechanisms may include particle rearrangement within the cake layer and the continual removal of excess particles deposited on the membrane surface. Region 3 represents the equilibrium region, where the increment in resistance is zero. This zone denotes that the flux has achieved steady state conditions. By definition, the fouling potential as described in Eq. (3.2) is the slope of the graph in region 1 where colloidal deposition is the predominant mechanism. Regions 2 and 3 are not suitable

for determining the fouling potential because there are other mechanisms competing with colloidal deposition.

3.5.2 Repeatability of the Fouling Potential Measure

To be an effective indicator of the tendency of the feed water to foul the membrane, the measurement has to be reproducible and its sensitivity or accuracy determined. Thirty filtration experiments were conducted on identical feed waters containing ST50 colloidal particles (diameter 30 nm) of concentration 3.62×10^{-4} v/v using the unstirred dead end system as shown in Fig 3.3. Polyethersulfone membranes of molecular weight cut off 5kDa (Biomax, Millipore, Bedford, USA) were used in all the filtration experiments. The membranes were reused at most three times, so as not to affect the results. The operational conditions, i.e. driving pressure (ΔP) 276kPa (40psi) and temperature (T) 24-25˚C, were kept constant for all filtration experiments. For each experiment the fouling potential was determined and the results are shown in Fig 3.7. The low regression coefficient for the data (R^2 = -0.05) proves that the fouling potential values determined are independent of the repeated filtration experiments conducted.

Analyzing the data statistically (Minitab® Software), the fouling potential values were found to fit a normal distribution by the Anderson-Darling normality test since the p-value = 0.845 ≥ 0.05 as shown in Fig 3.8. The mean and standard deviation of the fouling potential values are 1.73×10^{11} and 1.04×10^{10} Pa.s/m^2 respectively. The small standard deviation is indicative of the precision of the fouling potential under repeated experiments. Fouling potential values obtained are also highly sensitive given that the statistical power of the data is found to be 0.975. These findings are a good representation for the accuracy and sensitivity of the fouling potential measure to determine the fouling strength of feed water. This will permit confident elucidations of the impact of the critical physicochemical factors on colloidal fouling through measurements of the fouling potential.

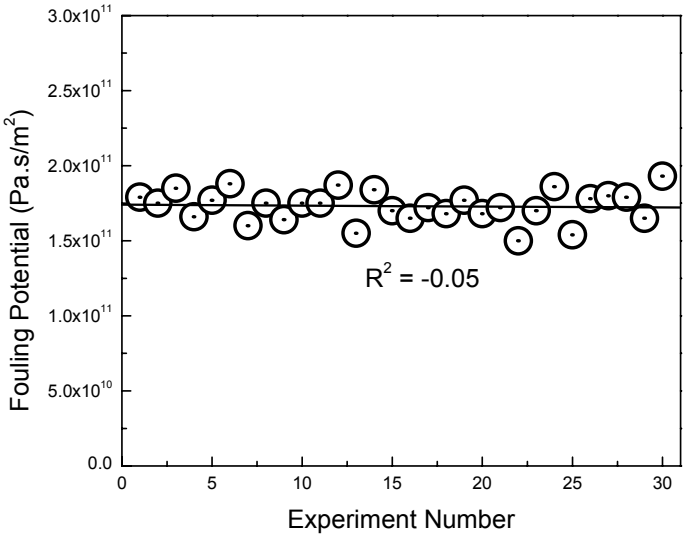

Fig. 3.7: Raw data of fouling potential obtained over 30 separate filtration experiments for feed water containing 3.62×10^{-4} (v/v) 30 nm silica particles (ST50) dispersed in deionized water using the same setup, membrane and operational conditions in all experiments.

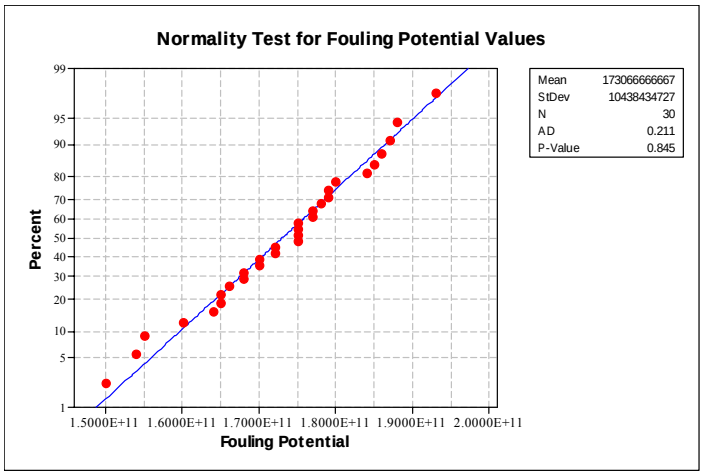

Fig. 3.8: Normal probability plot from output of Minitab® analysis for fouling potential data in Fig 3.7. The data shows that the fouling potential data collected for the identical feed water under the same operational conditions follows a normal distribution (p-value = 0.845 ≥ 0.05) with mean = 1.73×10^{11} and standard deviation = 1.04×10^{10}. This is a percentage difference of ± 6% indicating the variation in fouling potential is small and it is reproducible.

3.5.3 Influence of Colloid Concentration on the Fouling Potential

One of the most critical tests of an indicator of fouling is its relationship with the concentration of the foulants in the feed water. Theoretically, the fouling indicator should be linearly dependent on the concentration of the foulant. A critical shortcoming of the SDI method is its non-linear relationship with foulant concentration (Kremen and Tanner, 1998). Song *et al.*, (2004)* conducted filtration experiments on feed waters containing ST20L colloidal particles of differing concentrations under constant filtration conditions of driving pressure (ΔP) 276kPa (40psi), temperature (T) 24-25˚C, and crossflow velocity of 164cm/s using the tubular zirconia membrane of pore size 20 nm. The graphical approach described previously was used to analyze the experimental data and the results are presented in Fig 3.9. As seen, the fouling potential is linearly related to the concentration of colloidal particles in the feed water passing through the origin. Therefore when there are no foulants or colloidal particles in the feed water, the fouling potential is zero.

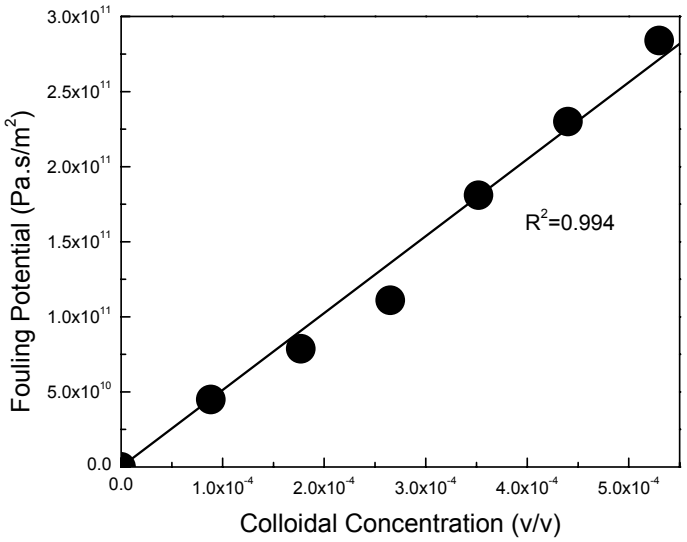

Fig. 3.9: Linear relationship between fouling potential and different concentrations of ST20L colloids in feed water. Filtration conditions employed are T = 24-25˚C, ΔP = 2.76 × 10^5 Pa, crossflow velocity = 164 cm/s. Data reanalyzed from Song *et al.*, (2004).

* Experimental and analytical work was carried out by the author of this thesis

This linear dependence is an important feature of the fouling potential, which allows meaningful assessment of the fouling capacities of different feed waters. It also overcomes a major shortcoming of the SDI method.

3.5.4 Influence of Driving Pressure on the Fouling Potential

The effect of driving pressure on the fouling potential of feed water was also investigated previously (Song *et al.*, 2004). Filtration experiments were conducted at different pressures on feed waters containing ST20L (84 nm diameter) and STZL (130 nm diameter) colloids at volume concentrations of 1.77×10^{-4} v/v and 4.06×10^{-4} v/v respectively. The experiments were all carried out using the tubular membrane system described in section 3.2 with the zirconia membrane of pore size 20 nm. The other operational conditions such as temperature (24-25°C) and crossflow velocity (164cm/s) were kept constant. The relationship between fouling potential and pressure analyzed using the graphical approach from the data of Song *et al.*, (2004) is shown in Fig 3.10.

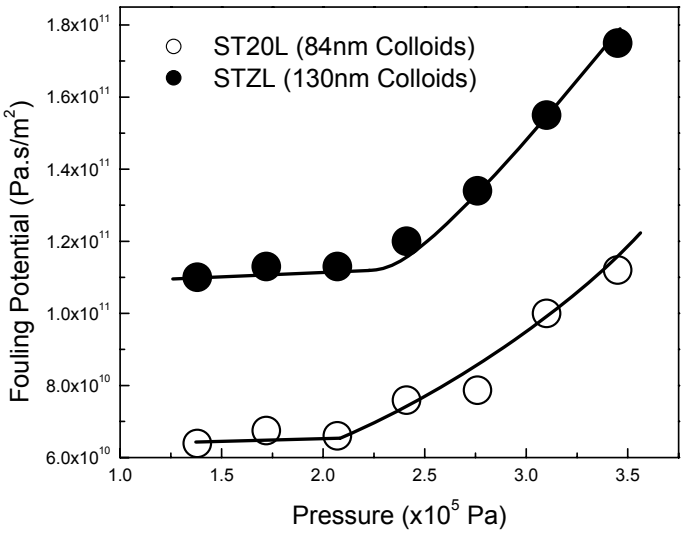

Fig. 3.10: Relationship between fouling potential and driving pressure for silica particles of diameter 84 nm (ST20L) and 130 nm diameter (STZL). The concentration for both particles is kept constant at 1.77×10^{-4} v/v and 4.06×10^{-4} v/v respectively. Filtration conditions employed are T = 24-25˚C, crossflow velocity = 164cm/s. The solid lines are to guide the eyes.

From Fig 3.10, it is observed that the fouling potential is independent of pressure at low driving pressure, but increases steeply when driving pressure increases for both types of feed water. The fouling potential is an intrinsic property of the feed water and should in principle be independent of system operational conditions. However, the independence may not be true if the fouling property of the feed water changes with the operational conditions. Such a situation arises when the fouling layer compacts or compresses under pressure, which will result in an increase in the fouling potential with pressure as observed at higher pressures for both colloidal feed waters. The compressibility behavior of the cake is discussed in greater detail in Chapter 6. It becomes apparent then that permeation drag or permeate flux velocity rather than driving pressure might be a more representative controlling parameter to compare fouling potential in different membrane systems.

3.5.5 The Fouling Potential of Identical Feed Waters in Different Membrane Systems

The effect of utilizing membranes of different materials and pore sizes on the fouling potential was investigated while keeping the feed water identical. Since driving pressure, which translates to permeation flux, has an effect on the compressibility of the particles as found in the previous section, experiments were conducted at the same initial permeate flux (v_0) instead. Therefore although the pressure and membrane resistance were different for each membrane and system, the initial permeate flux (v_0) was controlled at 2.50×10^{-5} m/s. The variation of fouling potential against the different membranes and systems were tested for four feed waters of composition a) colloid concentration = 4.89×10^{-4} v/v, b) colloid concentration = 9.73×10^{-4} v/v, c) colloid concentration = 4.89×10^{-4} v/v and NaCl concentration = 0.01M, and d) colloid concentration = 4.89×10^{-4} v/v and NaCl concentration = 0.05M and the results are as shown in Fig 3.11. In all experiments ST20L colloids were used and feed water temperature was controlled at 24-25°C. The membrane systems and membranes used, and their properties are summarized in Table 3.1.

Table 3.1: Summary of the membranes used in the fouling experiments.

Membrane Type	Membrane Module	Membrane/ (Manufacturer)	Pore Size/Rejection Size	Resistance of Membrane (Pa.s/m)
1	Tubular	Tubular Zirconia ceramic UF membrane/ (US Filters)	50 nm	9.73×10^8
2	Low Pressure Flat Sheet	Polysulfone UF (ER) membrane /(Osmonics)	30 000 Daltons	1.47×10^9
3	Tubular	Tubular Zirconia ceramic UF membrane/ (US Filters)	20 nm	2.30×10^9
4	Tubular	Tubular Titania, ceramic UF membrane/ (US Filters)	5000 Daltons	5.00×10^9
5	High Pressure Flat Sheet	Thin Film, NF (DL) membrane /(Osmonics)	96% $MgSO_4$	3.94×10^{10}
6	High Pressure Flat Sheet	Thin Film UF (GH) membrane /(Osmonics)	1000 Daltons	6.03×10^{10}
7	Dead End	Polyethersulfone UF (Biomax) membrane / (Millipore)	30 000 Daltons	9.60×10^8

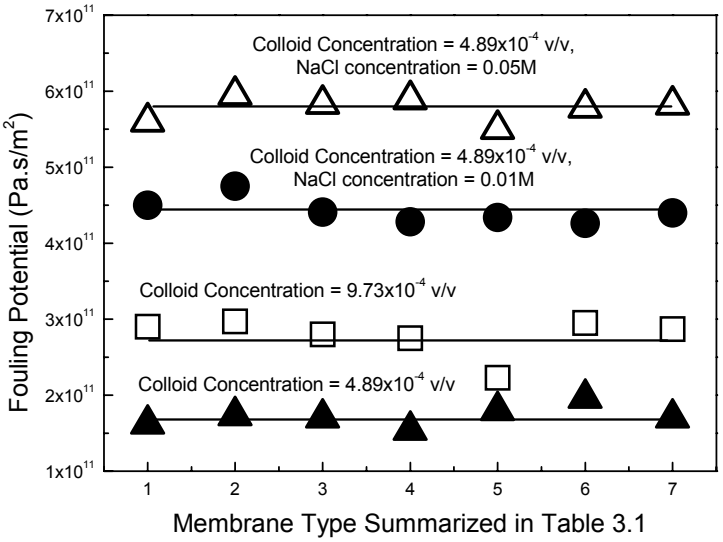

Fig. 3.11: Variation of fouling potential for four different feed water compositions filtered in various membranes and membrane systems, whose properties are summarized in Table 3.1. The horizontal solid lines indicate that the fouling potentials are independent of membrane type used.

From Fig 3.11, it is observed that the fouling potential is independent of the membrane and the membrane module configuration used. Instead it is dependent strictly on the feed water properties. This shows that the fouling potential measurement method can be used as a suitable universal indicator of colloidal fouling in different systems.

3.6 Summary

In this chapter, the fouling potential and the methods to determine it in both dead end and crossflow membrane systems were introduced. Emphasis was placed on the determination of fouling potential in crossflow membrane systems which are widely used and for which there is no current indicator of fouling. The mechanisms dominating the determination of the fouling potential in crossflow membrane systems were delineated. Preliminary tests on feed waters containing colloidal particles showed that the fouling potential was linearly related to the colloid concentration. This linearity is a fundamental requirement for any fouling indicator. It was also shown that the driving pressure had an effect on fouling potential which was greater at higher pressures. This indicated that there was a change to the colloidal foulant layer properties due to pressure. This aspect will be discussed in detail in Chapter 6. Therefore instead of pressure, a constant permeate flux or permeation drag force was used when the effects of different membranes and module configurations on the fouling potential were investigated. It was found that the fouling potential remained relatively constant for identical feed waters when different membranes and systems were used. This implied that the fouling potential was independent of the membranes and membrane systems and was confirmed using feed waters of different compositions. The findings clearly demonstrate that the fouling potential is (a) strongly dependent on the feed water properties, (b) is a sensitive measure of fouling and (c) a universal indicator which can be used for different membranes and systems. Therefore, it is in our opinion an ideal parameter for evaluating the effects of physicochemical parameters on colloidal fouling.

Chapter 4

Colloidal Fouling and Ionic Strength

4.1 Introduction

Membrane fouling, an inevitable phenomenon in membrane processes, results in inefficient membrane performance and reduces the economic viability of the process (Belfort *et al.,* 1994; Chen JC *et al.,* 2004). Although membrane fouling is affected by the operating conditions such as pressure and crossflow rate, the more fundamental and vital reason for membrane fouling lies in the properties of the feed water, i.e., the fouling potential of the feed water (Faibish and Cohen, 2001; Taniguchi *et al*., 2003; Belfer *et al*., 2004). Awareness of the impact of feed water properties on the fouling strength then forms the basis for an effective strategy in membrane fouling control and mitigation. Ionic strength is a primary feed water property whose impact on colloidal fouling has not been quantitatively evaluated.

Ionic strength, which is dependent on the valence and concentration of the ions in the feed water, influences the electrokinetic and interfacial properties of the colloids. This has a significant effect on the interaction between the colloidal particles and the fouling potential of the feed water. The effect of ionic strength on fouling can be directly observed by performing filtration experiments (Bowen and Jenner, 1995a; Tadros and Mayes, 1980; Chang *et al*., 1995; Elzo *et al*., 1998; Faibish *et al*., 1998). This qualitative phenomenological observation however may not assist much in understanding the intrinsic effect of ionic strength on colloidal fouling. A quantitative relationship between the defined fouling potential of feed water in Chapter 3 and a fundamental parameter of colloidal particles accounting for ionic strength effect is preferred, with which the well established theories, such as DLVO and EDL, can be used to explain the phenomenon observed from filtration experiments. The fouling potential will then serve as a bridge from which these theories can be applied to explain the

experimental results. This will inadvertently allow for better understanding and analysis of the experimental results.

In this chapter, the effects of different concentrations of monovalent NaCl on the fouling potential of colloidal silica particles at different concentrations were determined. A model to describe the effects of colloid concentration and NaCl concentration on the fouling potential was proposed and tested. Following this, the fouling potential of the colloidal feed water was determined with addition of different monovalent salts. The purpose was to investigate if salts of different counter-ion species but the same ionic strength had any effect on colloidal fouling. To wrap up the chapter, the effect of divalent salt, calcium chloride ($CaCl_2$), on the fouling potential was examined. The relationship between the critical coagulation concentration (C.C.C) of calcium chloride on the maximum fouling potential was also examined.

4.2 Experimental Section

4.2.1 Synthetic Feed Water

Commercially available colloidal silica particles, Snowtex 20L (ST20L) (Nissan Chemical Industries, Ltd., Tokyo, Japan), were used in this study as model foulants. The diameter of the colloidal particles as measured with the 90 Plus Particle Size Analyzer (Brookhaven Instruments Corp., Holtsville, NY) was confirmed to be 83 nm as highlighted in Chapter 3. Colloidal suspensions of the required concentrations were prepared in a 50L tank by dosing the concentrated commercial colloidal suspension to deionized water of conductivity less than 1 μS/cm. The pH value was measured to be 9.3 ± 0.3 for all feed waters used in this study. Reagent grade chloride salts of lithium, sodium, potassium, cesium, and calcium were used to adjust the ionic strength of the colloidal feed water. Conductivity (LF 538, Weilheim, Germany) and electrophoretic mobilities (Brookhaven Instruments Corp., Holtsville, NY) of

the colloidal particles in the feed water were measured to ensure no fluctuations occurred during the fouling experiments.

4.2.2 Filtration Protocol

All filtration experiments in this chapter were conducted in the tubular crossflow membrane system shown in Fig 3.2 using a tubular zirconia membrane of pore size 20 nm. At the start of the experiment, the required feed flow rate and driving pressure of the system were first obtained with deionized water. When the required flow rate and pressure were established, permeate was collected and weighed to determine the clean membrane resistance. After about 200mL of permeate was collected, the permeate valve was closed and permeate collected was poured back into the feed tank. The system was then equilibrated by running particle-free salt solution of the required ionic strength for approximately 2 hours. This was to ensure sufficient time for the permeate water flux to stabilize. Prior to initiating the fouling experiments, the permeate valve was opened and permeate collected was monitored at preset time intervals, which was 5s for most experiments conducted in this chapter. After about 100mL of particle-free permeate was collected, the required concentration of colloidal silica particles were added to the feed tank with constant mixing. Permeate collection was continuously monitored for approximately 30min. At the end of each experiment, the membrane was flushed with deionized water at a flow rate of 1.8 L/min for at least 3 hours. It was noted that at least 95% of the new membrane permeate flux was restored by this cleaning procedure. Chemical cleaning was carried out once a week as specified by the manufacturer.

4.2.3 Batch Aggregation Tests

Independent batch aggregation tests were conducted to determine the C.C.C of salt for different colloid concentrations. A number of 1L samples of the required colloidal concentration were adjusted to different ionic strengths by adding salt. After gentle mixing with a magnetic stirrer for approximately 15 minutes at 40 rpm, the samples were then

measured for their turbidity (Hach 2100N Turbidimeter Loveland, Colorodo, USA). The ionic strength that caused a sudden increase in turbidity was determined as the C.C.C. of salt for the tested colloidal concentration.

4.3 Results and Discussion

4.3.1 Dependence of Colloidal Fouling Potential on Ionic Strength

Fouling experiments were conducted for seven different feed waters at ionic strengths of 0.001M, 0.005M, 0.01M, 0.02M, 0.03M, 0.1M, and 0.2M. The feed concentration of the ST20L colloidal particles was fixed at 4.28×10^{-4} v/v and all other water chemistry conditions were kept constant. Experiments were controlled under a driving pressure of 276kPa (40psi) and crossflow velocity of 164 cm/s. It was found based on turbidity and particle size analysis that even at 0.2M NaCl, the colloids were not coagulated. This phenomena is attributed to the silanol and silicic acid ($Si(OH)_4$) groups that form a gel layer (also referred to as hairy layer) on the particle surface, adding monotonic short range (steric-like) repulsion to the double layer repulsion (Israelachvili, 1992; Vigil *et al*., 1994). Initial permeate flux values for the feed waters with different ionic strengths were found to be similar. This is expected as the electroviscous effects are negligible near the point of zero charge of the membrane surface which is close to the pH of the deionized water. Water fouling potentials determined for the abovementioned experimental conditions are presented in Table 4.1.

Table 4.1: Fouling potentials of feed waters containing ST20L colloidal particles at feed concentration of 4.28×10^{-4} v/v for different ionic strengths.

Ionic Strength (M)	0.001	0.005	0.01	0.02	0.03	0.1	0.2
Fouling potential ($\times10^{11}$ Pa·s/m^2)	2.25	3.72	4.52	5.50	5.89	6.85	7.32

It can be seen that ionic strength has a significant effect on colloidal fouling. For example, a 100-fold increase in ionic strength from 0.001M to 0.1M results in an increase in fouling potential of three times.

The trend of increasing fouling potential with increase in ionic strength is more discernible when depicted in Fig. 4.1. The relationship found suggests a maximum limit that the fouling potential of feed water can achieve when the ionic strength is increased. It is predicted that further increase of ionic strength near this limit could have minimal effects on the fouling potential of the feed water. If the C.C.C is reached, it could result in a porous cake layer and therefore a reduction of fouling potential. This aspect will be discussed in more detail in the subsequent sections.

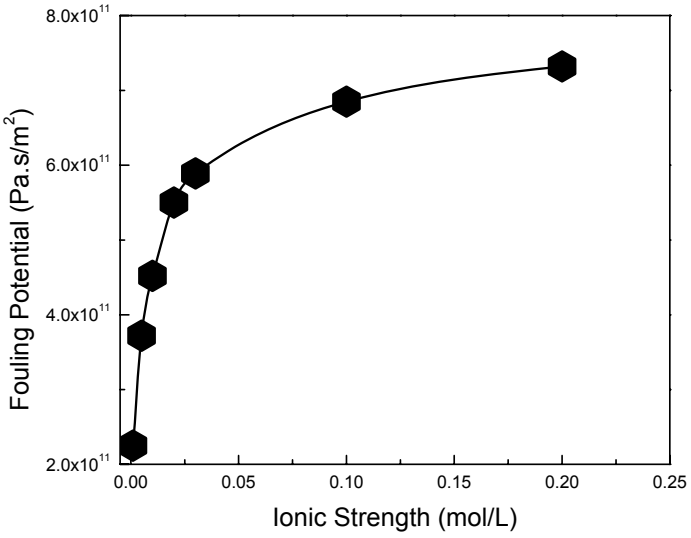

Fig. 4.1: Relationship between fouling potential and ionic strength for feed water containing ST20L colloidal particles at concentration of 4.28×10^{-4} v/v. T = 24-25 °C, $\Delta P = 2.76\times10^{5}$ Pa (40 psi), crossflow velocity = 164 cm/s. The solid line is to guide the eyes.

It is also observed that the fouling potential of the feed water increases non-linearly with the ionic strength of the water. The increase is attributed to the compression of the double layer around the colloids as ionic strength increases. This well accepted theory has been reported to be true for particles larger than 50 nm (Harding, 1971). The effect of ionic strength on the double layer thickness from Eq. (2.4) is expressed by:

$$\frac{1}{\kappa} = \sqrt{\frac{\varepsilon_0 \varepsilon_r k_B T}{2 \times 10^3 e^2 N_A I}} \tag{4.1}$$

κ is referred to as the Debye-Huckel parameter ($1/\kappa$ is the Debye-Huckel screening length traditionally called the double layer thickness), I (mol/L) the ionic strength of the feed water, and all other parameters as defined previously in Chapter 2. Strictly speaking, $1/\kappa$ is the distance away from the colloid surface where the potential drops to a value of 37% (1/e) of the surface potential. Therefore the Debye-Huckel screening length is sometimes referred to as a yardstick for characterizing the solution properties of charged particles that differ in ionic strengths. More importantly, Eq. (4.1) demonstrates that the Debye-Huckel screening length parameter, like ionic strength, is a water parameter as it is determined solely by the liquid properties, e.g. valence, concentration of salts and the dielectric properties of the liquid. Therefore, it would be an apt parameter to relate to the fouling potential, which is a measurement of the feed water characteristics.

4.3.2 Linearized Relationship between Ionic Strength and Fouling Potential

A strong linear relationship with correlation coefficient (R^2) of 0.99 is observed when the fouling potential is plotted against the natural logarithm of the ionic strength as shown in Fig. 4.2. Although the fouling potential measurement is applicable to both salt rejecting and non-salt rejecting membranes, it should be pointed out that additional phenomena such as cake enhanced osmotic pressure (Hoek and Elimelech, 2003) in salt rejecting membranes could affect the linear relationship. From the relationship expressed in Eq. (4.1), the fouling potential can also be linearly related with the natural logarithmic of Debye's screening length ($\ln(1/\kappa)$). The relationship suggests that the colloidal particles were operating in the low surface potential and Debye-Huckel approximated regime of screened electrostatic interactions. The term $\ln(1/\kappa)$ is a representative parameter of double layer effects and will be referred to as the double layer thickness for simplicity.

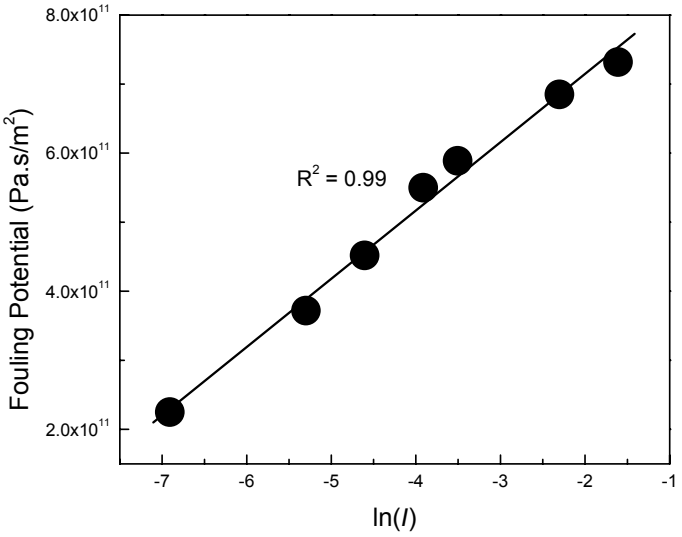

Fig. 4.2: Linear relationship between fouling potential and ionic strength parameter ln(*I*). *T* = 24-25 °C, $\Delta P = 2.76\times10^5$ (40 psi), crossflow velocity = 164 cm/s.

The relationship between fouling potential and either ln(*I*) or ln(1/κ)) may be useful and advantageous, depending on the situation and the preference of the user. For the purpose of this chapter, because of the direct reference of the Debye-Huckel parameter in many established theories in colloid chemistry like DLVO and EDL, it will be useful to limit discussions to only the linearized relationship between fouling potential and Debye-Huckel's screening length unless stated otherwise. The linear relationship found is extremely interesting as it shows for the first time a membrane fouling measurement that is directly related to the ionic strength of the feed water.

4.3.3 Effect of Colloid Concentration on the Linearized Relationship

Having established in the previous section the relationship between fouling potential and the double layer thickness, the effects of varying colloidal concentrations on the relationship are investigated in this section. Fouling experiments were conducted at four ionic strengths (0.005M, 0.01M, 0.02M and 0.03M) for three different feed concentrations of ST20L colloidal particles (1.08×10^{-4}, 2.65×10^{-4} and 5.13×10^{-4} v/v) at driving pressure of 276kPa

(40psi) and 164cm/s crossflow velocity. The fouling potentials of the feed water under the 12 different conditions were determined as previously described and are listed in Table 4.2.

Table 4.2: Fouling potentials × 10^{11} Pa.s/m^2 of feed waters with ST20L colloids at various concentrations and ionic strengths

Colloidal Concentration (× 10^{-4} v/v)	Ionic Strength (mM)			
	5	10	20	30
1.08	0.91	1.11	1.43	1.54
2.65	2.44	2.82	3.45	3.60
5.13	4.74	6.00	6.93	7.32

The fouling potential is plotted against the double layer thickness for each feed concentration in Fig. 4.3 and good linear correlations are found between the fouling potential and the double layer thickness at each feed concentration.

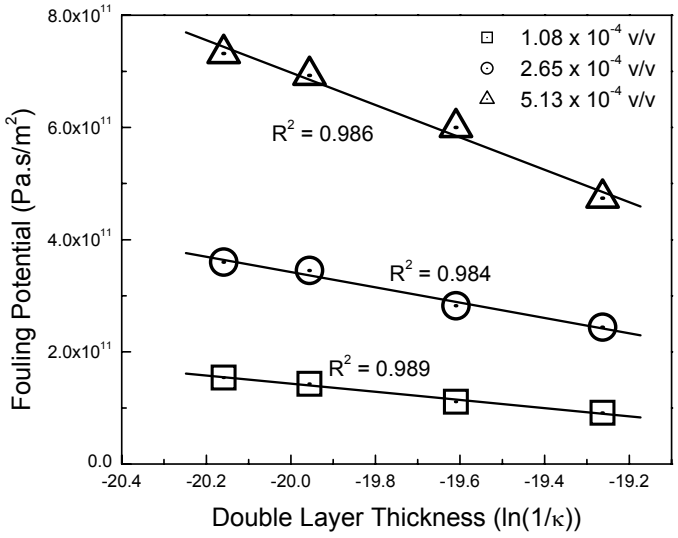

Fig. 4.3: Linear relationship between fouling potential and double layer thickness (ln(1/κ)) for feed waters containing different concentrations of ST20L colloidal particles as shown in the figure. T = 24-25°C, ΔP = 276kPa (40psi), crossflow velocity = 164 cm/s.

This further verifies the previous finding and confirms that the linear relationship between fouling potential and double layer thickness is valid for different colloidal concentrations. It is also noted from Fig. 4.3 that the slope of the lines increases (gets steeper) as the colloid

concentration increases. This implies that the rate of increase in fouling potential of the feed water per unit decrease in double layer thickness is higher for higher colloidal concentrations. The reason for this is because with higher colloid concentration, more colloidal particles would deposit on the membrane surface per unit permeate produced.

An alternative presentation of the data would be to express the fouling potential as a function of feed concentration at varying ionic strengths as in Fig. 4.4.

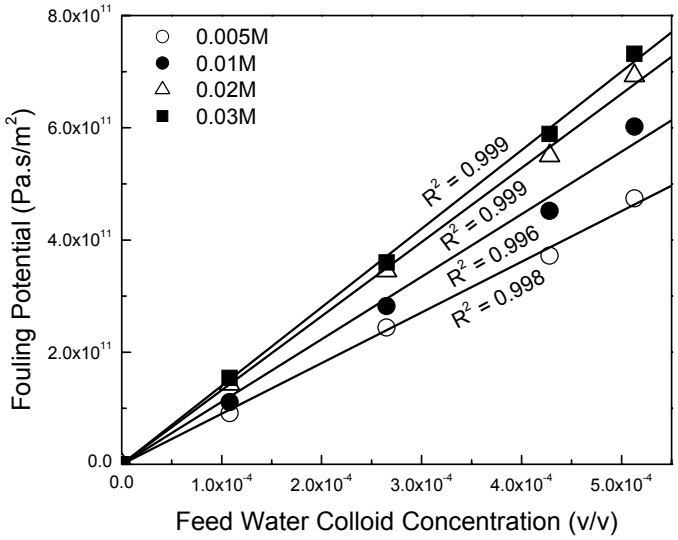

Fig 4.4: Linear relationship between fouling potential and feed water colloid concentration at increasing ionic strengths (mol/L) of a) 0.005, b) 0.01, c) 0.02, d) 0.03. T = 24-25 °C, ΔP = 276kPa (40psi), crossflow velocity = 164 cm/s.

Similar to chapter 3, Fig. 4.4 demonstrates the fouling potential to be linearly related to the feed colloid concentration. The linear correlation coefficients obtained for all lines are greater than 0.99**.** While this observation may seem foreseeable, it cements with experimental evidence that the fouling potential can reliably capture the propensity of the feed water to foul the membrane.

4.3.4 Bilinear Model

Based upon the linear relationships obtained between a) fouling potential and double layer thickness, b) fouling potential and colloid concentration in the feed water as found in the previous sections, a bilinear model is proposed in this section as expressed below to describe the dual effects of ionic strength and feed concentration on the fouling potential:

$$k = k_s \phi_b \tag{4.2}$$

Where k_s is the specific fouling potential which is defined as the fouling potential per unit volume fraction of colloids, and ϕ_b is the volume fraction of colloids present in the feed water. In writing Eq. (4.2), it is assumed that the two parameters k_s and ϕ_b are independent. This is largely true under normal conditions and for rigid i.e. non-deformable and stable colloidal foulants. Taking the derivative of Eq. (4.2) with respect to colloid concentration results in

$$\frac{dk}{d\phi_b} = k_s \tag{4.3}$$

Eq. (4.3) can be taken as the operational definition of the specific fouling potential, which is the rate of change of fouling potential per unit change of colloidal foulant concentration in the feed water. Therefore the specific fouling potential is simply the gradient of the relationship between the fouling potential and the colloidal concentration in the feed water.

The specific fouling potentials obtained from Fig 4.4 under varying salt concentrations are shown in Table 4.3. It can be seen that the specific fouling potential increases with ionic strength of the feed water. The exact effect of ionic strength on specific fouling potential can be determined by plotting it against the double layer thickness as shown in Fig. 4.5. A highly linear relationship with linear regression coefficient of R^2 = 0.997 is noted between the specific fouling potential and the double layer thickness.

Table 4.3: Specific fouling potential at different ionic strength

Ionic Strength (mM)	5	10	20	30
Specific fouling potential $k_s = \frac{dk}{d\phi_b}$ (× 10^{14} Pa.s/m^2)	9.10	11.15	13.21	14.00

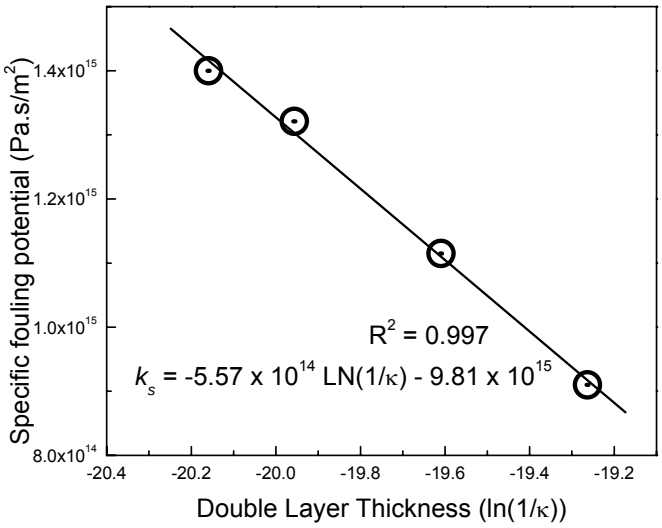

Fig. 4.5: Linear relationship between specific fouling potential (k_s) and parameter for double layer thickness (ln(1/κ))

Substituting the equation relating k_s to the double layer thickness into Eq. 4.3, the bilinear model is described by:

$$k = \left(-5.57\times10^{14}\ln(1/\kappa) - 9.81\times10^{15}\right)\phi_b \tag{4.4}$$

Similarly, by plotting k_s versus ln(I) a relationship can be formed between the fouling potential, the colloidal concentration and ln(I) given in terms of the bilinear model as:

$$k = \left(2.78\times10^{14}\ln(I) + 2.39\times10^{15}\right)\phi_b \tag{4.5}$$

These two equations relate the fouling potential to the colloidal concentration and ionic strength of the feed water. It is appropriate to point out at this juncture that the linear relationship and exact form shown above is valid only for the particle size and membrane used in this study. The influence of ionic strength for larger colloidal particles is diminished

and therefore will not significantly affect the fouling potential. In addition salt rejecting membranes would increase the salt concentration near the membrane surface significantly, which could have an effect on the relationship obtained. Nevertheless, the quantitative relationship shown above is very useful because it allows an estimate of the fouling potential of feed water with simple knowledge of colloid concentration and ionic strength, both of which can be determined easily. Although the practical application of the model is limited, it does provide a useful rule of thumb for evaluating the fouling potential of feed waters differing in these quantities. Analyzing the model further, it can be shown that when the ionic strength is increased ten-fold for a constant feed concentration, it has approximately the same effect on membrane fouling as increasing the colloidal foulant concentration by a factor of two under constant water chemistry and operating conditions. This underscores the importance of ionic strength on colloidal fouling in membrane processes.

4.3.5 Testing the Bilinear Relationship

The fouling potentials calculated with the model are compared to the ones obtained from the experimental data in Fig 4.6. From the graph it can be seen that the model fits the experimentally determined fouling potential values accurately within the range of colloid concentration and ionic strength tested. In addition to this, filtration experiments were conducted at arbitrary ionic strengths and colloid concentrations using both sodium chloride (NaCl) and potassium chloride (KCl) as electrolytes. The fouling potentials determined from the experimental data (k_{exp}) and the predicted values from the bilinear model (k_{mod}) are shown in Table 4.4.

It is deduced that the bilinear model is able to accurately predict within ±5% the fouling potential of the feed water for sodium chloride (NaCl) and within ±10% for potassium chloride (KCl). These percentages are well within experimental errors.

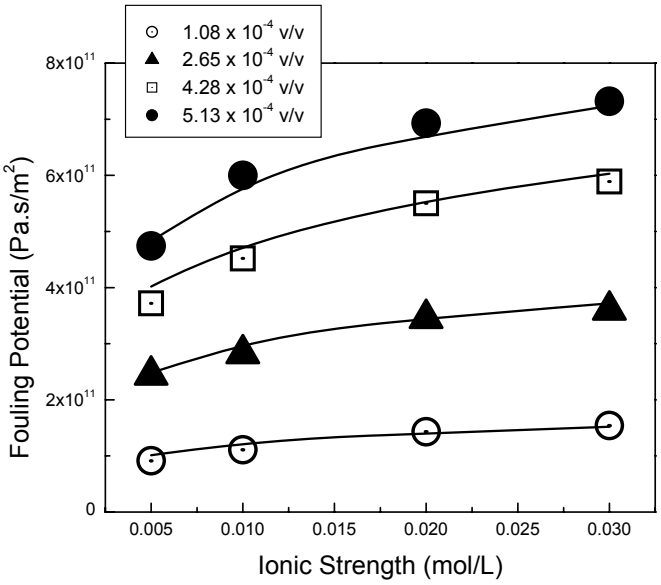

Fig 4.6: Fit of experimentally determined fouling potential values (data points) against bilinear model predicted fouling potential (solid lines) for feed concentrations of a) 1.08×10^{-4} v/v b) 2.65×10^{-4} v/v c) 4.28×10^{-4} v/v d) 5.13×10^{-4} v/v.

Table 4.4: Experimental and calculated fouling potentials of ST20L colloidal suspensions at varying concentrations and ionic strengths adjusted using NaCl and KCl

Salt	Ionic Strength (mM)	Colloid concentration ($\times 10^{-4}$ v/v)	k_{exp} ($\times 10^{11}$ Pa.s/m^2)	k_{mod} ($\times 10^{11}$ Pa.s/m^2)	Percentage Difference (%)
NaCl	25.0	2.65	3.50	3.60	2.8
	50.0	1.08	1.68	1.66	-1.2
	50.0	2.65	4.07	4.08	0.2
	200.0	5.13	10.1	9.98	-1.3
KCl	1.0	5.13	2.82	2.67	-5.3
	10.0	5.13	5.38	5.77	7.2
	20.0	4.28	5.61	5.58	-0.5
	100.0	4.28	6.99	7.39	5.7

The preliminary checks presented here suggest that the bilinear model is able to predict the fouling potential for colloidal suspensions containing monovalent electrolytes. However, this aspect would have to be further investigated with more monovalent electrolytes.

4.3.6 Effect of Li, Na, K and Cs Ions on the Fouling Potential

In this section, the effect of 4 monovalent chlorides of alkali metals, LiCl, CsCl, KCl and NaCl, on the fouling potential of feed waters with constant colloidal concentration are studied. The purpose is to examine quantitatively if different ions of the same valence and concentration exert an equivalent effect on colloidal fouling under identical conditions.

ST20L colloidal particles at feed water concentration of 5.13×10^{-4} v/v were used in the fouling experiments. The ionic strength was adjusted to 0.0005 M, 0.005 M, 0.02 M, 0.03 M, and 0.1 M, respectively, by adding the required amounts of the metal chloride being tested. All experiments were conducted under constant applied pressure (ΔP) of 276kPa (40psi) and crossflow velocity of 164cm/s. A plot of fouling potentials against ionic strength for the various salts is presented in Fig 4.7.

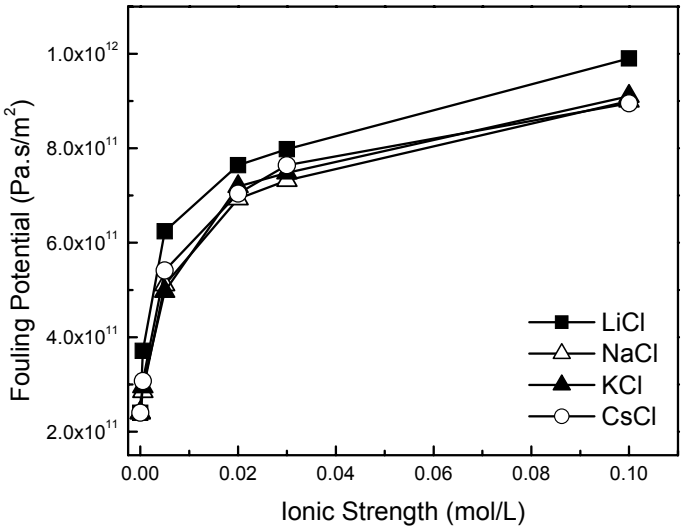

Fig 4.7: Fouling potential for feed waters at varying ionic strengths adjusted using monovalent LiCl, NaCl, KCl and CsCl salts. Colloid concentration in feed water = 5.13×10^{-4} v/v, ΔP = 276kPa (40psi), crossflow velocity = 164 cm/s.

From the plot, the fouling potentials obtained at the same ionic strength are approximately identical for NaCl, KCl and CsCl. The differences between the fouling potential values as shown in Table 4.5 are within ± 5% of each other for the 3 salts, well within the experimental

tolerance. This suggests that the fouling potential is insensitive to the type of salts and generically affected by ionic strength.

Table 4.5: Fouling potentials × 10^{11} Pa.s/m^2 under varying ionic strength for monovalent salts*

Salt	Ionic Strength (mM)				
	0.5	5.0	20.0	30.0	100.0
LiCl	3.71	6.24	7.64	7.98	9.90
NaCl	2.85	5.11	6.93	7.32	9.00
KCl	2.95	4.97	7.19	7.48	9.10
CsCl	3.07	5.41	7.04	7.64	8.95

* Colloidal concentration is 5.13 × 10^{-4} (v/v).

Second, the fouling potentials due to the addition of LiCl are constantly higher, albeit not by much, as shown in Table 4.5 compared with the other salts. It was previously reported that the adsorption behaviour of the alkali metals from lithium to cesium on colloidal silica differ by less than 20% (Abendroth, 1970). The results obtained for the conditions tested seem to support the claim, since the fouling potential values for all ions at the same ionic strength are less than approximately 25%. It should be pointed out that although the fouling potential is not a measure for adsorption on the silica surface, it is qualitatively related to it, since increased adsorption of alkali metals affects the interaction and packing of the colloids in the cake layer and hence the fouling potential. However, this does not account for the observation that only lithium salt shows a significantly higher fouling potential.

A more consolidated reason for the increase in fouling potential observed with lithium addition is likely due to the unique effect the lithium ion has on silica. The anomalous behaviour of silica particles in the presence of lithium ions has been reported by other researchers both in colloid science (Iler, 1979; Vivian, 1961) and in the field of concrete research (Collins *et al*., 2004; Mitchell *et al*., 2004). While it is accepted that lithium ions have a peculiar effect on the silica surface as compared to the other monovalent cations, the reason for the distinction remains elusive. It has been postulated that lithium adsorbs at the

silica interface, forming an impervious layer (Vivian, 1961) or primary hydration sheath (Persello, 2000) unlike the other monovalent cations. Iler (1979) suggested that lithium, having a higher hydrated radius as compared to other cations, does not adsorb as close to the silica surface. Here, it is speculated that the higher fouling potential is due to the impervious layer formed by lithium ions that screen the silica hairs (silicic and silanol groups) which are formed on the silica surface (Vigil *et al*., 1994). This impervious layer prevents the hairs from interacting with each other and therefore the particles can be pushed closer together. The closer packing results in a more compact cake layer and hence higher fouling potential value. This speculation is supported by the fact that the abnormal behavior of lithium cannot be explained with the classical electric double layer theory.

The fouling potentials of the colloidal suspension with additions of LiCl and average value of the fouling potentials for the 3 other salts are shown in Fig 4.8 with the differences indicated in the bar chart.

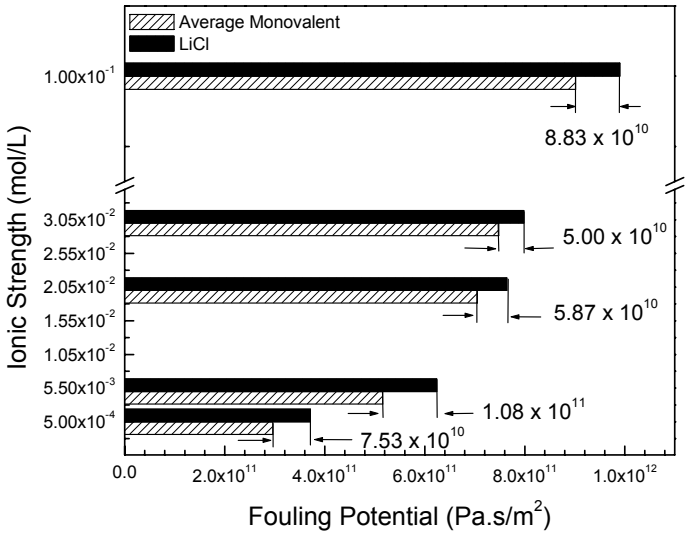

Fig. 4.8: Bar chart comparing the fouling potential due to LiCl and the average of NaCl, KCl and CsCl at varying ionic strength of (a) 0.0005M, (b) 0.005M, (c) 0.02M, (d) 0.03M and (e) 0.1M. The difference between the fouling potential values (x 10^{11} Pa.s/m^2) are (a) 0.753, (b) 1.08, (c) 0.587, (d) 0.500 and (e) 0.883 respectively.

The difference for the fouling potential for the various ionic strengths tested, ranging approximately between 0.5×10^{11} and 1.08×10^{11} Pa.s/m^2, is most likely due to the repulsive force induced by the silica hairs. This small range is fairly consistent with the findings of Vigil *et. al* (1994), who reported that the short range repulsive forces are independent of solution chemistry.

The third and final observation is that the trend of fouling potential against ionic strength is the same regardless of the type of monovalent salt used. It was previously shown (Section 4.3.4) that the fouling potential of feed water was dependent on the colloid concentration (ϕ_b) and natural logarithm of ionic strength (ln(I)) in a bilinear fashion shown below,

$$k = (\alpha + \beta \ln(I))\phi_b \tag{4.6}$$

where α and β are constants dependent on colloidal properties and their response to various operational conditions. Here, the bilinear model is tested by plotting the specific fouling potential for LiCl and the average specific fouling potential of the 3 other salts against ln(I) in Fig 4.9.

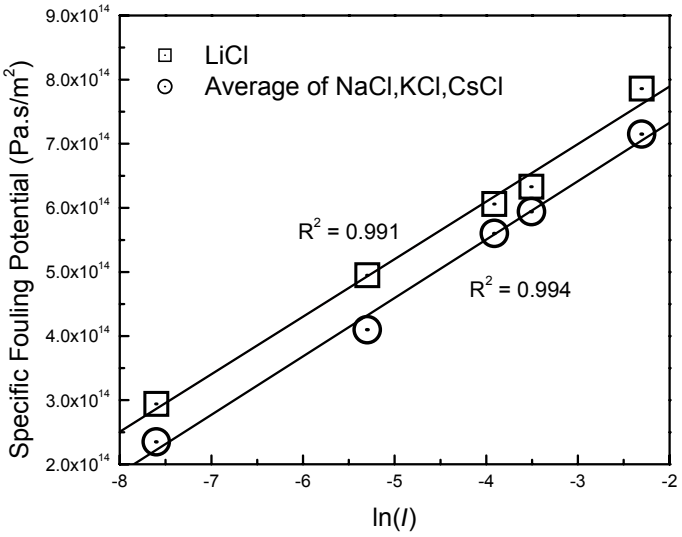

Fig. 4.9: Plot of specific fouling potential (k_s) against ln(I) for LiCl and the average of NaCl, KCl and CsCl. Colloidal concentration = 5.13 × 10^{-4} v/v, ΔP = 276kPa (40psi), crossflow velocity = 164 cm/s. Both plots indicate a highly linear relationship between *ks* and ln(I).

The plot shows that a strong linear relationship exists between the two groups of fouling potentials and the logarithm of ionic strength. While the α value is higher, the β value is similar for LiCl as compared to the average of the 3 other monovalent salts. This clearly shows that changing the salt concentration which affects the electrical double layer around the colloidal particles has an equivalent effect on the colloidal fouling potential regardless of the salt used. An additional mechanism, in this case postulated to be the screening of the silica hairs by the lithium ions, is present and is represented by the difference in the α values.

4.3.7 Effect of Divalent Calcium Ions on Fouling Potential

Because calcium ion is one of the most common cations in natural water sources (Snoeyink and Jenkins, 1980), calcium chloride ($CaCl_2$) was used to investigate the effect of divalent cations on colloidal fouling. For simplicity and consistency, all measurements for $CaCl_2$ in this chapter are expressed in terms of ionic strength. It may be useful to note that the $CaCl_2$ concentration is 1/3 that of the ionic strength. Fouling experiments were conducted at 5 ionic strengths of 0.0003 M, 0.0015 M, 0.003 M, 0.0045 M, and 0.009 M $CaCl_2$ for a constant feed water colloidal concentration of 1.08×10^{-4} v/v. All other operational conditions were kept constant as per the monovalent salt experiments. The fouling potentials under various ionic strength of $CaCl_2$ are tabulated in Table 4.6 and plotted in Fig. 4.10.

Table 4.6: Colloidal fouling potential for feed waters adjusted using $CaCl_2$ at varying ionic strengths*

	Ionic Strength (mM)				
	0.3	1.5	3.0	4.5	9.0
Fouling Potential ($\times 10^{11}$ Pa.s/m^2)	0.76	1.26	1.63	0.89	0.86

* Feed water colloidal concentration is 1.08×10^{-4} v/v.

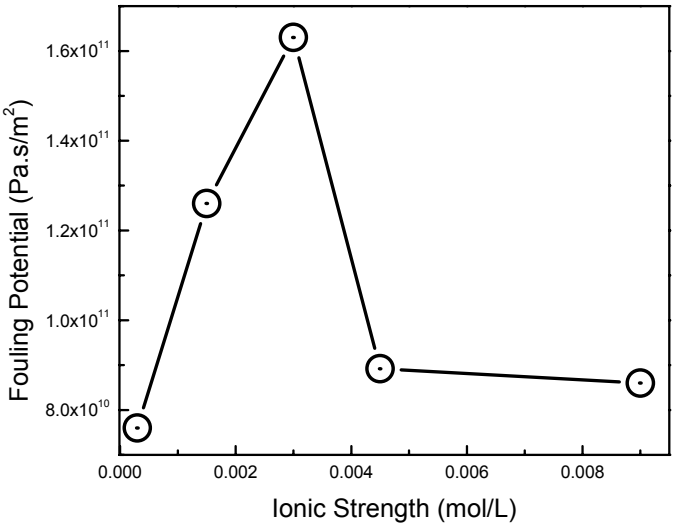

Fig 4.10: Fouling potential at varying ionic strength of calcium chloride. Colloidal concentration in the feed water = 1.08×10^{-4} v/v, ΔP = 276kPa (40psi), crossflow velocity = 164 cm/s.

From the graph it can be seen that the fouling potential increases with ionic strength, reaching a maximum at ionic strength of 0.003M, and then decreases. This behavior of fouling potential with ionic strength was not observed for monovalent cations.

Independent batch aggregation tests were conducted to elucidate the reason for the occurrence of the peak in the fouling potential. The turbidity of identical colloidal suspensions (1.08×10^{-4} v/v) with differing $CaCl_2$ ionic strength was measured and is presented in Fig. 4.11. The turbidity remains constant for low ionic strengths and starts increasing at ionic strength of 0.003M. This indicates that the aggregation of the colloidal particles occur at this ionic strength of $CaCl_2$. The concentration of salt at which coagulation occurs is termed the critical coagulation concentration (C.C.C) and is marked as the critical salt concentration in Fig. 4.11. Interestingly the C.C.C as found from the independent batch aggregation tests was found to coincide with the ionic strength for the maximum fouling potential observed in Fig. 4.10. This denotes that the greatest fouling potential of colloidal particle laden feed water will occur just before aggregation begins.

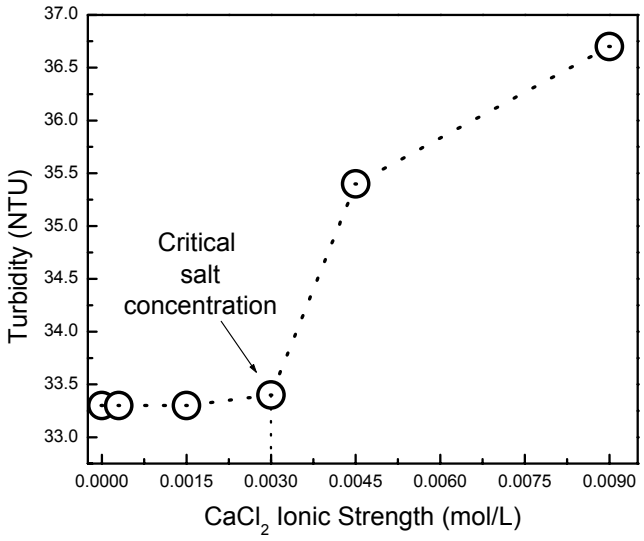

Fig. 4.11: Turbidity results from independent batch aggregation tests for varying $CaCl_2$ ionic strength at colloidal concentration of 1.08×10^{-4} v/v. Turbidity remains constant up to 0.003M and increases subsequently. This is termed the critical salt concentration or critical coagulation concentration.

The fouling potential is consistently higher for the divalent ions than for the monovalent ions at the same ionic strength below the C.C.C as seen from Table 4.6 and Table 4.2. This implies that another mechanism besides the electrokinetic phenomena is present between the colloidal particles due to multivalent cations. It has been suggested that for silica colloidal particles, bridging by Ca^{2+} ions could be responsible for the heightened attraction between the particles (Tadros and Lyklema, 1969; Iler, 1979). This bridging effect is stronger for the divalent salt than the monovalent salt because it not only neutralizes the negatively charged silica surface but also acts as a positive charge site bringing another silica particle closer. Below the C.C.C or peak in fouling potential, the fouling potential increases with divalent ionic strength, similar to the case with monovalent salts. Fig. 4.12 shows a plot of fouling potential (k) versus $\ln(I)$ for the divalent salt $CaCl_2$ with the one previously obtained for monovalent NaCl (data from Table 4.2) at the same colloidal concentration and operational conditions.

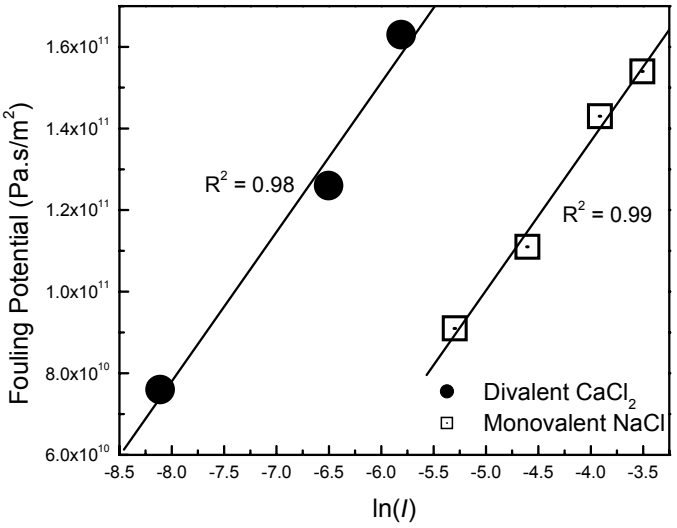

Fig. 4.12: Plot of fouling potential (k) against ln(I) for the addition of $CaCl_2$. The plot of k versus ln(I) for NaCl as presented previously (data from Table 4.2) is added for comparison. All experiments at colloidal concentration = 1.08×10^{-4} v/v, ΔP = 276kPa (40psi), crossflow velocity = 164 cm/s.

The regression coefficient of 0.98 indicates that the fouling potential with a divalent salt obeys the bilinear relationship just as well as that with monovalent salts does. However, precaution should be taken here because only three experimental data points are presented. It is observed that a significantly smaller calcium chloride ionic strength is required to induce the same fouling potential as compared to sodium chloride. The β value (trendline slope) is equivalent between the two salts, suggesting that the fouling potential due to a change in salt concentration is controlled by the double layer. The difference in the α values is due to the additional bridging mechanism induced by the divalent salt.

Beyond the C.C.C., coagulation of the colloidal particles occurs resulting in a more porous cake layer of bigger aggregates and reduction in the fouling potential. For monovalent salts, the decline in fouling potential was not observed because the experiments were conducted well below the C.C.C. value which was experimentally found to be at 0.45M and 0.49M for KCl and NaCl respectively for feed water colloidal concentration of 5.13×10^{-4} v/v.

4.3.8 Effects of Colloid Concentration on Fouling Potential with Divalent salt

In the previous section it was found that the relationship between fouling potential and ionic strength of divalent salt could be divided into two segments. Fouling potential increased with ionic strength concavely to a peak value then decreased in a convex fashion. In this section, the fouling potential at different combinations of divalent ionic strengths and colloid concentrations are investigated. The results are shown in Fig 4.13., and summarized in Table 4.7.

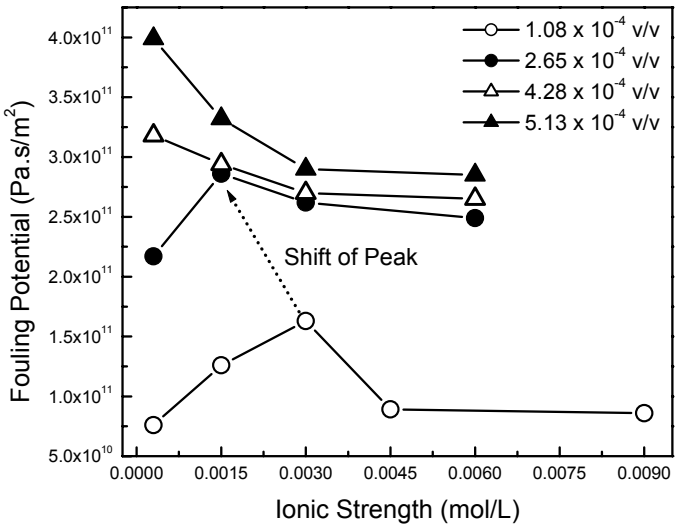

Fig. 4.13: Fouling potential for feed waters at varying ionic strengths of calcium chloride and colloid concentrations. ΔP = 276kPa (40psi), crossflow velocity = 164 cm/s. The peak fouling potential is observed to shift to the left as colloidal concentration is increased.

Table 4.7: Fouling potential x 10^{11} for feed waters containing different colloidal concentrations and ionic strengths adjusted with $CaCl_2$.

Colloid Concentration (× 10^{-4} v/v)	Ionic Strength (mM)			
	0.3	1.5	3.0	6.0
2.65	2.17	2.86	2.62	2.49
4.28	3.18	2.94	2.70	2.65
5.13	3.99	3.32	2.90	2.80

It is observed from Fig. 4.13 that a higher colloidal concentration generally results in a higher fouling potential, and a peak value at lower ionic strength. The peak fouling potentials occur at 0.003M and 0.0015M, respectively, for 1.08×10^{-4} v/v and 2.65×10^{-4} v/v colloidal concentrations. At higher colloidal concentrations of 4.28×10^{-4} and 5.13×10^{-4} v/v, it is observed that the fouling potential, declines monotonically with ionic strength. The peak of fouling potential is not discernible from Fig. 4.13 for these two colloidal concentrations because it may occur at much lower ionic strengths that were not tested.

Batch aggregation tests for 2.65×10^{-4} v/v colloidal concentration were conducted and the results are shown in Fig. 4.14. Similar to the case of 1.08×10^{-4} v/v colloidal concentration presented in Fig. 4.11, the point where turbidity starts to increase corresponds exactly with the ionic strength that causes the peak in the fouling potential which is 0.0015M. This confirms that the decrease in fouling potential after the peak value is due to the aggregation of colloidal particles.

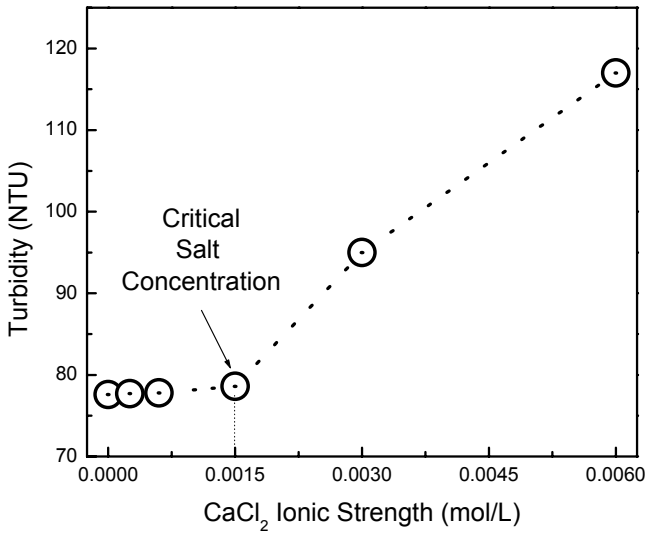

Fig 4.14: Turbidity versus ionic strength for $CaCl_2$ for colloidal concentration of 2.65×10^{-4} v/v. The critical salt concentration is found to be at 0.0015M.

This is a useful finding, since the C.C.C. for any salt and colloidal suspension can be easily ascertained from batch aggregation tests. The value can then be used to determine the ionic strength at which the greatest fouling potential will take place in the membrane filtration system. Beyond the C.C.C. the fouling potential declines for all concentrations of colloidal particles in the feed water with further increase in ionic strength. This observation is attributed to the increase in permeability of the cake layer formed on the membrane surface due to the aggregation of the colloidal particles.

4.3.9 Effect of Colloidal Concentration on the Stability Diagram

It was previously shown, that the peak in fouling potential occurred at the C.C.C. as found from independent batch aggregation tests. Therefore knowledge of how the C.C.C varies with various solution chemistry properties such as pH, counterion type, colloidal material, concentration, etc will aid in understanding the conditions under which the fouling strength of the colloidal feed water will be the greatest. The variation of C.C.C with various parameters is often represented by stability diagrams. The aggregation behaviour of silica colloidal particles under the influence of calcium ions at various pH values have been previously investigated, most notably by Iler (1975) and Zerrouk *et al*. (1990). However, a literature review revealed that the effect of silica colloidal concentration on the critical concentration of calcium ions for aggregation was not available, although it is commonly accepted that a higher particle concentration usually results in a lower critical coagulation concentration.

Batch aggregation tests were conducted for a series of colloidal concentrations of 4.90×10^{-5} v/v, 1.08×10^{-4} v/v, 1.47×10^{-4} v/v, 2.65×10^{-4} v/v, and 5.70×10^{-4} v/v to determine their critical coagulation concentrations using calcium chloride. The test results are presented in terms of silica concentrations in Table 4.8.

Table 4.8: Critical coagulation concentration of calcium chloride at different colloidal concentrations

Colloidal Concentration ($\times 10^{-4}$ v/v)#	Silica Concentration (mM)*	- log [Silica] = *p*[Silica]	Critical Coagulation Concentration [Ca] (mM)	-log [Ca] = *p*[Ca]
0.49	16.00	1.796	9.00	2.046
1.08	35.20	1.453	3.00	2.523
1.47	48.00	1.319	2.70	2.569
2.65	86.40	1.063	1.50	2.824
5.70	192.0	0.717	0.54	3.268

20% of commercial colloidal suspension is silica as specified by the manufacturer
* Molecular weight of 60g/mol and specific gravity of 1.2 for silica colloidal particles is used.

As shown in Fig. 4.15, there is a good linear relationship between *p*[Ca] and *p*[Silica] with a relatively high regression coefficient of 0.989. The linear regression line divides the domain in Fig. 4.15 into two regions. The stable region falls above the line where the colloidal particles remain dispersed in the feed water, and the unstable region below the line is where aggregation occurs. The salt concentration which results in the peak fouling potential for the different colloidal concentrations is represented by the line.

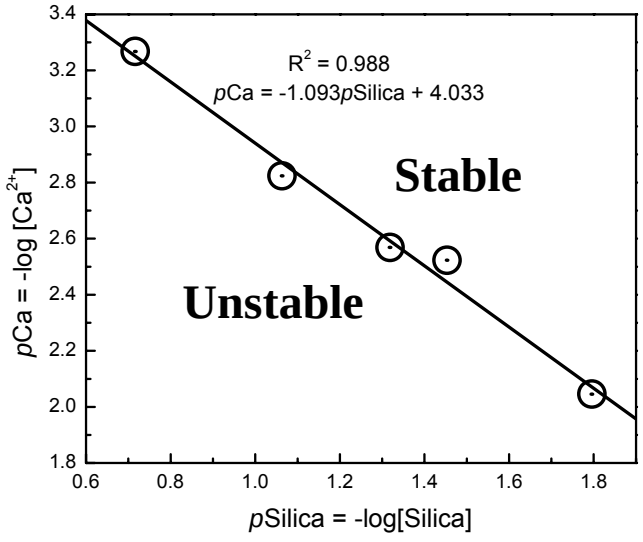

Fig 4.15: Stability diagram for increasing concentration of colloidal particles. Stable and unstable domains are separated by a straight line with a slope of -1.09.

4.4. Summary

In this chapter the effect of ionic strength and colloidal concentration in the feed water on the fouling potential was quantitatively evaluated. The fouling potential of the feed water was found to be linearly related to the double layer thickness ($\ln(1/\kappa)$) with all other conditions kept constant. By defining the specific fouling potential as the fouling potential per unit concentration of colloidal particles, a predictive bilinear model was developed by empirically relating the fouling potential of feed water to the ionic strength parameter and the colloidal concentration. It was found that the model was able to predict accurately to within ±5% the fouling potential of feed water of varying ionic strength and colloid concentration when sodium chloride was used. The model was also able to predict accurately the fouling potential to within ±10% when potassium chloride was used. The quantitative fouling potential and predictive model are novel techniques to study and understand the effects of ionic strength on colloidal fouling. A clearer and better understanding of the dual effects of colloidal concentration and ionic strength on colloidal fouling emerged from this chapter as a result of this. For example it was found that a ten-fold increase in ionic strength from 0.001M to 0.01M has an equivalent effect on the fouling potential as an increase in colloidal concentration of approximately two-fold. This highlights clearly, the importance of ionic strength on colloidal fouling.

Subsequently, the effects of various monovalent salts on the fouling potential of the colloidal feed waters under constant operational conditions were investigated. It was found that within the range of ionic strengths tested, there was insignificant difference between the effects of sodium chloride, potassium chloride, and cesium chloride on the fouling strength of the feed water. Lithium chloride however resulted in higher fouling potential values at all ionic strength tested. This particular behavior was most likely attributed to the unique interaction properties of the silica colloidal particles in the presence of lithium ions. Nevertheless, the

fouling potential under various ionic strengths of all monovalent salts tested can be well correlated with the bilinear model.

Unlike monovalent cations, divalent calcium resulted in higher fouling potentials and induced aggregation of the colloidal particles at relatively smaller salt concentrations. This was attributed to additional mechanisms such as the 'bridging effect' between the colloidal silica particles due to the calcium ion. Colloidal aggregation resulted in an increase in the permeability of the cake layer and consequently a reduction of the fouling potential. This assertion was supported by independent aggregation tests at two different colloidal concentrations. Below the critical coagulation concentration, the fouling potential increased with ionic strength in a similar fashion to that found for monovalent salts. The finding that the peak fouling potential occurs at the salt concentration at which the aggregates start to form may have important practical implications. The C.C.C. of calcium cation or other high valence cations can be determined first from independent batch tests, which is much easier. Then the ionic strength of the cations that would cause maximum fouling in the membrane processes could be anticipated and preventive measures could be taken. Having shown that ionic strength plays a critical role in colloidal fouling, attention in the next chapter turns to the effect of solution pH which was constant and not considered in this chapter.

Chapter 5

Colloidal Fouling and Feed Water pH

5.1 Introduction

Mounting experimental evidence suggests that solution chemistry (pH and Ionic strength) could play the primary role in influencing the fouling of colloidal particles because of their small size (Bowen and Jenner, 1995c; Zhu and Elimelech, 1997; Faibish *et al.*, 1998). In the previous chapter, the effect of ionic strength on colloidal fouling was quantitatively evaluated and found to be significant. Solution pH is another critical water chemistry parameter that influences colloidal fouling and is often used to control it (Winfield, 1979; Teixeira and Rosa, 2003; Van der Meeren *et al.*, 2004). Silica colloidal particles found in the natural environment are normally negatively charged at neutral pH conditions with $-SiO^-$ groups on the surface of the particle. The adsorption of protons (H^+) due to the presence of acids lowers the surface charge of the particle by forming silanol groups. These surface silanol groups (—SiOH) are quite stable and further adsorption of protons to form —Si—OH_2^+ groups on the surface only occur under very acidic conditions (pH<isoelectric point). The lowering of the surface charge by the addition of acids reduces the repulsion between the colloidal particles and increases colloidal fouling. While these trends have been reported qualitatively (McDonogh *et al.*, 1992; Faibish *et al.*, 1998; Fu and Dempsey, 1998; Waite *et al.*, 1999; Kilduff *et al.*, 2005; Li *et al.*, 2005), a quantitative relationship between colloidal fouling and solution pH remains elusive and has not been attempted. As a result it is not clear to what extent solution pH affects colloidal fouling. Furthermore, the dual effects of solution pH and ionic strength on colloidal fouling need to considered in combination.

Strong acids such as sulphuric acid (H_2SO_4) and hydrochloric acid (HCl) are often added into the feed water to prevent scaling of sparingly soluble salts in nanofiltration and reverse osmosis processes in water and wastewater treatment (Winfield, 1979; Abdel-Jawad *et al.*,

1997; Boerlage *et al*., 1999; Zidouri, 2000; Teixeira and Rosa, 2003; Al-Shammiri, 2005). However, their adverse effects on the exacerbation of colloidal fouling have not been investigated previously. Various acids are also used in the semiconductor industry during the manufacturing process, generating large volumes of wastewaters containing colloidal silica particles (Hong *et al.*, 2004). This is another area, where an assessment of the effect of the different acids on colloidal fouling would be beneficial. Furthermore, due to the presence of the gel layer (Vigil *et al.*, 1994) around the silica particle surface, sorption of ions, molecules, compounds and other macromolecules on its surface can alter significantly the interfacial properties of the particles. The sorption of acid species which can occur through chemical forces (covalent or co-ordinate bonding), hydrogen bonding force, electrostatic force, hydrophobic association force or molecular force (Lu *et al.*, 2005) could have a significant impact on colloidal fouling in membranes. For example, in Chapter 4, it was found that lithium ions had a greater effect on the fouling potential of the colloidal feed waters as compared to other monovalent ions such as sodium, potassium and cesium at the same ionic strength. The results were attributed to the reduced repulsion between the colloids as a result of the interaction between the hydrated lithium ions and the silanol groups on the particle surface.

In this chapter, the objective is to assess the effects of changes in solution chemistry on colloidal fouling in membrane processes. In the first part of the chapter, the variations in fouling potential with feed water chemistry are deliberated in terms of bulk particle interaction parameters such as zeta potential (ζ) and ionic strength which was covered independently of solution pH in Chapter 4. Subsequently, the extent of using different acids (hydrochloric, nitric, sulphuric, phosphoric, acetic and citric) to control feed water pH on colloidal fouling will be investigated.

5.2 Experimental Section

5.2.1 Synthetic Feed Water

Commercially available Snowtex 20L (ST20L) and Snowtex ZL (STZL) (Nissan Chemical Industries, Ltd., Tokyo, Japan) colloidal particles were used in this study. The particles were delivered in liquid form and used as received. Particles of the required concentration were dispersed in deionized water (DI) with conductivity < 1μS/cm obtained from a Milli-Q-system (Millipore, Bedford, MA). As the experiments were conducted at different times of the year, colloidal particles from two different batches of ST20L were obtained from the supplier. The first batch (referred to as ST20L-1) had slightly larger particles of hydrodynamic diameter 84±3 nm and the second batch, (referred to as ST20L-2) had particles of hydrodynamic diameter 67±5 nm as determined by dynamic light scattering (90 Plus Light Scattering, Brookhaven Instruments Corp., Holtsville, NY, USA). The particle size for the STZL colloids measured by the same method was 130±5nm. Since, the investigations in each section are independent; the slight difference in particle sizes between the ST20L colloidal particles is inconsequential to the analytical outcomes in this chapter.

5.2.2 Adjustment of Feed Water Chemistry

The particles, when suspended in DI water without chemical adjustment, had a feed water pH of approximately 9. Solution chemistry of the feed water was adjusted by first performing alterations on smaller 1L samples. To 1L of DI water the required colloidal concentration to be used in the filtration experiments diluted 40 times was added under constant mixing at 300rpm. The samples were then adjusted to the required ionic strength based on molar concentration with sodium chloride (NaCl) (Reagent Grade Sigma Aldrich, Germany). Subsequently titration of the sample to the required pH was performed and the volume of acid or base required was determined. Acids used in this chapter included strong acids such as hydrochloric acid HCl (37% Prolabo, France), nitric acid HNO_3 (65% Merck, Germany), and sulfuric acid H_2SO_4 (95-97% Merck, Germany), and weak acids such as citric acid $C_6H_8O_7$

(99.5+% A.C.S Reagent, Germany), phosphoric acid H_3PO_4 (85% A.C.S Reagent, Mexico) and acetic acid CH_3COOH (100%, Merck, Germany), all prepared to 0.1M concentration before use. The alkali used was sodium hydroxide (NaOH) (≥98% Riedel-de Haen, Germany) also prepared to a molar concentration of 0.1M.

Each sample adjusted this way constituted a batch test. For each pH value, 3 batch tests were conducted and the volume of acid or base required was ascertained to within 5% variation. The average of the batch tests for each acid or base at a particular pH was used to determine the amount to be added during the filtration experiments by multiplying by 40, since the feed water volume used in all experiments was 40L. The feed water pH in the filtration experiments could be controlled to within ± 0.1 pH units using the method above. Batch tests were conducted just prior to the filtration experiment using the same materials to minimize any discrepancy between the two conditions.

5.2.3 Filtration Experiments

Filtration experiments were carried out at different feed water chemistries using the crossflow experimental setup and filtration protocol as described in sections 3.4.1 and 4.2.2 respectively. The membrane used in these experiments was a tubular ceramic membrane made of Titania, (T1-70-25, USFilter Corp., Warrendale, PA) with a molecular weight cut-off (MWCO) of 5000 Daltons. The isoelectric point (i.e.p.) of the membrane has been previously determined as pH 6 (Szymczyk *et al.*, 1998). Above this pH value the membrane is negatively charged and it is positively charged below it. The allowable pH range, pressure and temperature limit as specified by the manufacturer are 1-13, 112psi (784kPa) and 95°C respectively. The rejection of the acids and salt by this membrane was found to be negligible.

5.2.4 Monitoring of Feed Water Properties during Filtration

The pH (Horiba Ltd., Kyoto, Japan) and conductivity (conductivity meter LF 538, Weilheim, Germany) of the feed water was monitored with probes in the feed tank throughout the experiments and were found to remain constant. Particle size and turbidity measurements of the feed water were made before and after each experiment to ensure that no fluctuations occurred during the fouling experiments. All experiments were conducted with the particles in a stable state, i.e. no aggregation occurred. The electrophoretic mobility of the particles in the feed water was evaluated at the start, middle and the end of each filtration experiment using the Zeta Potential Analyzer (Brookhaven Instruments Corp., Holtsville, NY). The zeta potential (ζ) was automatically calculated by the instrument using the Smoluchowski Equation.

5.3 Results and Discussion

5.3.1 Influence of pH on Fouling

Several filtration experiments at different pH values were conducted for both the ST20L-1 and STZL colloids at constant particle concentrations of 6.83×10^{-4} v/v, and controlled operating conditions of ΔP = 280kPa and crossflow velocity = 164cm/s. The ionic strength of the feed water in all experiments was maintained at 3mM with the addition of NaCl and pH was adjusted using HCl and NaOH. All experiments at each condition were conducted at least twice. The average fouling potentials with the error bars indicating the actual fouling potential for each condition are plotted against the pH values of the feed water in Fig 5.1. As observed, there is a decreasing trend in the fouling potential of the feed waters between the pH values of 2 and 9 and a slight increase in fouling potential between pH 9 and 10.3 for both particles.

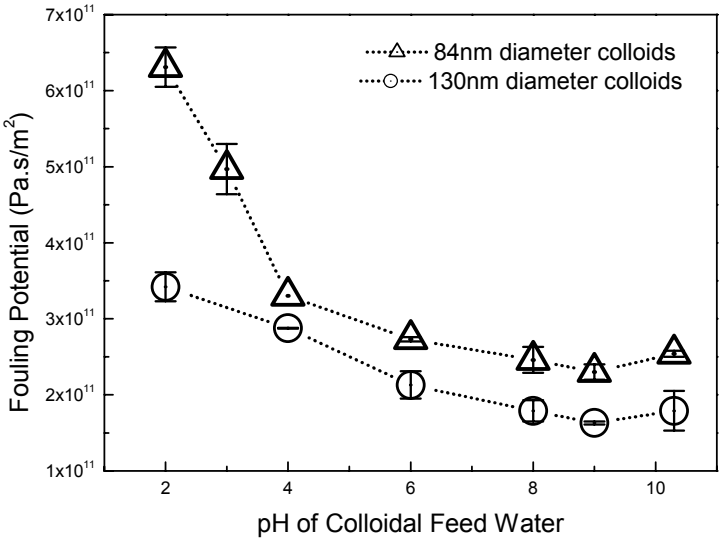

Fig 5.1: Relationship between fouling potential and pH of the feed water containing ST20L-1 (84 nm diameter) and STZL (130 nm diameter) colloidal particles. Experiments at each pH value were conducted twice at constant operational conditions of ΔP = 2.76×10^5 Pa (40psi), crossflow velocity = 164cm/s, T = 25˚C, feed water ionic strength = 3mM, and both colloidal concentrations = 6.83×10^{-4} v/v.

The effect of pH on the modification of the colloidal silica surface silanol groups (-*Si*-*OH*) is summarized in Eq. (5.1) for hydroxide (OH^-) and Eq. (5.2) for hydrogen ion (H^+) adsorption.

$$-Si-OH+OH^- \leftrightarrow -Si-O^- + H_2O \tag{5.1}$$

$$-Si-O^-+H^+ \leftrightarrow -Si-OH \tag{5.2}$$

For acidic feed water, there is excess hydrogen ion concentration in the feed water which adsorbs on the negatively charged colloidal silica surface, thereby neutralizing its charge. This reduces the repulsion between the colloidal particles and leads to a denser colloidal cake layer. As the pH is reduced further, the screening effect increases, resulting in higher fouling potential values. Theoretically, in the alkali pH range, the adsorption of hydroxide ions increases the negative charge on the particles and therefore reduces the fouling potential. Zeta potential measurements of the particles shown in Fig 5.2 confirm that the interparticle repulsion between the colloids decreases as the feed water acidity increases. The silica particles are observed to remain stable, having a negative zeta potential, for all pH values

used in the experiments. The isoelectric point for silica particles is reported in the literature to be between pH 1 and 2 (Iler, 1979).

Interestingly, the fouling potential increases between pH 9 and 10.3, contrary to the explanation above. The increase in fouling potential is attributed to the dissolution of silica particles to form silicate ions ($HSiO_3^-$) above pH 10 (Iler, 1979). Zeta potential measurements of the particles shown in Fig. 5.2 were also found to increase (less negative) between pH 9 to 10.3 in accordance with the fouling potential results.

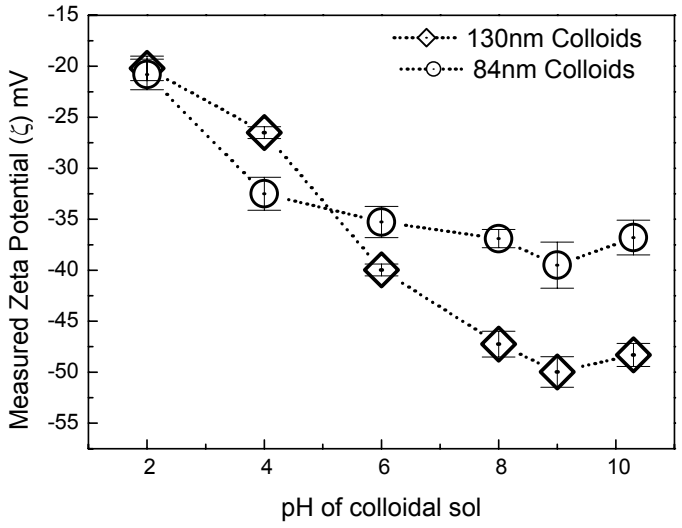

Fig 5.2: Variation of measured particle zeta potential (ζ) with pH of colloidal solution. All measurements were repeated three times with samples taken directly from the feed tank at the start, middle and end of the experiment. Feed water and filtration conditions are as described in Fig. 5.1.

5.3.2 Relationship between Zeta Potential and Fouling Potential

The similarity in trends between the zeta potential and the fouling potential with pH of feed water suggests that a relationship between the two parameters is probable. The fouling potential at each pH value is plotted against the corresponding zeta potential for the pH in the range 2 to 10.3 in Fig 5.3. The graph indicates a strong linear relationship between the fouling potential and zeta potential for both ST20L and STZL colloidal particles for the range of the

experiments conducted. To our knowledge, this is the first time a direct relationship between particle zeta potential and membrane fouling has been shown.

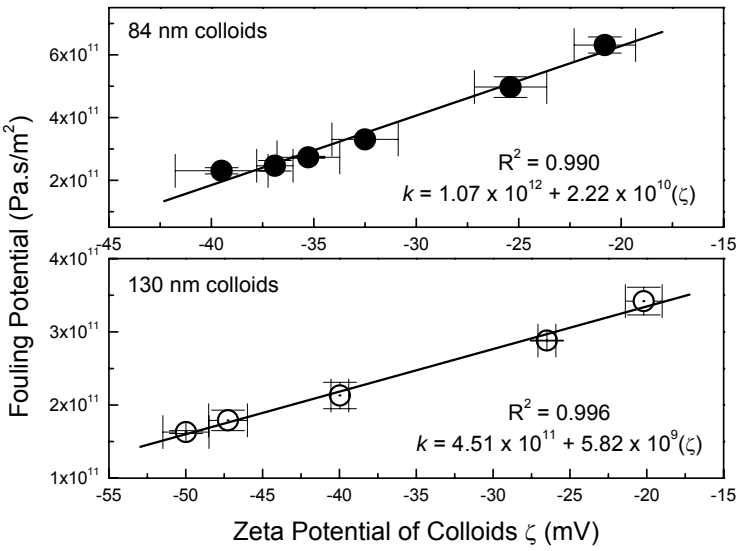

Fig. 5.3: Strong linear relationship between fouling potential and zeta potential of the particles was observed for both ST20L-1 (84 nm diameter) and STZL (130 nm diameter) colloids.

Analyzing the linear equations presented in the figures, the fouling potential at the isoelectric point (set as $\zeta = 0$) would be 1.07×10^{12} Pa.s/m^2 and 4.51×10^{11} Pa.s/m^2 for the ST20L-1 and STZL silica particles respectively. These values represent the fouling potential due to the packing of hard-sphere (no interparticle interactions) particles in the cake layer. For hard-spheres, assuming the maximum packing volume fraction of 0.64 is achieved, the ratio of the specific resistance (r_c) of the cakes formed for the two particles will be dependent on the inverse square ratio of their particle sizes. This is consistent for the data presented here where the ratio of fouling potentials ($4.51\times10^{11}/1.07\times10^{12} = 0.421$) is in close agreement with the inverse square of the particles ($(84/130)^2 = 0.418$).

The slope of the line provides an indication of the increment in fouling for a given variation in zeta potential of the particles which is dependent on the intrinsic property of the particles such as particle size, electrostatic properties, material properties, particle shape, etc. Accordingly,

the smaller ST20L-1 colloidal particles exhibit greater variations in fouling behaviour for changes to zeta potential as compared to the larger STZL particles. This indicates that the fouling potential is more strongly influenced by the solution properties for smaller colloidal particles than for the larger particles.

5.3.3 Effect of Colloid Concentration on the Relationship between Fouling Potential and Feed Water pH

The relationship between fouling potential and feed water pH was further investigated for two other colloidal concentrations of 3.43×10^{-4} v/v and 1.02×10^{-3} v/v using ST20L-1 colloids. All other conditions were kept constant as described in section 5.3.2. For each feed water condition, filtration experiments were conducted twice and the fouling potential values determined. The average fouling potential values plotted (error bars denote actual fouling potential values of each experiment) against pH are shown in Fig. 5.4.

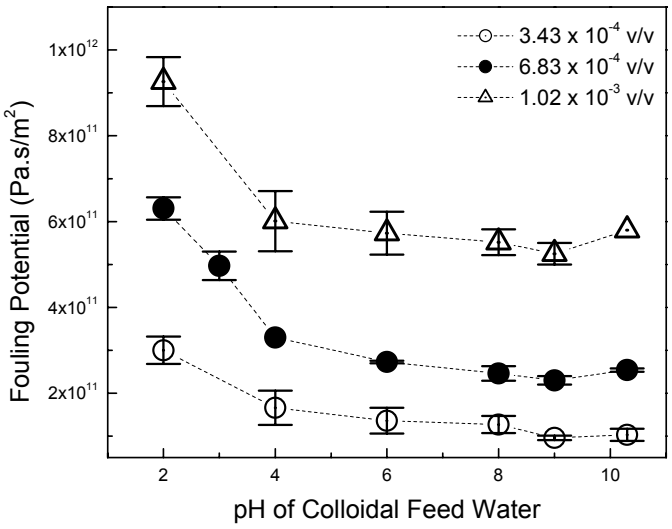

Fig. 5.4: Variation of fouling potential with pH for feed waters containing colloidal particles of concentrations a) 3.43×10^{-4} v/v, b) 6.83×10^{-4} v/v, c) 1.02×10^{-3} v/v. All experiments were conducted with ST20L-1 colloids (84 nm diameter) at T = 25°C, $\Delta P = 2.76\times10^{5}$ Pa (40 psi), crossflow velocity = 164 cm/s. The ionic strength of the feed water was controlled at 3mM.

The experimental data from Fig. 5.3 for colloidal concentration of 6.83×10^{-4} is also shown for completeness. As shown, the general trend where the fouling potential decreases as feed water pH increases from 2 to 9 is adhered to for different concentrations of colloidal particles. Between pH 9 and 10.3, the fouling potential is observed to increase for all colloidal concentrations. The similarities in the trends indicate that the relationship between the specific fouling potential and feed water pH is independent of the particle concentration.

5.3.4 Effect of Ionic Strength on the Relationship between Fouling Potential and Feed Water pH

Previously, all membrane filtration experiments were conducted at a constant ionic strength of 3mM with different feed water pH values. The effect of pH on the fouling potential was investigated for further ionic strengths of 0.01M, 0.05M, 0.10M and 0.15M to feed waters containing ST20L-1 colloidal particles at concentration 6.83×10^{-4} v/v. The average fouling potential values for each feed water pH and ionic strength are shown in Fig 5.5. Error bars again indicate the range of fouling potentials obtained for each condition.

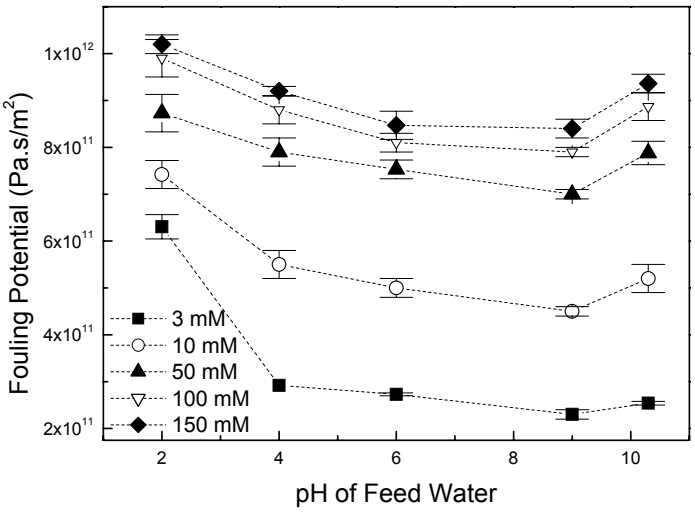

Fig. 5.5: Variation of fouling potential with pH for feed water containing colloidal particles at different ionic strength. All experiments were conducted using ST20L-1 colloidal particles (84 nm diameter) at colloidal concentration = 6.83×10^{-4} v/v, T = 25°C, $\Delta P = 2.76\times10^{5}$ Pa (40 psi), crossflow velocity = 164 cm/s.

The general trend of decreasing fouling potential between pH 2 to 9 and increasing fouling potential between pH 9 to 10.3 is observed for all feed water ionic strengths. The increment in fouling potential from pH 9 to pH 10.3 appears more pronounced with ionic strength. This is in agreement with previous work on dissolution of the silica colloidal particles (Iler, 1979). It is also observed that at higher ionic strength the decline in fouling potential with increasing pH is gentler. This is attributed to the increasing ratio of the counter-ions $\left(Na^{+}\right)$ to the potential determining ions (H^{+}) at higher ionic strength thus rendering any variation in pH to have a smaller effect on the silica surface potential due to strong counter-ion screening. This finding implies that for high ionic strength waters, changes to pH would not have a substantial effect on colloidal fouling behaviour. This might have useful ramifications for colloidal fouling control in seawater desalination.

In chapter 4, it was empirically determined that the fouling potential is linearly related to the natural logarithm of ionic strength for feed water at a single pH value. The data presented in Fig. 5.6 shows that the linear relationship holds true for all pH values tested.

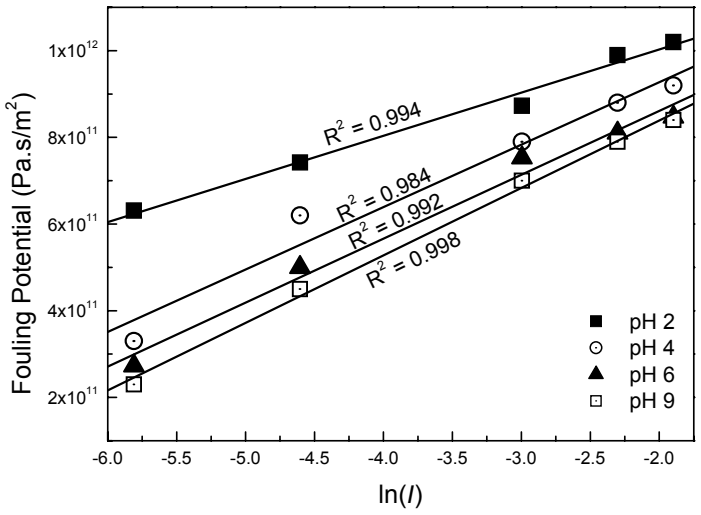

Fig. 5.6: Strong linear relationships (as seen from regression coefficients) between colloidal fouling potential and ln(*Ionic Strength*) were found for the feed water pH tested. An increase in the slope of the relationship is found as feed water pH becomes more alkali.

The slope of the relationship increases as feed water pH increases in alkalinity. At low pH values, the surface potential on the colloidal silica surface is significantly lower than that at higher pH values; therefore it is less sensitive to changes in feed water ionic strength as compared to at higher pH values. Since ionic strength is directly related to the double layer thickness (1/κ), a similar relationship between fouling potential and the natural logarithm of the double layer thickness (1/κ) would also exist.

5.3.5 Relationship between Fouling Potential and Zeta Potential for Different Feed Water Ionic Strengths

The fouling potential values from Fig. 5.5 plotted against the measured zeta potential values of the colloidal particles under the conditions tested except for pH 10.3 are shown in Fig 5.7.

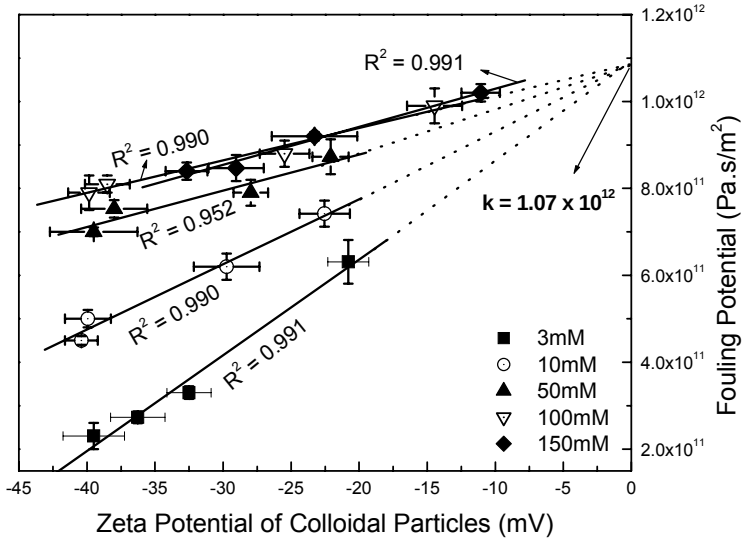

Fig. 5.7: Linear relationships between fouling potential and colloid zeta potential for feed waters containing colloidal particle at ionic strengths of a) 3mM, b) 10mM, c) 50mM, d) 100mM and e) 150mM. The trendlines for the linear relationships and the regression coefficients are shown in the graph. For 100mM and 150mM ionic strength, the trendlines obtained were almost identical. All the trendlines converge at the isoelectric point of the colloids (ζ = 0mV) to a fouling potential value of 1.07×10^{12} Pa.s/m^2.

The graph shows a linear relationship between fouling potential and zeta potential of colloids at all feed water ionic strengths. Extrapolated data from the trendlines shown as dotted lines

converge at fouling potential = 1.07×10^{12} Pa.s/m^2 which occurs at the colloid isoelectric point ($\zeta = 0$). As discussed previously, this corresponds to hard sphere fouling in membranes which is not influenced by the feed water ionic strength. The slope of the relationship between fouling potential and zeta potential becomes gentler when the ionic strength of the feed water is increased due to the stronger counter-ion screening of the colloidal particles. The linear dependence of the fouling potential on the particle zeta potential at various feed water ionic strengths provides a useful correlation to evaluating colloidal fouling.

5.3.6 Impact of Feed Water Acidification on Colloidal Fouling

Hydrochloric and citric acids were used as representative strong and weak acids to investigate their effect on colloidal silica fouling at the same feed water pH value. Filtration experiments were carried out with ST20L-1 colloids at concentration of 6.83×10^{-4} v/v in the feed water, at constant driving pressure of 280 kPa and crossflow velocity 164 cm/s. Sodium chloride of 3mM was added in all experiments as the background electrolyte. The average fouling potentials of two parallel filtration experiments at each pH value are reported in Fig 5.8.

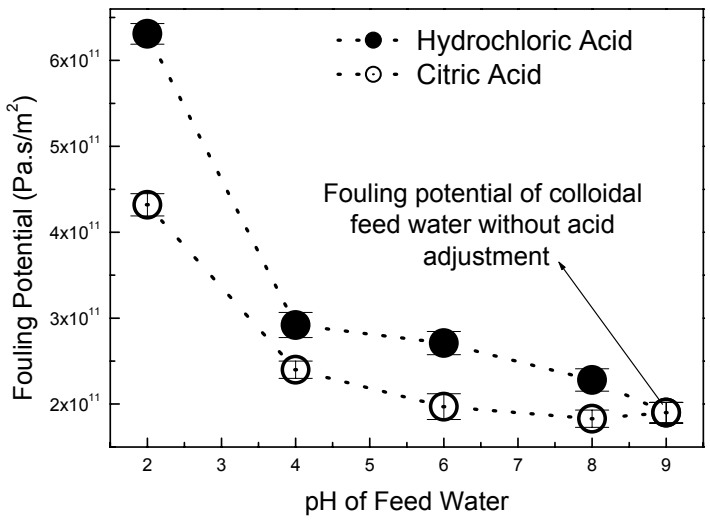

Fig. 5.8: Fouling potential determined at different feed water pH adjusted using hydrochloric acid and citric acid. The colloidal fouling potential is found to be higher when hydrochloric acid is used as compared to citric acid irregardless of the adjusted pH. Feed water and operational conditions are as described in Fig. 5.5.

The small error bars indicate good reproducibility of the fouling potential. From the graph it is observed that the colloidal fouling potential increases as the feed water pH decreases (i.e. more acidic) irregardless of the type of acid used. The fouling potential of feed waters with hydrochloric acid addition is higher than that with citric acid addition at every pH. The absolute values of zeta potential of the colloidal particles as shown in Fig. 5.9 decreases (becomes less negative) as the pH of the feed water approaches the isoelectric point (pH 1-2) of the silica colloids.

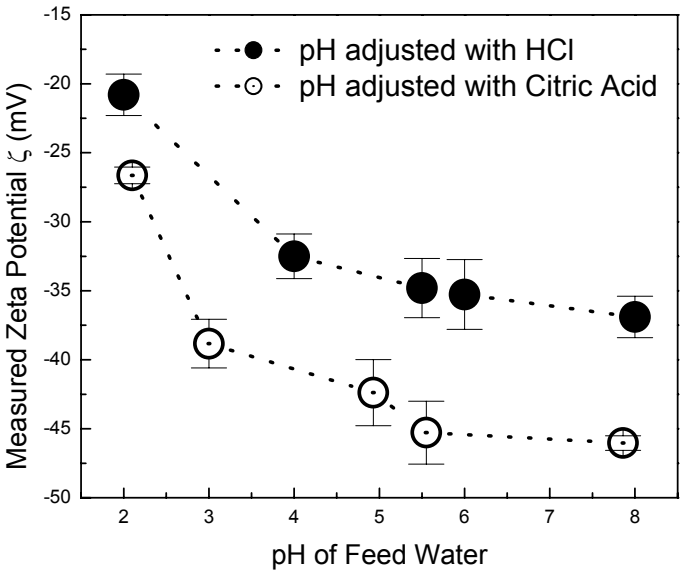

Fig. 5.9: Particle zeta-potential measured for different feed water pH. The particle zeta-potential is of higher magnitude when feed water pH is adjusted by citric acid as compared to hydrochloric acid. The same feed water and operational conditions described in Fig. 5.8 are used here.

It is noted that the absolute values of zeta potential for the colloidal particles are greater (more negative) for citric acid adjusted feed waters as compared to that of hydrochloric acid adjusted ones. It can be seen from Figs 5.8 and 5.9 that the fouling potential is well correlated to zeta potential. The reduction in zeta potential weakens the electrostatic repulsive force between the particles, which allows closer packing of the colloids in the deposited cake layer and therefore results in a higher fouling potential. It should be noted that the results discussed here are deliberated only in terms of particle – particle interactions which are adjudged to play a more

pivotal role in colloidal fouling than particle – membrane interactions (Bowen and Jenner, 1995a; Bowen and Jenner, 1995b; McDonogh *et al*., 1989).

The higher absolute value of zeta-potential and the resulting lower fouling potential with citric acid is most likely due to surface interactions between citric acid and the silica colloids in the feed water. Hong *et al*. (2004) found similar effects of citric acid on silica zeta-potential and attributed their findings to the adsorption of citrates on the silica surface that occurs most likely by hydrogen bonding. Citrates contain three carboxylic groups (-COOH) which deprotonate as the feed water acidity increases. The adsorption of citrates on the silica surface results in carboxylic acid-functionalized silica particles. When the carboxylic groups deprotonate ($-COO^-$), stronger repulsive forces develop between the particles (Biggs *et al*., 1995; O'Brien and White, 1978).

5.3.7 Strong and Weak Acids Effect on Fouling Potential

The impact of the acidification of feed water on the colloidal fouling potential was further investigated with more acids, including strong acids of hydrochloric, sulphuric, and nitric acids, and weak organic/inorganic acids of acetic, phosphoric, and citric acids. The experiments were conducted in exactly the same conditions as the previous section, except for the pH and the colloidal particles used. A fixed pH of 3 and the ST20L-2 silica colloids were employed in the experiments. The fouling potential of the feed waters adjusted using the different acids are summarized in Fig 5.10. The conductivities of the feed waters with the various acids used are also shown.

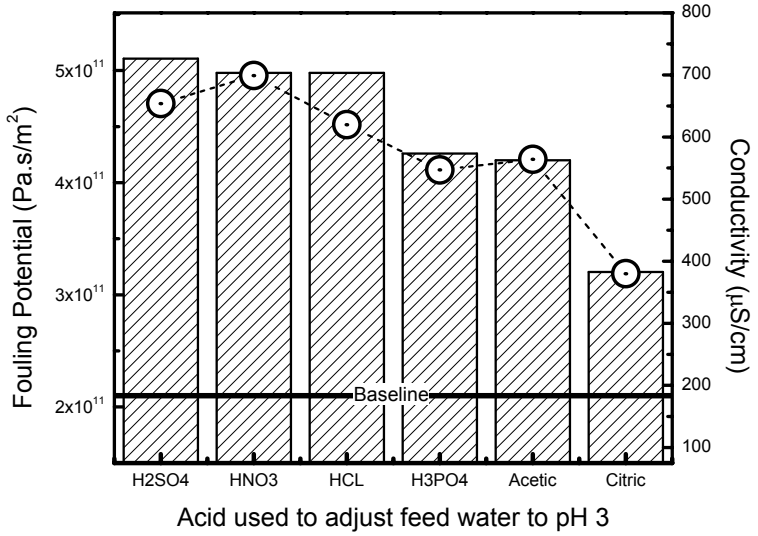

Fig. 5.10: The fouling potential (bar charts) for feed waters adjusted to pH 3 for different acids. Feed waters also consist of ST20L-2 colloidal particles of concentration 6.83×10^{-4} v/v with 3mM NaCl operated at applied pressure ΔP = 280kPa, crossflow velocity = 164cm/s and temperature T = 25°C. The dotted points (⊙) indicate the feed water conductivity after the individual acid adjustment. The solid line represents the baseline fouling potential and conductivity without acid adjustment.

The solid line in the figure represents the fouling potential (2.1×10^{11} Pa.s/m^2) of the colloidal feed water without acid addition and can be used as a baseline for comparison. It is noticed that the fouling potential is constant at approximately 5×10^{11} Pa.s/m^2 when the strong acids such as sulphuric, nitric and hydrochloric acid are used to adjust feed water pH. This is 2.4 times higher than the baseline fouling potential. The fouling potential of the feed water with the addition of phosphoric or acetic acids are about 2 times higher than the baseline value but 15% lower than that for the strong acids. Feed water pH adjustment using citric acid resulted in the smallest increase in colloidal fouling potential (≈ 1.5 times of the baseline fouling potential), which is approximately 35% lower than that with the strong acids.

Fouling potentials of feed waters at higher colloid concentration (ST20L-2, 1.08×10^{-3} v/v) and adjusted to pH 3 with the various acids were determined under the same experimental conditions and the results are shown in Fig. 5.11. The fouling potential for the feed water

containing colloids at the same conditions except for acid addition is represented by the solid line (baseline) in the figure.

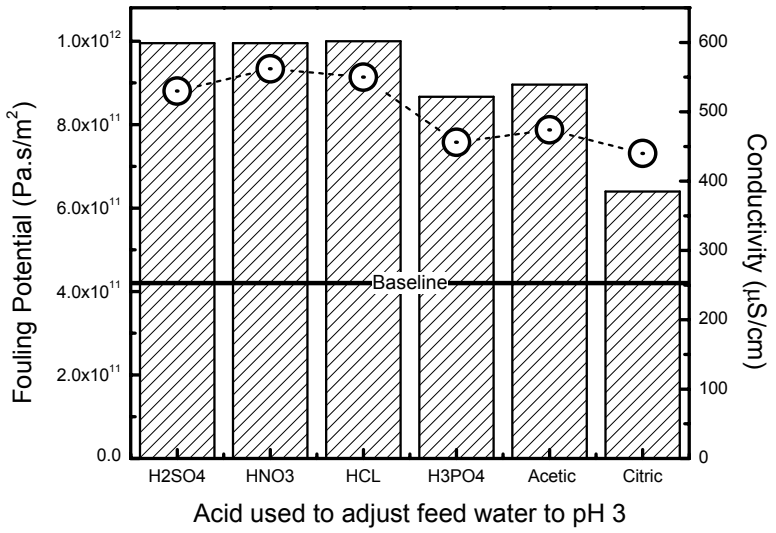

Fig 5.11: Fouling potential obtained using different acids (bar chart) to adjust the feed water pH to 3. Feed waters also consist of ST20L-2 colloids of concentration 1.08×10^{-3} v/v with 3mM NaCl operated at applied pressure 280kPa, crossflow velocity 164cm/s and temperature 25°C. The dotted points indicate the feed water conductivity (⊙) after the individual acid adjustment.

The percentage differences between the fouling potentials for the feed waters adjusted using the strong and weak acids are similar to those found for the smaller colloid concentration feed water described above. This indicates that the impact of acids on the fouling potential is not affected by the colloid concentration.

The lower fouling potential obtained with the weak acids is attributed to the adsorption of weak acid anions (acetates, citrates and phosphates) by hydrogen bonding to the surface silanol groups (Iler, 1977; Murashov and Lezczynski, 1999) as described for citric acid in the previous section. Adsorption of these anionic species increases the surface potential of the colloidal particles. This is supported by the zeta-potential measurements of the ST20L-2 colloidal particles of concentration 6.83×10^{-4} v/v at pH 3 for the different acids presented in Fig 5.12.

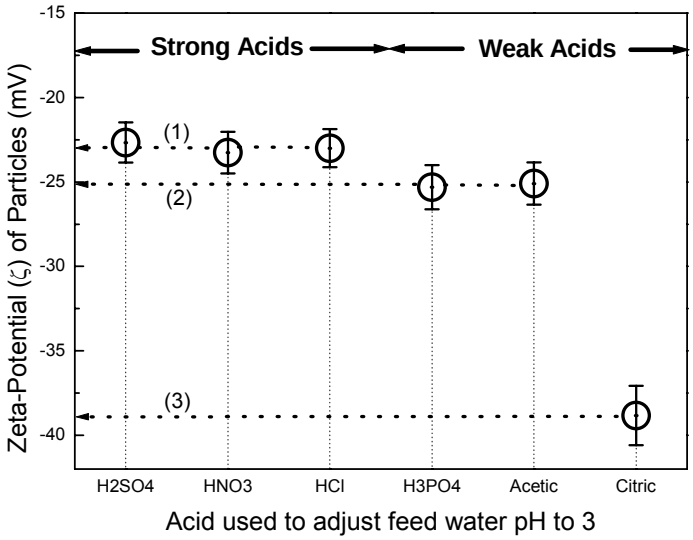

Fig. 5.12: Zeta-potential of colloidal particles for different acids used to adjust the feed water pH to 3. Dotted lines with arrows are the zeta potential values for (1) average of H_2SO_4, HNO_3 and HCl, (2) average of H_3PO_4 and Acetic acid, (3) Citric acid. All other feed water conditions are as summarized in Fig. 5.10.

The absolute values of zeta-potential measured for the colloidal particles were higher (indicating more repulsive interfacial interaction) for weak acids as compared to that for the strong acids, with citric acid resulting in the highest absolute potential value. It can be seen that citric acid addition results in an even lower fouling potential than the other two weak (acetic and phosphoric) acids. This particular phenomenon may be attributed to the stronger hydrogen bonding between citrate and the silanol groups on the silica surface (Iler, 1977).

The conductivity of the feed water measured after acid adjustment presented in Figs. 5.10 & 5.11 indicated that the strong sulphuric, hydrochloric, and nitric acids had a higher conductivity than the weak acids. This is likely attributable to the adsorption of weak acids on the silica surface and the reduced mobility of the weak acid ions because of higher concentration of weak acids in the water than the strong acids at the same pH. Experiments were subsequently conducted with ST20L-2 colloidal particles of concentration 6.83×10^{-4} v/v under the same operating conditions to investigate the possible effect of feed water conductivity on the colloidal fouling potential. For this purpose, sodium chloride was added

to maintain a constant feed water conductivity of 730±5 μS/cm after acid addition. Comparison of the data in Fig. 5.13 and Fig. 5.10 shows that the conductivity adjustment of the feed water increased the fouling potential marginally for all acids.

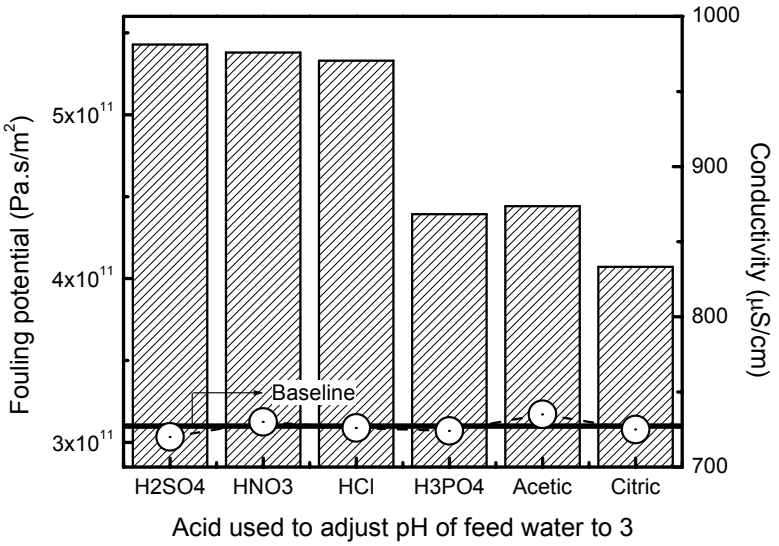

Fig 5.13: Fouling potential determined for feed water adjusted to pH 3 using the different acids. The feed water conductivity (⊙) was adjusted using sodium chloride to achieve a constant conductivity of 730±5 μS/cm. All other feed water and operating conditions summarized in Fig. 5.10. The solid line represents the baseline fouling potential of feed water under the same conditions except without the addition of acid.

Despite the constant conductivity, the strong acids still registered the highest colloidal fouling potential, and the relative positions of all the acids in exacerbating colloidal fouling were unchanged. Therefore, the deviation in conductivity was not the primary reason for the difference in fouling potential when different acids were used in feed water acidification.

5.3.8 Feed Water Acidification at High Ionic Strength

At low feed water conductivity of 730μS/cm, experimental data revealed the significant role that the type of acid used in feed water acidification played on the colloidal fouling. More experiments were conducted with ST20L-2 colloidal particles at 0.1M NaCl concentration (conductivity ≈ 11860μS/cm) to investigate the impact of feed water acidification on colloidal fouling at high ionic strength. Colloidal concentration of 6.83×10^{-4} v/v was used in the

experiments and feed water pH was adjusted to 3 separately with the six acids under investigation. The fouling potential values determined from the experiments are summarized in Fig. 5.14.

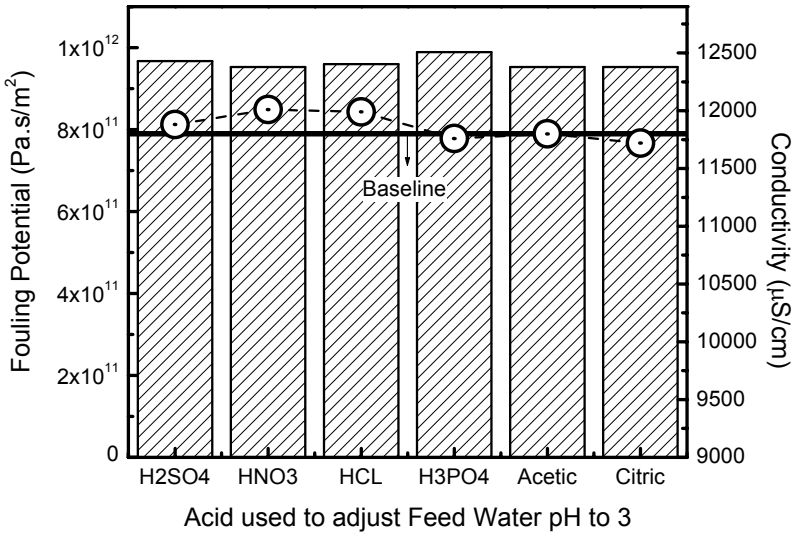

Fig 5.14: Fouling potential determined for feed water adjusted to pH 3 using the different acids. The feed water ionic strength was adjusted to 0.1M with sodium chloride. All other feed water and operating conditions summarized in Fig. 5.10. The solid line represents the baseline fouling potential of feed water under the same conditions except without the addition of acid.

It is noticed that the fouling potential only increases slightly over the baseline fouling potential (1.2 times of baseline) at 0.1M sodium chloride (solid line) for all acids. There is no significant difference between the fouling potentials with the addition of different acids. The results suggest that at high salt concentrations, screening of the colloidal silica surface by the counter-ions takes place, which suppresses the impact of different acid addition on colloidal fouling. In other words, ionic strength is the predominant controlling factor on the colloidal interactions at high salt concentration.

5.4 Summary

Solution chemistry has a significant effect on colloidal fouling in membrane processes. Feed water combinations of low pH and high ionic strength induce the greatest fouling effect on the silica colloidal particles. For example the fouling potential of feed water containing silica

colloids at a pH of 2 and an ionic strength of 0.15M was 4.3 times higher than that of an identical feed water but at pH of 9 and ionic strength of 0.003 M for the same operating conditions.

Subsequently, the effects of pH and ionic strength were quantitatively related to the fouling potential. A linear relationship between fouling potential and zeta potential was experimentally found when feed water pH was adjusted for a wide range of solution ionic strengths. Interestingly, the extrapolated fouling potential values at different ionic strengths converged to 1.07×10^{12} Pa.s/m^2 at the isoelectric point of the colloids ($\zeta = 0$). This value was envisaged to be the fouling potential of similar sized hard-sphere (rigid) colloids. Ionic strength which affects the extent of the diffuse double layer and therefore screening of the charges on the colloidal surface was found to increase colloidal fouling at all pH values tested. A linear relationship between colloidal fouling potential and the natural logarithm of ionic strength as reported previously in chapter 4 was confirmed for all pH values tested.

The effects of acidification of feed water with strong and weak acids on the fouling potential of colloidal particles were investigated. Although colloidal fouling potential was generally increased by feed water acidification, notably smaller increases in fouling potential were found for weak acids at the same pH. This was attributed to the adsorption of anionic groups of the weak acids (citrates, acetates and phosphates) on the silica surface. As a result, inter-particle repulsive interaction increased and resulted in a less compact cake layer on the membrane surface. The results demonstrate that the general impact of the pH value on colloidal fouling potential could be modified by the anionic parts of the acids used, at least for low salinity feed water acidification. At high ionic strength, the adsorption of these groups on the silica surface was suppressed and the effect of the anionic parts of the acids used in acidification on the colloidal fouling potential was diminished. This study implies that the proper choice of acids in feed water acidification can considerably reduce the adverse impact of colloidal fouling in membrane filtration for the low salinity waters.

Chapter 6

Cake Compressibility and Feed Water Chemistry

6.1 Cake Compressibility

Cake formation due to colloidal deposition is of practical importance in many engineering applications (Tiller *et al.*, 1987; Antelmi *et al.*, 2001). Examples include granular filtration (deep-bed filtration), sludge dewatering, landfill lining, and sedimentation (Almy and Lewis, 1912; Walker and Lewis, 1927; Ruth *et al.*, 1933; Chen *et al.*, 1997). Of particular interest is cake formation due to the deposition of colloidal particles in membrane processes.

The formation of a cake layer of deposited colloidal particles on the membrane results in an additional layer of resistance to the permeate flow. The necessary condition to hold the deposited colloidal particles onto the membrane surface is that the driving pressure is greater than the so-called critical pressure of the colloids to be separated (Song and Elimelech, 1995). Membrane processes are usually operated at pressures much greater than the critical pressure for higher permeate production. Therefore, it is inevitable for colloidal cake formation to occur in most membrane processes. The resistance of a given amount of deposited colloidal particles to permeate flow is strongly dependent on the density of the cake layer. It is well documented that the density of the colloidal cake layer may vary under different pressures (Hong *et al.*, 1997; Lee and Clark, 1998; Kim and Hoek, 2002). An increase in the cake layer density in response to an increase in pressure is defined as the compressibility of the cake.

Cake packing density or the specific cake resistance is controlled by the long-range interactions between the colloidal particles, which is affected by solution chemistry. Therefore cake compressibility is strongly dependent on the solution chemistry, e.g. ionic strength and pH of the solution (Howe and Clark, 2002; Zhang *et al.*, 2003; Mavredaki *et al.*,

2005). Cake compressibility is also contingent upon the intrinsic property of the colloidal particles present in the water and their interactions at close separation distances in the cake layer. It has been shown in the previous chapters that increasing the ionic strength or reducing pH exacerbates colloidal silica fouling due to the tighter packing density in the cake brought about by the compression of the electrical double layer and reduction of surface potential around the silica particles respectively. However, the effects of solution chemistry on compressibility have not been addressed despite its significance to fouling.

In this chapter, the compressibility of colloidal silica particles in a membrane filtration process is investigated. Filtration experiments on colloidal feed waters were conducted in a bench scale crossflow UF setup to determine the fouling potentials under different driving pressures. Through analysis of the experimental results the compressibility of the colloidal cakes formed for different feed waters was determined. The effects of adjustments to the ionic strength and pH of the colloidal feed waters on the compressibility of the cakes were then quantitatively analyzed.

6.2 Relating Compressibility to the Fouling Potential

Cake compressibility is related to the specific resistance of the cake layer (Tiller and Tsai, 1986; Tosun, 1986) and therefore it is also associated to the fouling potential of the colloidal feed water. A quantitative relationship between these two parameters is developed below, starting with an empirical relationship widely applied in deep-bed filtration and membrane filtration (Almy and Lewis, 1912; Belfort *et al.*, 1994; Hwang *et al.*, 1998; Matsumoto *et al.*, 1999; Chun *et al.*, 2001):

$$r_c / \phi_c = \alpha(\Delta P)^{\omega} \tag{6.1}$$

where r_c is the specific resistance of the cake layer, ϕ_c is the particle concentration (volume fraction) in the cake layer, α is the leading coefficient, ΔP is the driving pressure, and ω is the cake compressibility coefficient which shows the dependence of the specific cake resistance

on the applied pressure. The increment in resistance due to cake formation at any time *t* can be expressed as (Song, 1998a)

$$\Delta R_t = r_c \delta_c(t) = \frac{r_c \phi_b}{\phi_c} \int_0^t v dt \tag{6.2}$$

where $\delta_c(t)$ is the thickness of the cake layer at time *t* and ϕ_b is the bulk colloidal concentration in the feed water. Combining Eqs. (3.2), (6.1) and (6.2), an expression relating cake compressibility to the fouling potential is obtained.

$$k = \alpha(\Delta P)^{\omega} \phi_b \tag{6.3}$$

The advantage of Eq. (6.3) over Eq. (6.1) is obvious due to the ease in which the fouling potential can be determined from the filtration experiments. Otherwise, the specific cake resistance may be unknown because the thickness and concentration of particles of the cake layer in a membrane device is difficult to determine. Rearranging Eq. (6.3) and taking logarithm of both sides result in:

$$\ln\left(\frac{k}{\phi_b}\right) = \ln(k_s) = \ln(\alpha) + \omega \ln(\Delta P) \tag{6.4}$$

The compressibility coefficient of the cake layer is the slope of the line when $\ln(k/\phi_b)$ is plotted against $\ln(\Delta P)$. The term (k/ϕ_b) represents the specific fouling potential (k_s) as discussed in Chapter 4. When a linear relationship exists between the fouling potential and the colloidal concentration, the compressibility coefficients obtained through this approach should be independent of the colloidal concentration in the water. It is also postulated, that through this approach the compressibility is independent of the membrane resistance and dependent on the feed water properties.

6.3 Experimental Section

6.3.1 Synthetic Feed Water Properties

All feed waters were prepared using deionized (DI) water obtained from a Milli-Q system (Millipore, Bedford, MA) of conductivity < 1μS/cm. Monodispersed colloids, ST20L,

(Nissan Chemical Industries, Ltd., Tokyo, Japan) were used in this study as model colloidal foulants. The particle size of the colloids as measured by 90 Plus Light Scattering (Brookhaven Instruments Corp., Holtsville, NY) was 67±5 nm. The required amount of colloidal suspension was measured volumetrically and added to the DI water to prepare the required colloidal feed water in a 50L tank. Reagent grade sodium chloride (NaCl) (Sigma-Aldrich, Gmbh, Germany), was added as required to achieve the appropriate ionic strength. The colloidal particles were found to remain stable even at the highest salt concentration of 0.1M NaCl used in the experiments since this is below the C.C.C. of 0.49M as determined in Chapter 4. The pH of the feed solution was adjusted using either hydrochloric acid (37% Prolabo, France) or citric acid (99.5+% A.C.S. Reagent, Germany) when required. The unadjusted pH of the colloidal feed water was relatively constant at 9.5 ± 0.4 for all the experiments. Conductivity (Conductivity meter LF 538, Weilheim, Germany) and particle electrophoretic mobility (Brookhaven Instruments Corp., Holtsville, NY) in the feed water were measured during the fouling experiments. Turbidity and particle size of the water in the feed tank were tested both before and after each experiment and were found to remain constant.

6.3.2 Filtration Experiments

All filtration experiments were conducted in the tubular crossflow membrane filtration device detailed in section 3.4.1. The membranes used in this study were the tubular ceramic membranes of zirconia and titania (T1-70-25Z and T1-70-25, USFilter Corp., Warrendale, PA), housed in a cylindrical stainless steel casing (USFilter Corp., Warrendale, PA), of pore size 20 nm and molecular weight cut-off (MWCO) 5000 Daltons respectively. Fig. 6.1 shows the permeate fluxes at varying driving pressures at the beginning, after 20 filtration experiments, and at the end of the study.

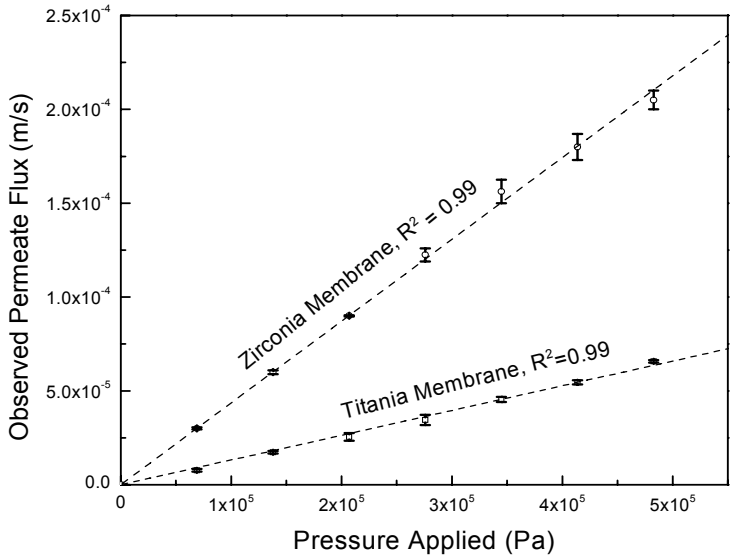

Fig 6.1: Permeate fluxes observed at different pressures for zirconia and titania membranes. The error bars indicate the difference in values obtained at the beginning, in the middle, and at the end of the study.

The resistances of the zirconia and titania membranes determined from the experiments are 2.29×10^{9} and 7.58×10^{9} Pa.s/m respectively, which are invariant with pressures. The MWCO of a membrane can be approximately related to the characteristic pore size of the membrane by the following method. The diffusion coefficient (D) of representative dextran particles to be filtered is related to molecular weight (M_w) by (Brandrup and Immergut, 1975).

$$D = 8.7\times10^{-6} M_w^{-0.48} \tag{6.5}$$

The pore size of the membrane (d_p) can then be determined from the Stokes-Einstein equation by assuming the MWCO of the membrane to be equal to the molecular weight of dextran particle (M_w),

$$d_p = \frac{1.1\times10^{10} k_B}{\pi\mu M_w^{-0.48}} \tag{6.6}$$

where k_B is the Boltzmann's constant and μ is the viscosity of the feed water. Based on this relationship, the pore size of the 5kDa membrane is found to be approximately 3.4 nm by the substitution of appropriate values. Therefore, the colloidal particles are completely retained

by both ceramic membranes because their pore sizes are much smaller than the size of the colloids used in the experiments.

The isoelectric points (i.e.p.) of the membranes occur at approximately pH 5.6 and 6.7 with the titania membrane having the lower i.e.p. (Kosmulski, 2003). The pressure and temperature limits for both membranes are 784kPa (112psi) and 95°C respectively. In all experiments the filtration protocol described in section 4.2.2 was used, and the feed water chemistry was adjusted following the procedure specified in section 5.2.2. The temperature of the feed water was maintained at 24-25°C throughout the fouling experiment.

6.4 Results and Discussion

6.4.1 Cake Compressibility of Colloidal Silica Particles

Fouling experiments were conducted on feed waters at three colloidal concentrations (9.82×10^{-5} v/v, 2.45×10^{-4} v/v, and 4.89×10^{-4} v/v) under five driving pressures (210, 280, 350, 420, and 490kPa) using the zirconia membrane and two colloidal concentrations (5.28×10^{-4} v/v and 1.45×10^{-3} v/v) under the same driving pressures using the titania membrane. The fouling potentials determined from the experiments and plotted in Figs 6.2a and 6.2b for the zirconia and titania membranes, respectively. Deviations between the fouling potentials of the repeated experiments were found to be less than 5%. The experimental results clearly indicate that fouling potentials increase with pressure regardless of the membrane. This implies that a certain level of compressibility exists in the cake layer of the colloidal silica particles.

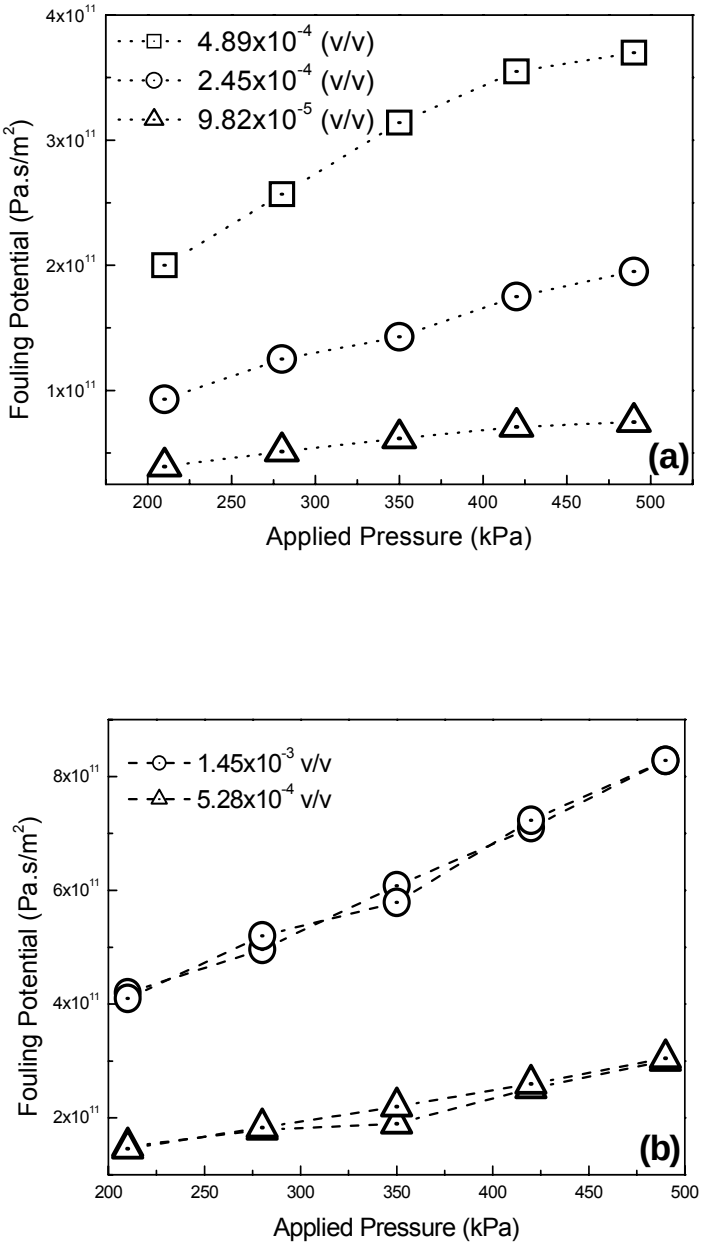

Fig. 6.2: Fouling potentials at different pressures for different feed water colloidal concentrations shown in the graphs, determined on (a) zirconia and (b) titania membranes. It is observed that the fouling potential increases with applied pressure for all concentrations tested.

The linear dependence of the fouling potential on feed water colloidal concentration was reported previously in Chapters 3. In this study, the experimental data further confirms that the linear relationship between fouling potential and colloidal concentration in the feed water

holds for different applied pressures. Figs 6.3a and 6.3b show that the fouling potential data points of different feed water colloidal concentrations for each pressure are well correlated with a straight line for both the zirconia and titania membranes. The strong linearity (R^2 > 0.99) between fouling potential and colloidal concentration in the feed water suggests that the coefficients α and ω in Eq. (6) are not affected by the colloidal concentration.

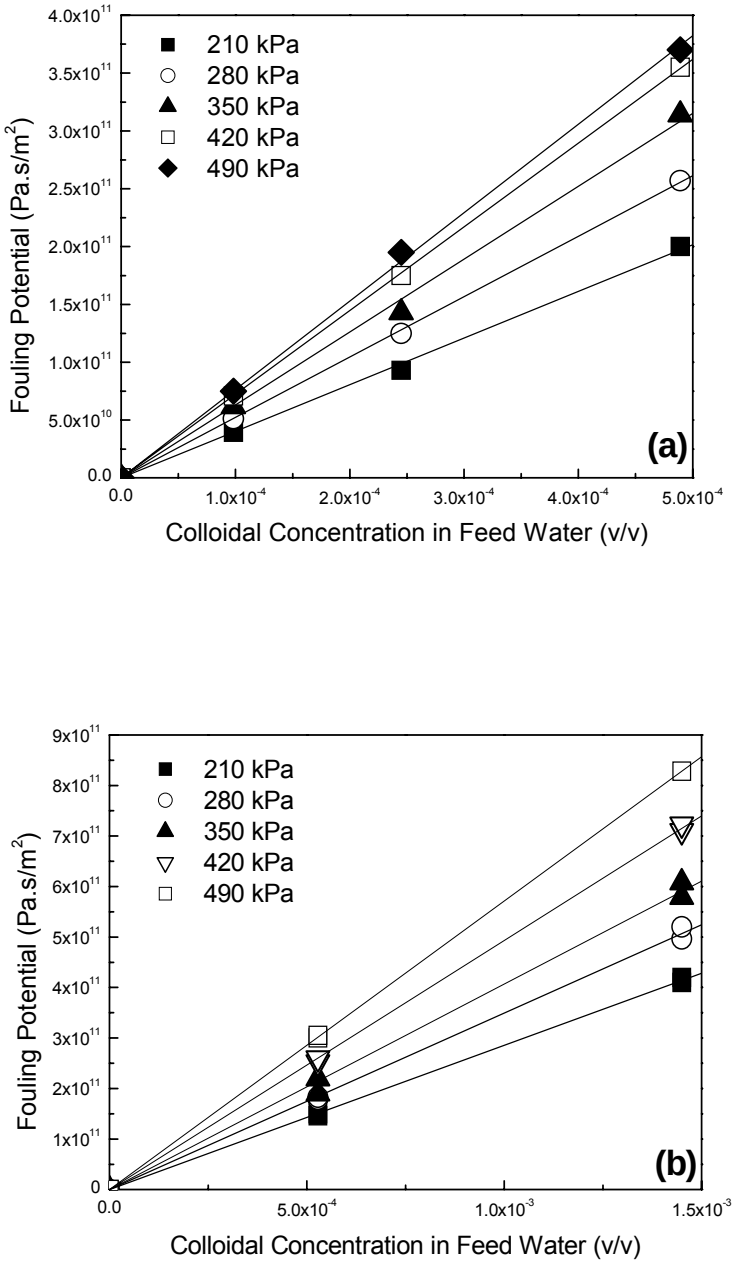

Fig. 6.3: Linear relationships are observed between fouling potential and colloidal concentration in the feed water at all pressures tested with (a) zirconia and (b) titania membranes. All regression coefficients are greater than 0.99.

According to Eq. (6.7), the compressibility coefficient can be determined by plotting $\ln(k/\phi_b)$ versus $\ln(\Delta P)$ for all colloidal concentrations and pressures. Figs 6.4 and 6.5 show that all data are well fitted with straight lines with regression coefficient (R^2) of about 0.99 for both the zirconia and titania membranes.

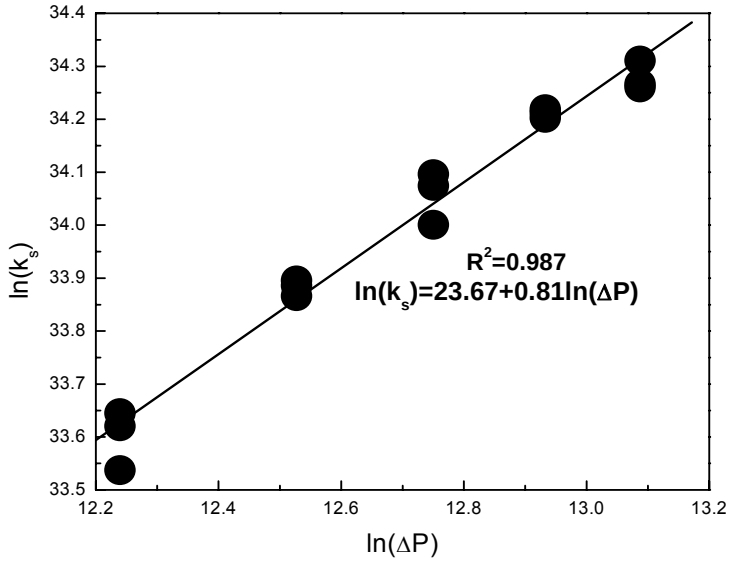

Fig. 6.4: Specific fouling potentials plotted against driving pressure in natural logarithmic scales (●) experimentally determined with the zirconia membrane and linear regression with Eq. (6.7). The compressibility and α value are shown in the graph.

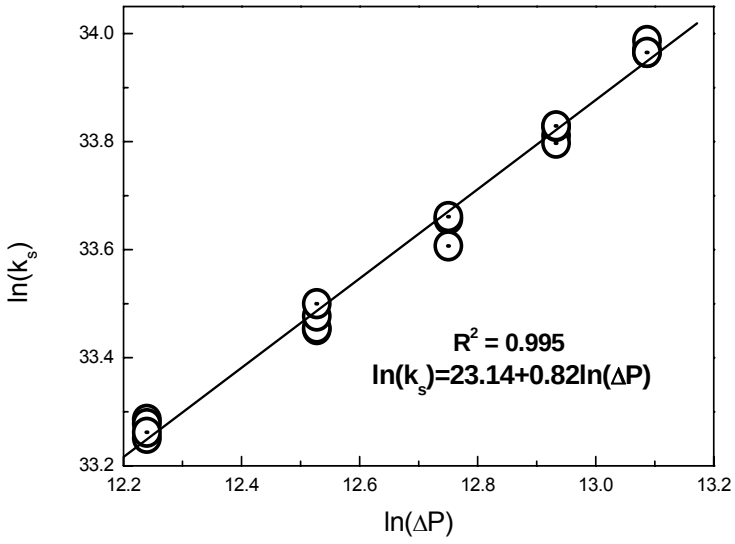

Fig. 6.5: Specific fouling potentials plotted against driving pressure in natural logarithmic scales (⊙) experimentally determined with the titania membrane and linear regression with Eq. (6.7). The compressibility and α value are shown in the graph.

The slopes of the best-fit lines in the two figures reveal that the compressibility coefficients are 0.812±0.04 and 0.826±0.02 for the zirconia and titania membranes, respectively. The compressibility coefficients for the colloidal cake in both membranes differ by less than 2%. This supports the understanding that the cake compressibility is independent of membranes and controlled by the colloidal properties and water chemistry which will be described later.

The relatively high compressibility coefficients indicate that the cake layer is quite compressible even though silica colloids are generally considered non-deformable. Electrostatic repulsion manifests itself as one of the major colloidal interactions when the particle sizes are small (<0.1μm). Therefore a possible reason for the compressibility of the cake layer is due to the repulsive EDL interactions between the colloidal particles that separates them. The separation distance between the colloids could decrease under increased pressure.

6.4.2 Ionic Strength and Cake Compressibility

Ionic strength in the solution has a strong impact on the thickness of the double layer and therefore on the compressibility of the cake layer. The effect of ionic strength on the compressibility of the cake is investigated in this section. Feed waters with colloidal concentration of 2.45×10^{-4} v/v and ionic strengths of 0.005, 0.01, 0.05, and 0.10M NaCl were filtered using the zirconia membrane while feed water with colloidal concentration of 5.28×10^{-4} v/v and ionic strengths of 0.001, 0.01, and 0.10M NaCl were filtered using the titania membrane. Based on conductivity measurements, the initial salt concentrations are 2.0×10^{-4} M and 3.9×10^{-4} M for the 2.45×10^{-4} and 5.28×10^{-4} v/v colloidal concentration feed waters, respectively, without any salt addition.

The experimental results are plotted in Fig 6.6a and Fig. 6.6b for the zirconia and titania membranes respectively.

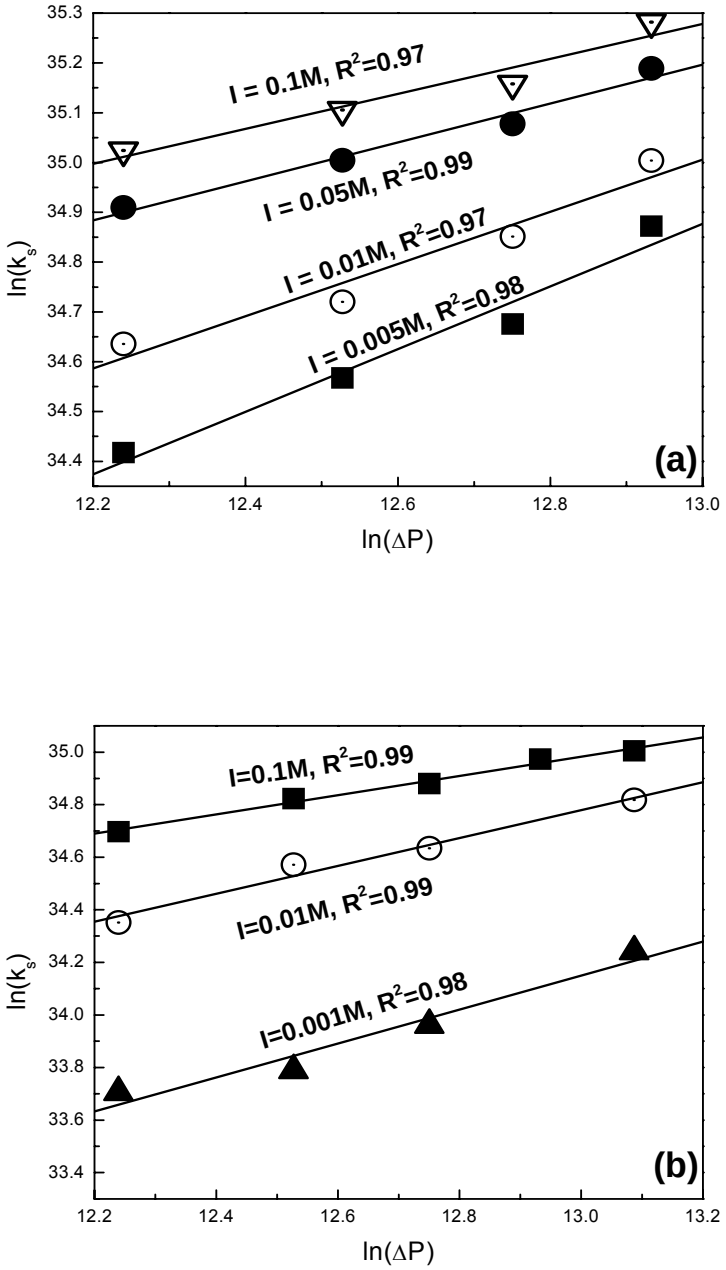

Fig 6.6: Specific fouling potentials and driving pressure in natural logarithmic scales at various ionic strengths experimentally determined with (a) zirconia and (b) titania membranes and linear regressions with Eq.(6.7). The ionic strength (I) and regression coefficient (R^2) are shown in the figure.

The compressibilities of the colloidal cakes at different ionic strengths determined from the graphs in Fig. 6.6 are tabulated in Table 6.1. It can be seen from the table that the compressibility coefficient decreases as the feed water ionic strength increases. The result

verifies that the compressibility coefficient of colloidal silica cakes is related to the thickness of the electric double layer and is affected substantially by the ionic strength in the solution.

Table 6.1: Compressibility coefficients determined with the zirconia and titania membranes for colloidal feed waters of different salt concentrations

Added salt concentration (mM)	0.00*	1.00	5.00	10.0	50.0	100
Zirconia Membrane	0.812	-	0.629	0.524	0.391	0.351
Titania Membrane	0.826	0.694	-	0.531	-	0.362
%Δ in Compressibility	1.67	-	-	1.15	-	3.09

* The initial salt concentrations in the colloidal suspensions were about 2.0×10^{-4}M and 3.9×10^{-4}M without salt addition for the zirconia and titania membrane experiments respectively, as determined from conductivity measurements.

From Table 6.1 it is observed that the compressibility coefficients obtained with the two membranes under the same feed water ionic strengths are very similar. The result further confirms that cake compressibility is an intrinsic property of the colloids and its response under given water chemistry conditions, which is independent of the membranes used in the measurements. It should be pointed out that low salt rejecting membranes were used in this study and the compressibility could be significantly affected if high salt retaining membranes are used. As shown in Fig. 6.7, the relationship between compressibility and the ionic strength of the feed water fits a power-law function of the form:

$$\omega = a(I)^b \tag{6.7}$$

where a and b are coefficients. The compressibilities obtained from both the zirconia and titania membranes are included in Fig. 6.7. It is noted that all the data points are well fitted with a straight line and the regression coefficient R^2 is 0.98. The coefficients a = 0.262 and b

= -0.148 in Eq. (6.7) can be determined by regression for the colloidal particles used in this study. Interestingly, the compressibility is also well related to the natural logarithm of ionic strength by the equation as shown in Fig. 6.7. Based on current information, both relationships can be deemed as suitable. However, it is important to emphasize that the exact relationship is not as important here, as the fact that compressibility is related to ionic strength and not affected by the type of membrane used.

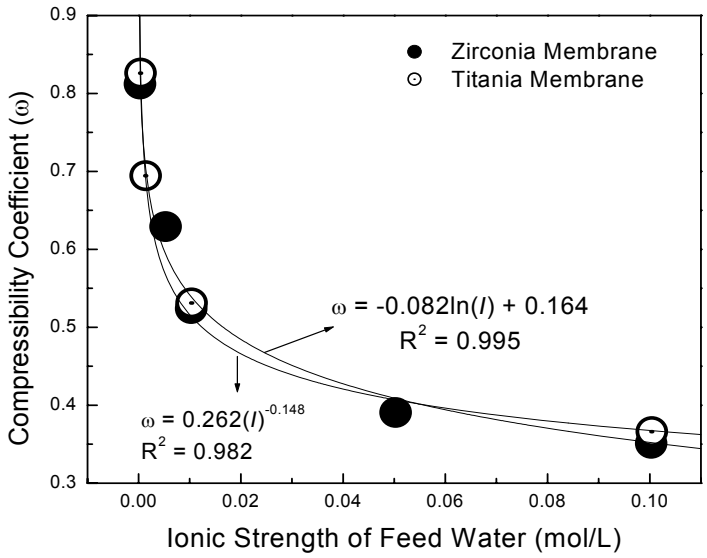

Fig 6.7: The compressibility coefficient is found to be strongly related to ionic strength of the feed water. Both a power law relationship and a natural logarithmic function can be used to fit the two parameters. Experimental data from zirconia (●) and titania membranes (○) are shown in the figure.

6.4.3 Solution pH and Cake Compressibility

Solution pH affects the surface charge of the colloids and therefore the packing within the colloidal cake layer. To investigate the effects of solution pH on the compressibility of colloidal cakes, filtration experiments were carried out for feed waters containing silica colloidal particles (ST20L) of concentration 2.45×10^{-4} v/v. All experiments were conducted using the zirconia membrane. The feed water pH was adjusted using either HCl or citric acid and the ionic strength was kept constant at 3mM using NaCl. The plot of specific fouling

potential against pressure in natural logarithmic scales is shown in Fig 6.8a and 6.8b for feed waters adjusted with HCl and citric acid respectively.

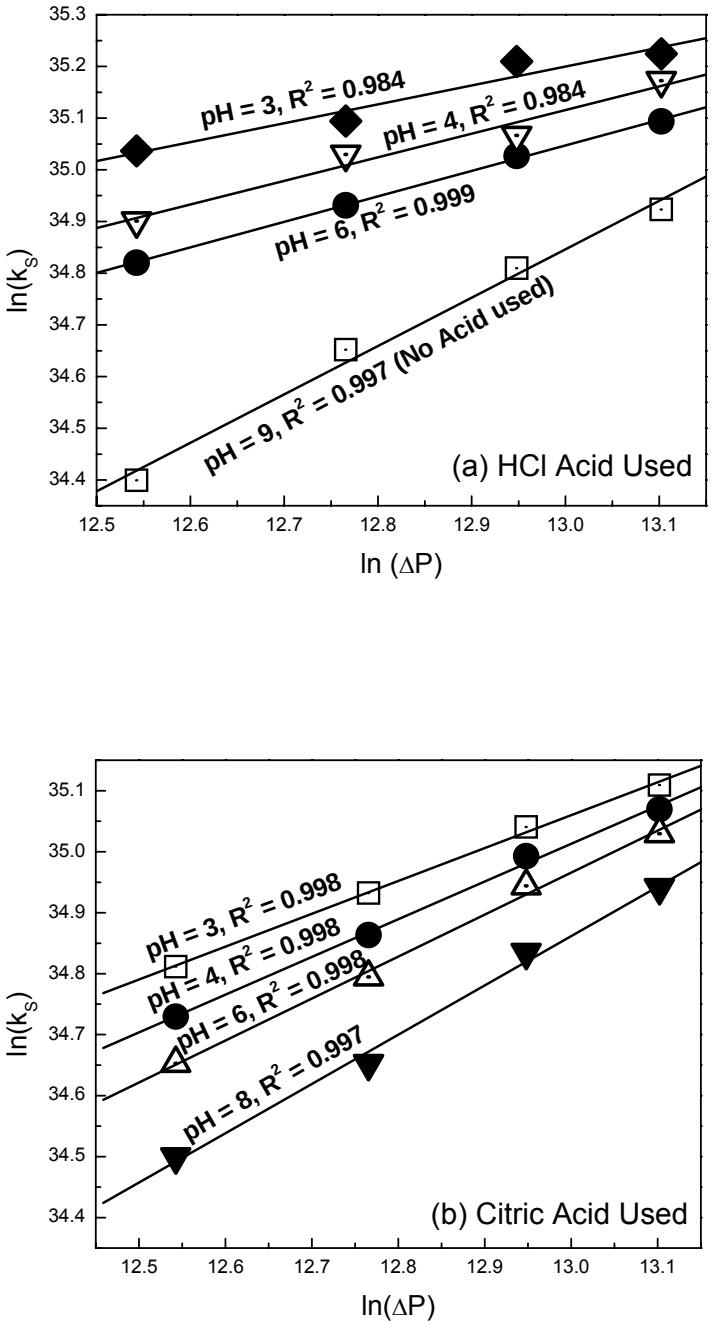

Fig 6.8: The plot of specific fouling potential against driving pressure on natural logarithmic scales. The regression coefficients and pH of the feed water adjusted using a) hydrochloric acid and b) citric acid are shown in the respective graphs. Data for feed water without pH adjustment (i.e. pH =9) is shown for comparison in Fig. 6.8a.

The data indicates that the linear relationship derived in Eq.(6.4) remains consistent when the feed water pH is adjusted as seen from the high regression coefficients. The slope of the lines, i.e. the compressibility of the colloidal cake, decreases as the feed water pH becomes more acidic for both types of acids used. This is better represented, by the plot of compressibility against pH of the feed water as shown in Fig 6.9. Compressibility at feed water pH = 9 represents the value for feed water containing the same colloidal particle concentration but without the addition of any acid.

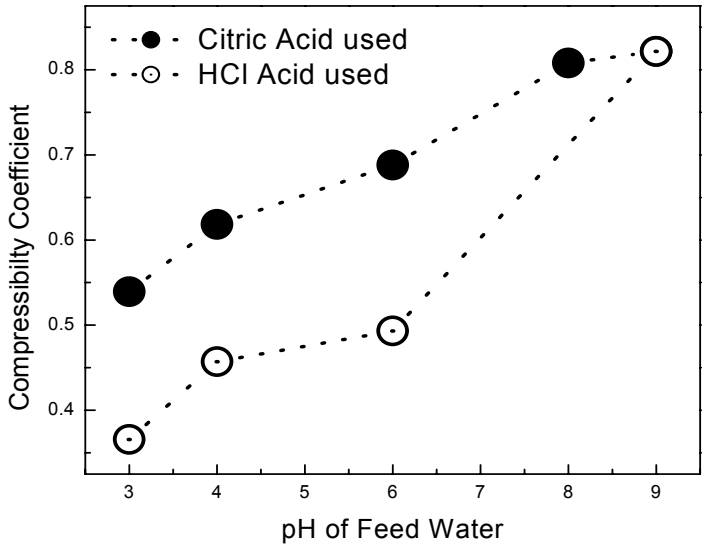

Fig 6.9: Relationship between compressibility of colloidal cake layer and pH of feed water. Compressibility decreases as feed water pH becomes more acidic regardless of the type of acid used. pH adjustment using citric acid results in higher compressibility values as compared to when hydrochloric acid is used.

The compressibility of the cake layer is higher for feed waters adjusted with citric acid as compared to HCl. This is attributable to the higher zeta potential of the colloidal silica particles in the presence of citric acid as compared to HCl at the same feed water pH, as discussed in Chapter 5. The data here suggests that adsorption of charged ions and molecules on the surface of the silica colloids in water can have strong effects on the compressibility of the colloidal cakes on the membrane surface.

6.5 Summary

Cake compressibility of feed waters containing colloidal silica particles under variable solution chemistries was investigated in a UF system in this chapter. Fouling experiments were conducted with two UF membranes for feed waters of various colloidal concentrations and water chemistries under different driving pressures. A quantitative relationship was theoretically established between the fouling potential of the feed waters and the cake compressibility. With the relationship, the cake compressibility under different experimental conditions was investigated. Experimental data revealed that cake compressibility is dependent on the intrinsic properties of the colloidal particles and is independent of the colloid concentration in the feed water and the membranes used in the fouling experiments. The feed water ionic strength was found to have a significant influence on the compressibility of the colloidal cake. Experimental data indicated a strong linear relationship between compressibility and feed water ionic strength, which could be related by either a power law function or a natural logarithmic function. Solution pH also has an important effect on colloidal cake compressibility, which decreased as feed water acidity increased. However, the adsorption of ions and molecules on the colloidal silica surface could have a substantial influence on the compressibility of the colloidal cakes. This was evident from the higher compressibility of feed waters with pH adjusted using citric acid as compared to HCl. Adsorption of citrates on the silica surface increased the colloidal surface potential resulting in stronger repulsive forces within the cake layer and therefore higher compressibility values.

Through the results in this study, a better understanding of the effects of solution chemistry on the compressibility of colloidal cakes emerges. Charged colloidal particles commonly present in aquatic environments would exhibit high compressibilities in membrane processes. On the other hand, uncharged colloidal particles (rigid) would pack at the maximal cake concentration and therefore under pressure would not undergo significant compressibility. Changes to feed water properties such as increasing ionic strength and adjusting solution pH

to values nearer the point of zero charge of the colloidal particles can reduce compressibility as shown from the experimental data in this chapter. Ideally such changes to feed water cause the colloids to behave like rigid particles that exhibit no charge characteristics. From this chapter, it becomes evident that compressibility is controlled by the balance of the permeation drag force applied by the driving pressure on the colloidal cake and the counter-acting repulsive EDL forces which dominate the colloidal interactions within the cake layer. The balance of these external (permeation drag) and internal (colloidal interaction) forces is critical to fouling and will be further discussed in the next chapter.

Chapter 7

Predicting the Fouling Potential of Colloidal Feed Waters

7.1 Introduction

In Chapters 4 and 5 it was empirically shown that the colloidal fouling potential is strongly affected by the properties of the feed water or its chemistry e.g. its ionic strength, pH, colloidal concentration, etc. Subsequently in chapter 6, the impact of the physical hydrodynamic drag force on colloidal fouling was quantified and investigated for different solution chemistries. The strong dependence of colloidal fouling on these physicochemical factors alludes to the possibility of a theoretical correlation between the basic feed water parameters (e.g. ionic strength, colloid size, colloid zeta potential, etc) and the colloidal fouling potential. An attempt will be made in this chapter to numerically calculate the colloidal fouling potential from fundamental principles of colloidal interactions and membrane fouling theories.

It is generally accepted that colloidal fouling results in a colloidal cake, wherein the colloidal particles are in a "frozen" or immobile state due to the confinement of neighboring particles. The validity of assuming the formation of a cake layer on the membrane surface will be revisited subsequently in the chapter. An immediately apparent distinction of the cake layer to the bulk solution is it's much higher colloidal or solids volume fraction as shown pictorially in Fig. 7.1. The colloidal volume fraction of the cake layer is difficult to measure or determine experimentally (Bacchin *et al.*, 2002; Tarabara *et al.*, 2004). Colloidal particles within the cake layer are subject to the influence of hydraulic and colloidal interfacial interaction forces. As schematically shown in Fig. 7.1, the colloidal particles in the cake layer achieve equilibrium or are "solidified" in their specific positions by the balance of the forces acting on them. If the equilibrium position of a particle in the cake under the influence of various forces

can be calculated, and the interparticle distance, h_{cake}, known, then the colloidal volume fraction of the cake layer can be determined.

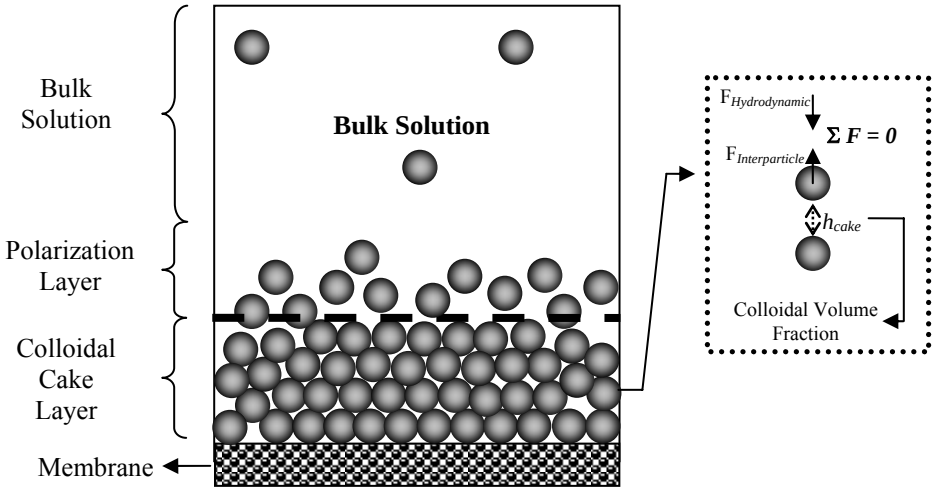

Fig 7.1: The interparticle distance and solids volume fraction of the colloidal cake layer can be found by determining the equilibrium position of a particle in the cake layer under all forces.

Generally, the colloidal volume fraction of a cake layer is usually sufficient for the determination of the colloidal cake resistance. However, often mathematically predicted colloidal fouling models do not fit with experimental results and, inevitably, correction factors are introduced (Hwang *et al.*, 1998; Kim and Hoek, 2002; Bowen *et al.*, 2003; Kim *et al.*, 2006). A possible factor which could contribute significantly to colloidal fouling is postulated to be the viscosity of the liquid within the narrow pores of the colloidal cake. It is suggested here that the liquid viscosity within the pores of the cake for small colloids, could deviate substantially from that in the bulk solution. This would contribute greatly to the determination of the resistance of the cake layer.

In this chapter, the main objective is to predict the fouling potential based on water properties and membrane operating conditions, through fundamental principles of colloidal interaction. Through this predictive model, a better understanding of how the various physicochemical factors affect colloidal fouling will be sought.

7.2 Theoretical Development

7.2.1 Colloidal Volume Fraction of the Cake Layer

The colloidal volume fraction of the cake layer is a fundamental parameter representing the characteristics of the cake which dictates the fouling potential. The determination of the colloidal volume fraction of cake layer is therefore a primary step for evaluating the colloidal fouling potential. In the colloidal cake layer, interparticle interactions coupled with hydrodynamic forces determine all the dynamic and static properties of the colloidal particles in it.

The balance of these forces on individual particles within the cake layer eventually establishes the equilibrium configuration of the cake and its average colloidal volume fraction. Here, a simplified analytical approach considering the summation of all the forces acting between two particles set to zero is used to determine the average interparticle distance (h_{cake}) in the colloidal cake layer as summarized in Eq. (7.1) below

$$\sum F(h) = F_{LW}(h) + F_{EDL}(h) + F_{AB}(h) + F_{HD}(h) = 0 \qquad (7.1)$$

The forces with subscripts *LW*, *EDL*, *AB* and *HD* depicted above are the London-van der Waals, Electrical double layer, Acid-Base and Hydrodynamic Drag forces respectively. Gravitational force and axial forces due to crossflow velocity are negligible because the colloidal particles in this study are smaller than 0.1μm (Wiesner et al., 1989; McDonogh et al., 1992; Bacchin et al., 1995). The average interparticle distance where the net force acting between two particles is zero, represents the configuration of minimum interaction energy under isothermal and isobaric conditions. Although microscopically the consideration of forces between two particles may not be exact due to multi-body effects, it is an acceptable approximation for the macroscopic interparticle packing distance in the cake layer and has been used previously to model particle interaction forces in the cake layer (Jonsson and Jonsson, 1996; Hwang *et al.*, 1998; Kim *et al.*, 2006). The mathematical expressions used for the forces are presented below.

London-van der Waals (LW) Interaction Force

The LW interaction force (F_{LW}) between two spherical particles of radius (a_p) separated by distance (h) is determined by differentiating Eq. (2.2) with respect to h resulting in (Gregory, 1981).

$$F_{LW} = \left(\frac{A_H a_p}{12h^2}\right)\left[1 - \frac{1}{1+\frac{\lambda}{bh}}\right] \tag{7.2}$$

The term in the square brackets accounts for retardation effects. λ is the 'characteristic wavelength' ($\lambda = 2\pi c/\sigma$, where c is the speed of light and σ the dispersion frequency) for the interaction and is assumed here to be 100 nm (Hwang *et al.*, 1998), the constant b = 5.32 and A_H is the Hamaker's constant taken to be 4.61×10^{-21} J for silica particles (Bergstrom, 1997). The closest approach between two particles (h_0) is assumed to be 0.158 nm, because the particles would experience infinitely high Born repulsion for approaches smaller than this value (Elimelech *et al.*, 1995).

Electrical Double Layer (EDL) Interaction Force

For low surface potentials, assuming constant surface charge as the particles approach, the repulsive EDL force between the particles is given by (Wiese and Healy, 1970).

$$F_{EDL} = -2\pi a_p \varepsilon_o \varepsilon_r \zeta^2 \kappa \left(\frac{\exp(-\kappa h)}{1-\exp(-\kappa h)}\right) \tag{7.3}$$

κ is the Debye-Huckel parameter which is the inverse of the double layer thickness and is related to the ionic strength (I) of the solution as defined in Eq. (2.4) and ζ is the zeta-potential of the colloids. The above equation is valid for cases where the particle size is large, such that $\kappa a_p > 10$. When the double layer around the particle is thick (i.e. $\kappa a_p < 5$), the EDL interaction force at constant surface charge is obtained by differentiating Eq. (2.8) with respect to h as (Verwey and Overbeek, 1948).

$$F_{EDL} = -2\pi a_p \varepsilon_o \varepsilon_r \zeta^2 \kappa \exp(-\kappa h) \tag{7.4}$$

For simplicity in Eq. (7.1), the EDL interaction force denoted in Eq. (7.4) is used only when $\kappa a_p < 5$; for all other conditions the force shown in Eq. (7.3) will be used. The negative signs for the forces indicate that they are repulsive.

Acid Base (AB) Interaction Force

The free energy of interaction due to acid-base (U_{AB}) interactions between two colloidal particles of radius (a_p) separated by distance (h) can be approximated by (van Oss, 1994)

$$U_{AB}(h) = \pi a_p l_{AB} U_{h0} \exp(\frac{h_0 - h}{l_{AB}}) \tag{7.5}$$

Where l_{AB} is the correlation length, i.e. the scale over which the interaction force will decay. For repulsive acid-base interactions the correlation length is smaller than 1.0 nm, with a value of 0.6 nm generally used (van Oss, 1990). This equation is valid for $h > l_{AB}$. Differentiating Eq. (7.5), an expression for the interaction force is obtained

$$F_{AB}(h) = -\pi a_p U_{h0} \exp\left(\frac{h_0 - h}{l_{AB}}\right) \tag{7.6}$$

Where U_{h0} is the interaction energy between two parallel flat surfaces at the minimum equilibrium distance (h_0 = 0.158 nm). This value is taken to be 6.57×10^{-3} J/m^2 as measured by Kim *et al.*, (2006) for similar silica colloidal particles used in this study.

Hydrodynamic Drag Force

The hydrodynamic (HD) or permeation drag force is the most fundamental force dictating cake formation in membrane processes and originates from an external force (driving pressure) applied to the feed water. The hydrodynamic force is expressed by the modified Stokes-Einstein equation as (Happel and Brenner, 1991; Elimelech and Bhattacharjee, 1998);

$$F_{HD} = \frac{k_B T}{D} v A_S \tag{7.7}$$

Where v is the permeate velocity, D is the diffusion coefficient, and A_S is the hydrodynamic correction factor. For concentrated colloidal systems such as in a cake layer, the Happel's

sphere-in-cell model is commonly used for the hydrodynamic correction factor as shown in Eq. (7.8) where ϕ_c is the solids or colloidal volume fraction of the cake (Happel and Brenner, 1991; Bhattacharjee *et al.*, 1999):

$$A_S = \frac{1+\frac{2}{3}\phi_c^{\frac{5}{3}}}{1-\frac{3}{2}\phi_c^{\frac{1}{3}}+\frac{3}{2}\phi_c^{\frac{5}{3}}-\phi_c^2} \tag{7.8}$$

In a dilute liquid medium, the diffusion coefficient (D) of a particle is given by the Stokes-Einstein equation

$$D = \frac{k_B T}{6\pi\mu a_p} \tag{7.9}$$

Where μ is the viscosity of the surrounding liquid (Bulk water viscosity is 8.9×10^{-4} Pa.s at 25°C). Therefore the expression for the hydrodynamic drag force between the colloidal particles in the cake layer is given by

$$F_{HD} = 6\pi\mu a_p v\left(\frac{1+\frac{2}{3}\phi_c^{\frac{5}{3}}}{1-\frac{3}{2}\phi_c^{\frac{1}{3}}+\frac{3}{2}\phi_c^{\frac{5}{3}}-\phi_c^{2}}\right) \tag{7.10}$$

Once the average interparticle distance, h_{cake}, is known, the colloidal volume fraction of cake layer is then determined from Eq.(7.11),

$$\phi_c = \phi_{\max}\left(\frac{2a_p}{2a_p+h_{cake}}\right)^3 \tag{7.11}$$

where $\phi_{\max}$ is the theoretical maximum random packing colloidal volume fraction for monodispersed particles, which is 0.64, ϕ_c is the colloidal volume fraction of the cake layer, and a_p the mean radius of the colloidal particles.

7.2.2 Resistance of the Cake Layer

Classically, the resistance to permeate transport through an assemblage of particles is the product of the thickness of the layer (δ) and the specific cake resistance (r_c) as shown below.

$$R_C(t) = r_c \delta(t) \tag{7.12}$$

δ is related to the deposition rate (= $v\phi_b$, where ϕ_b is the colloidal volume fraction in the bulk) of the particles on the membrane surface and is given by (Romero and Davis, 1990),

$$\delta(t) = \frac{1}{\phi_c - \phi_b} \int_0^t v\phi_b .dt \tag{7.13}$$

The specific cake resistance in this study is calculated with the Carman-Kozeny method (Eq. (2.16)), which is approximately equivalent to the Happel model for a Kozeny constant of 5 as discussed in Chapter 2.

$$r_c = \frac{45\mu\phi_c^2}{a_p^2(1-\phi_c)^3} \tag{7.14}$$

Eqs. (7.13) and (7.14) coupled with Eq. (2.11) can be solved simultaneously to obtain the permeate flux and cake thickness, with an iterative approach similar to that of Kim *et al*. (2006). This permits the calculation of the fouling potential as described in Eq. (3.2).

A relatively thin cake layer that is built up due to the production of 10^{-4} m^3 of permeate per unit area of membrane is considered in this study. Therefore a constant colloidal volume fraction of the cake layer can be reasonably assumed.

7.2.3 Liquid Viscosity in the Pores of the Colloidal Cake Layer

The liquid viscosity within the pores of an assemblage of colloidal particles on the membrane surface is postulated here to affect colloidal fouling. The impact of liquid viscosity within the pores has been rarely contemplated in previous studies of colloidal fouling and the bulk viscosity (colloidal suspension viscosity) or water viscosity is commonly used. While the use of bulk viscosity might be appropriate for macroscopic particles (micrometer range and

above), it may not be so for colloidal particles where the pores are narrow and in the nano-scale (Nirschl and Schafer, 2005).

Although the knowledge of liquid properties in narrow spaces and nano-sized pores is still rudimentary, it is universally accepted that the liquid rheology in these confines is significantly different from bulk water (Happel and Brenner, 1991; Lyklema, 1991; Hunter, 2000). The viscosity of water in fine capillaries with diameters in the range of tens of nanometers has been found to be significantly higher than the bulk liquid viscosity (Bowen and Jenner, 1995b; Churaev, 2000). This increase in liquid viscosity in narrow confines has been attributed to the structuring of water near the surface of the solid walls or electroviscous effects. However, the electroviscous effect as described in Chapter 2, is inconspicuous for capillaries of radii $\leq$ 50nm (Churaev, 2000) and so may not play a significant role for the colloidal cakes in this study. The vicinal liquid or water structurally modified due to its proximity to a particle interface has a much higher viscosity compared to that of the bulk liquid as shown in Fig. 7.2 (Schufle *et al.*, 1976; Lyklema, 1991; Hunter, 2000).

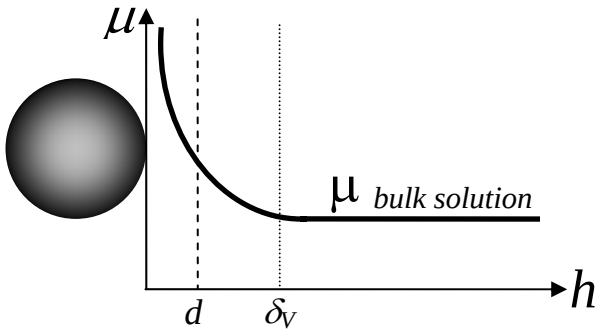

Fig. 7.2: Variation of liquid viscosity with distance away from the surface of the particle is shown by the solid line (Lyklema, 1991; Hunter, 2000). *d* and δ_V represent the surface of shear and the thickness of the vicinal water layer.

The viscosity gradually decreases from an infinite viscosity at the surface of the particle to the bulk solution viscosity as shown by the solid line in Fig 7.2. δ_V and *d* represent the thickness of the vicinal water layer and the shear plane, respectively. The ratio of vicinal water

thickness to particle size increases with decreasing particle diameters (Schufle *et al.*, 1976), making the consideration of viscosity in the pores of colloidal (especially nanoparticles) cakes more critical than larger particulate cakes. Determination of viscosity within the pores of the colloidal cake layer is complex. Besides the difficulty in studying the properties of a liquid near a surface, other complexities stem from the ambiguous nature of the cake layer, making it impossible to mimic the actual conditions for measurement of viscosity ex-situ. Given the heterogeneous nature of the pores within the cake layer, the value of viscosity of the liquid within the pores can only be an average value at best. Nevertheless, liquid viscosity in the porous colloidal cake layer could be a crucial parameter in fouling assessment because it influences the hydrodynamic forces between the particles (Eq. 7.10), as well as the determination of specific resistance of the cake layer (Eq. 7.14).

A dimensionless parameter, the relative viscosity ($\mu_r = \mu^*/\mu$ with μ^* and μ being water viscosities in the concentrated cake and dilute suspensions, respectively), is introduced as a correcting factor for the possible elevated viscosity of water in the pores of the cake. Initially, the value of $\mu_r = 1$, is used to determine the theoretical fouling potential based on the fundamental colloidal interaction and cake formation equations as highlighted in the numerical procedure. Any difference between the experimentally determined fouling potential and theoretical fouling potential is then attributed to the liquid viscosity in the pores of the colloidal cake. In this study the relative viscosity is treated as a constant, i.e. it does not vary with time.

7.2.4. Numerical Procedure

The numerical procedure for determining the colloidal fouling potential theoretically is shown in Fig. 7.3. Input parameters are first initialized, which include the colloidal volume fraction in the feed water (ϕ_b), relative viscosity, zeta potential of the colloids (ζ), ionic strength (I), mean radius of the colloids (a_p), driving pressure (ΔP), and membrane resistance (R_0). In

addition, the time step (Δt) and the volume of permeate to be collected (V_{limit}) for which the analysis is conducted are also specified.

The calculation of permeate flux and cake resistance at any time step is determined by a successive iteration procedure (Kim *et al.*, 2006). First, an arbitrary value for the permeate flux, v, is chosen. This permits the determination of the hydrodynamic force shown in Eq. 7.10 and the interparticle distance (h_{cake}) obtained from the force balance (Eq. 7.1). With the interparticle distance, the colloidal volume fraction of the cake layer (ϕ_c) can be calculated from Eq. 7.11. The thickness of the cake layer can then be determined by numerical integration of Eq (7.13). Following this, the cake resistance (R_c) can be calculated from the cake specific resistance through Eq. 7.14 and the cake thickness. The permeate flux is then calculated from the general filtration equation and compared with the initial permeate flux v. If the difference between the two permeate fluxes is greater than the tolerance level (set as 10^{-9} m/s in this study), the initial permeate flux is replaced by the new calculated permeate flux and the steps described above are repeated until the tolerance is met. The volume of permeate collected for that time step, $V(t)$, is calculated by the trapezoidal rule. Therefore, a small time step is recommended to minimize numerical errors. The numerical procedure will then proceed to the next time step until the cumulative volume of permeate collected (V_{limit}) is reached (10^{-4} m is used here). The theoretical colloidal fouling potential (k_{mod}) is then determined from the total increment in membrane resistance (ΔR) and the total volume of permeate collected as described in Eq. (3.2).

Since the relative viscosity (μ_r) is unknown, an additional iteration step is added to determine its value as shown by the dotted section in Fig. 7.3. The calculated fouling potentials are compared against the experimentally determined ones (k_{exp}) under the same condition. The relative viscosity is successively iterated by a linear interpolation method until the absolute percentage difference between the fouling potentials is less than 0.1%.

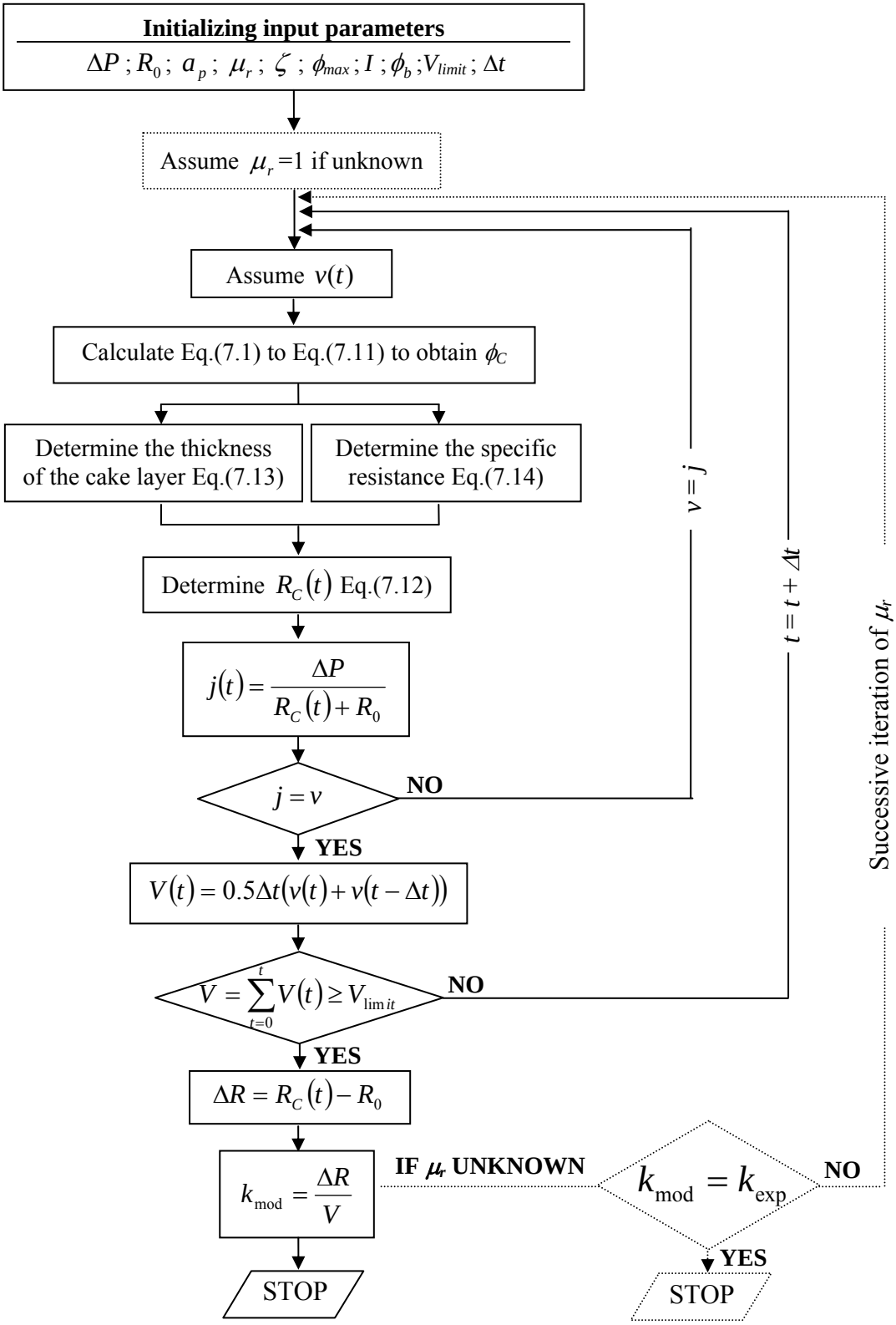

Fig 7.3: Numerical algorithm to determine the theoretical fouling potential from the physicochemical conditions. The determination of the relative viscosity if unknown is shown in the dotted section.

7.3 Calibration with Experiments

7.3.1 Permeate Flux Decline

As an example, the numerical simulation of the permeate flux decline curve from the model is plotted against the experimental data in Fig. 7.4 for different relative viscosity values. The filtration experiment was conducted on feed water containing ST20L colloids of a_p= 35 nm, ϕ_b= 5.28×10^{-4} v/v, zeta-potential= -39.3mV, ionic strength= 0.1M, in a crossflow tubular, titania membrane (see sections 3.4.1) of resistance= 7.58×10^{9} Pa.s/m under an applied pressure= 490kPa. For water viscosity within the pores assumed to be equal to the bulk water viscosity, i.e. μ_r = 1, the predicted flux decline curve severely underestimates the experimental flux. This implies that the relative viscosity within the pores is much higher than the bulk liquid viscosity. The best fit between the experimental and simulated permeate flux data is observed for μ_r = 7.33, which was numerically determined by the method described above. The simulated permeate flux curve declines more severely as the relative viscosity value increases, as seen for μ_r = 12.

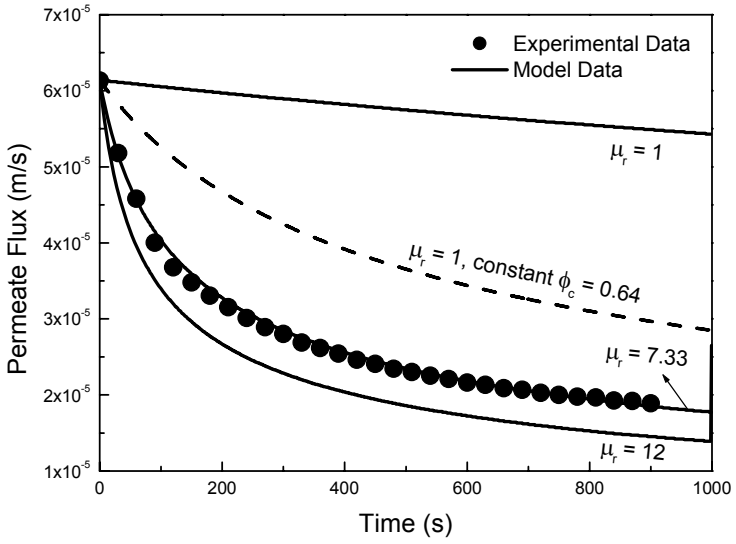

Fig. 7.4: Simulated permeate flux decline curves for different relative viscosity values and conditions against experimental data.

The difference between experimental and model predicted colloidal fouling data is often minimized by introducing drag force corrections or additional interaction forces between the particles (Hwang *et al.*, 1998; Bowen *et al.*, 2003; Kim *et al.*, 2006). As noted from Eq. (7.1) and (7.11) these corrections affect the cake volume fraction. To evaluate if the difference in our theoretical and experimental data could be due to these factors, the simulated permeate flux curve for $\mu_r = 1$ and assuming the cake to be at the maximum volume fraction of 0.64 throughout the filtration is shown as the dashed line in Fig. 7.4. This corresponds with the situation where the particles in the cake layer are in contact with each other (i.e. $h_{cake} = 0$) and at the tightest permissible cake structure as defined by maximum random close packing. As seen, the simulated flux still underestimates the experimental flux, indicating that these factors, even if present, do not aid in minimizing the difference between the experimental and theoretical data. From this observation, it is concluded that there is another mechanism, which is unaccounted for, that is controlling colloidal fouling. In this chapter, that mechanism is attributed to the higher relative viscosity within the pores of the colloidal cake. With this understanding, it is necessary to investigate how the relative viscosity value changes under various conditions.

7.3.2 Relative Viscosity and Cake Volume Fraction

Fouling potentials previously determined from filtration experiments, reported in Chapters 4 and 6, are used to determine the relative viscosity in the cake layer under varying feed water conditions and driving pressures. For each set of conditions, the relative viscosity value is determined by setting the absolute difference between the experimental fouling potential (k_{exp}) and the theoretical one (k_{mod}) to smaller than 0.1% in the numerical model. The numerically obtained relative viscosities and cake volume fractions under 40 different physicochemical conditions are summarized in Table 7.1 and Fig. 7.5.

Table 7.1: Relative viscosities for different combinations of salt concentration, colloidal concentration, driving pressure, membrane resistance, zeta potential and particle radius.

(ϕ_b) Colloid Concentration in bulk $\times10^{-4}$	(ΔP) Applied Pressure (kPa)	(I) Ionic Strength (mol/L)	(ζ) Zeta Potential (mV)	(a_p) Particle radius (nm)	(R_0) Membrane Resistance $\times10^{9}$ (Pa.s/m)	(k_{exp}) Fouling Potential $\times10^{11}$ (Experimental)	(μ_r)* Relative Viscosity	(ϕ_c)* Cake Volume Fraction
Data from Chapter 4								
1.08	280	0.005	-40	42	2.29	0.91	6.57	0.542
1.08	280	0.01	-40	42	2.29	1.11	6.84	0.561
1.08	280	0.02	-40	42	2.29	1.43	7.70	0.576
1.08	280	0.03	-40	42	2.29	1.54	7.91	0.582
2.65	280	0.005	-40	42	2.29	2.44	7.05	0.546
2.65	280	0.01	-40	42	2.29	2.82	7.03	0.562
2.65	280	0.02	-40	42	2.29	3.45	7.63	0.575
2.65	280	0.03	-40	42	2.29	3.60	7.62	0.580
5.13	280	0.005	-40	42	2.29	4.74	7.09	0.545
5.13	280	0.01	-40	42	2.29	6.00	7.55	0.564
5.13	280	0.02	-40	42	2.29	6.93	7.88	0.576
5.13	280	0.03	-40	42	2.29	7.32	7.97	0.581
4.28	280	0.001	-40	42	2.29	2.25	7.53	0.479
4.28	280	0.005	-40	42	2.29	3.72	7.74	0.543
4.28	280	0.01	-40	42	2.29	4.52	7.01	0.561
4.28	280	0.02	-40	42	2.29	5.50	7.57	0.575
4.28	280	0.03	-40	42	2.29	5.89	7.73	0.580
4.28	280	0.1	-40	42	2.29	6.85	8.07	0.592
4.28	280	0.2	-40	42	2.29	7.32	8.26	0.597
Data from Chapter 6								
2.45	210	0.005	-39.5	35	2.29	2.17	7.81	0.481
2.45	280	0.005	-39.5	35	2.29	2.52	7.32	0.509
2.45	350	0.005	-39.5	35	2.29	2.81	7.00	0.528
2.45	420	0.005	-39.5	35	2.29	3.42	7.23	0.547
2.45	210	0.01	-40.4	35	2.29	2.70	7.62	0.512
2.45	280	0.01	-40.4	35	2.29	2.94	7.17	0.530
2.45	350	0.01	-40.4	35	2.29	3.35	7.18	0.546
2.45	420	0.01	-40.4	35	2.29	3.90	7.49	0.559
2.45	210	0.05	-39.5	35	2.29	3.55	6.80	0.559
2.45	280	0.05	-39.5	35	2.29	3.90	6.93	0.568
2.45	350	0.05	-39.5	35	2.29	4.20	7.07	0.574
2.45	420	0.05	-39.5	35	2.29	4.69	7.49	0.580
2.45	210	0.1	-39.3	35	2.29	3.98	6.89	0.570
2.45	280	0.1	-39.3	35	2.29	4.32	7.07	0.577
2.45	350	0.1	-39.3	35	2.29	4.55	7.15	0.582
2.45	420	0.1	-39.3	35	2.29	5.15	7.74	0.587
5.28	210	0.1	-39.3	35	7.58	6.20	6.21	0.545
5.28	280	0.1	-39.3	35	7.58	7.03	6.63	0.552
5.28	350	0.1	-39.3	35	7.58	7.45	6.75	0.557
5.28	420	0.1	-39.3	35	7.58	8.17	7.10	0.561
5.28	490	0.1	-39.3	35	7.58	8.43	7.33	0.564

* Values obtained from model predictions

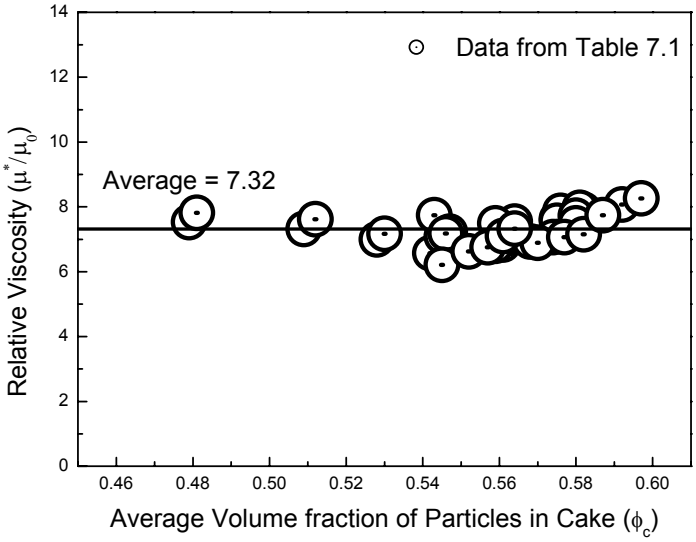

Fig. 7.5: Plot of relative viscosities and colloidal cake volume fractions. The relative viscosity is independent of colloidal volume fraction with an average relative viscosity, μ_r of 7.32.

The relative viscosity values determined, fall in a narrow range from 6.21 to 8.26 (the statistical mean and standard deviation are 7.32 and 0.44 respectively) and are independent of the cake volume fraction. As noted from Table 7.1, the relative viscosity values are also relatively independent of the feed water chemistry and the membrane operating conditions. Interestingly, the liquid viscosity in the pores of the colloidal cake layer ($\approx 6.5\times10^{-3}$ Pa.s), is more than 7 times the bulk liquid viscosity. This is much higher compared to the relative viscosity found in fine capillaries, which tend to range from 1.5 to 2.0 (Churaev, 2000). Assuming that the theoretical development and the assumptions made are representative of actual conditions, the higher relative viscosity could be due to the more tortuous three dimensional paths through which the liquid traverses in the colloidal cake layer thus inducing greater friction. In contrast, the flow in an engineered capillary is smooth and uni-dimensional. The objective here, however, is not to go into the details of the relative viscosity within the pores of the colloidal cake but rather the prediction of the colloidal fouling potential from the numerical model developed. For this purpose, a universal relative viscosity of 7.32 will be used in all the subsequent analysis in this study. To address more

comprehensively the issue of the relative viscosity within the pores of the colloidal cake, a future study with better experimental design is required. However, this lies outside the scope of the current study. In the next section, focus is shifted briefly to the issue of colloidal cake formation which was assumed throughout this thesis.

7.3.3 Colloidal Cake Formation

It is widely accepted that a colloidal cake layer forms as a result of the filtration of the feed waters containing colloidal particles. Cake formation is supported by many experimental and theoretical studies. In this section, an additional and novel means for indicating the formation of a cake from the fundamental colloidal interactions is presented.

According to the order-disorder theory in fluid rheology, there exists an order-disorder colloidal volume fraction ($\phi_{o/d}$) for colloidal systems under which the suspension undergoes a transition from a disordered liquid state to an ordered solid state (Barker and Henderson, 1967; Russel *et al*., 1989). For charged colloidal systems, the colloidal suspension becomes an ordered, face-centered cubic solid above the order-disorder colloidal volume fraction given below as

$$\phi_{o/\,d} = 0.55\left(\frac{2a_p}{d_{eff}}\right)^3 \tag{7.15}$$

where d_{eff} is the effective collision diameter for charged colloidal particles (Russel *et al.*, 1989). By applying a superposition approximation, the effective collision diameter for charged particles (d_{eff}) is given by (Barker and Henderson, 1967; Chan *et al.*, 1968).

$$d_{eff} = 2a_p + \int_{2a_p}^{\sigma}\left[1-\exp\left(-U/k_bT\right)\right]dr \tag{7.16}$$

Where r is the centre-to-centre distance between the colloids, U is the total interaction energy potential and σ is the distance such that $U(\sigma) = 0$. With this expression the order-disorder solids volume fraction can be determined.

The critical order-disorder volume fractions calculated with Eqs (7.15) and (7.16) for the colloidal suspensions in Table 7.1 are plotted as solid data points (●) against the double layer thickness (1/κ) in Fig. 7.6. The order-disorder volume fraction for hard spheres is 0.55 as shown by the horizontal line in the figure. The order-disorder colloidal volume fraction for the charged sphere decreases from the hard sphere order-disorder volume fraction of 0.55 with increasing double layer thickness as reported previously (Hachisu and Kobayashi, 1974). The colloidal volume fraction of the fouling layer (last column in Table 7.1) determined in the calculation of the colloidal fouling potential are also indicated (⊙) in Fig. 7.6.

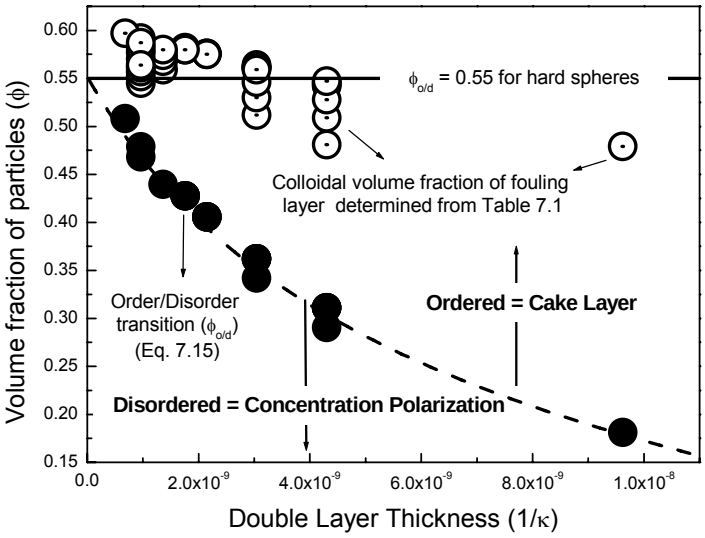

Fig. 7.6: The order-disorder colloidal volume fraction obtained from Eq. (7.15) using the input parameters from Table 7.1 are shown as solid points (●). The dotted line is to guide the eyes. The colloidal volume fractions of the fouling layer determined from the theoretical study all fall above this line indicating that a cake forms on the membrane surface.

From the plot, it is evident that for all experiments, the colloidal volume fractions of the fouling layer are much higher than the corresponding critical order-disorder colloidal volume fraction. The result verifies that the colloidal fouling layer on the membrane surface is in an ordered, immobile state i.e. a cake. To our knowledge, this is the first time such an approach has been used to determine if the fouling layer exists as a cake.

7.3.4 Verification of Predicted Fouling Potential with Experiments

A relative viscosity value of 7.32, as found previously, is used in all the theoretical calculations of the fouling potential and comparisons are made against the experimentally determined fouling potential values. Initially, comparisons between the predicted fouling potentials from the numerical procedure and the experimental fouling potential are made for data presented in Table 7.1. Subsequently, independent experimental data from Chapter 5, where the zeta potential changes significantly, are used for the comparison between the two fouling potentials for this constant relative viscosity value.

In Fig. 7.7, experimental fouling potentials for feed waters containing different colloidal concentrations and feed water ionic strengths from Chapter 4 are shown as data points. The theoretical predictions for the fouling potential from the numerical procedure under those feed conditions and using a constant relative viscosity of 7.32 are indicated by the solid lines. The graph indicates a relatively close fit between the numerically predicted and experimentally determined fouling potential values. The average percentage difference between the predicted and experimentally determined fouling potential values is approximately 8%.

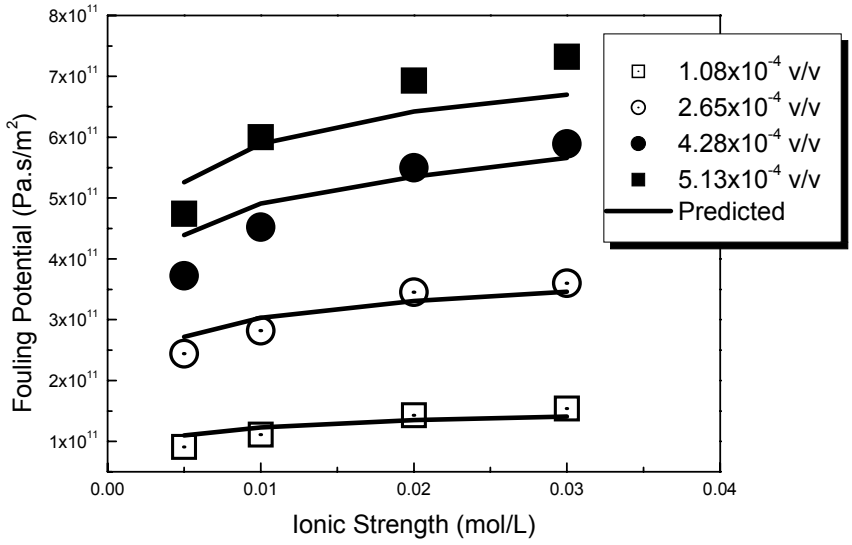

Fig. 7.7: Theoretical fits with experimental data from Chapter 4 (Table 4.1 & 4.2). Theoretical simulations were made with a relative viscosity value of 7.32.

Similarly, a close fit between the fouling potentials determined experimentally and through the numerical procedure are found when the driving pressure and membrane resistance are varied as shown in Figs 7.8a & 7.8b for data obtained from Chapter 6 (Fig 6.6a and 6.2b respectively). The average differences between the predicted and experimental fouling potentials are 5.6% and 3.8%, respectively.

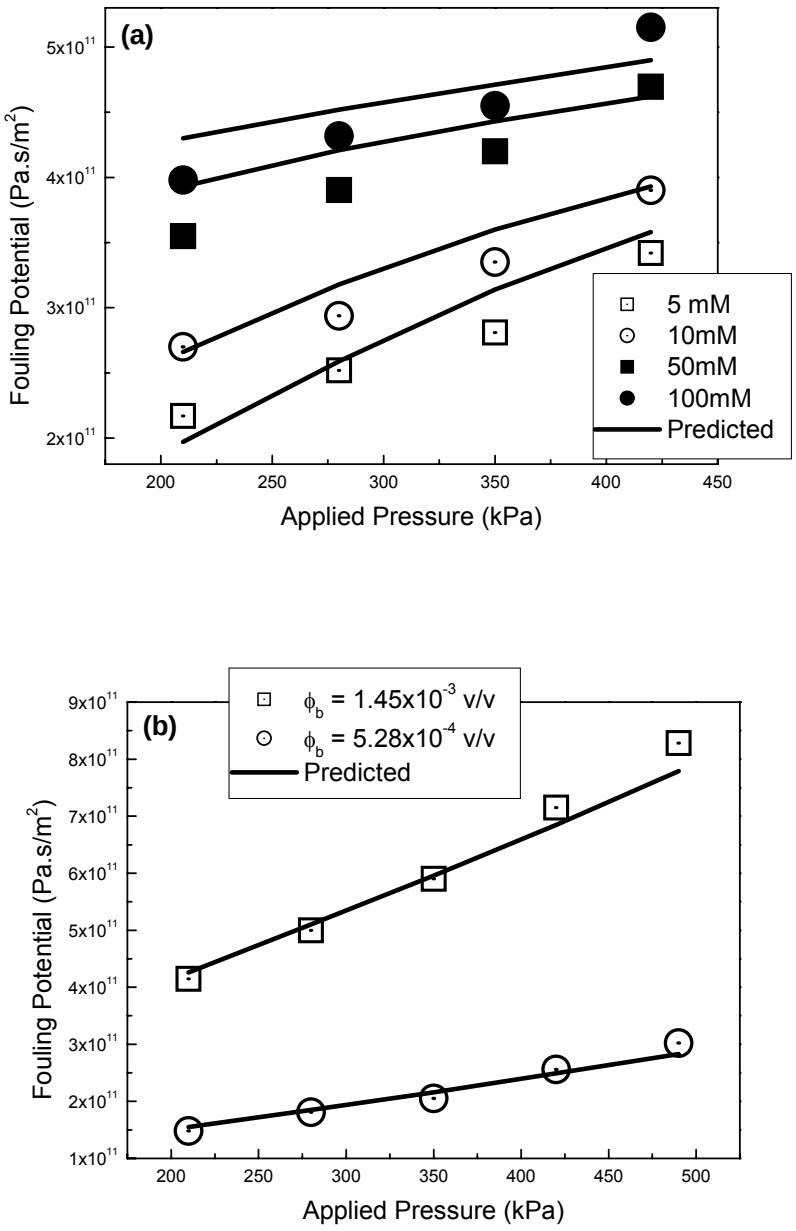

Fig. 7.8: Comparison of the predicted fouling potential using relative viscosity = 7.32 against experimental fouling potentials at various driving pressures for (a) colloidal concentration = 2.45×10^{-4} v/v on a zirconia membrane of resistance 2.29×10^{9} Pa.s/m (Fig. 6.6a) (b) various colloidal concentration on a titania membrane of resistance 7.58×10^{9} Pa.s/m (Fig. 6.2b).

Experimental data of the feed water fouling potential under various ionic strengths and pH values from Chapter 5, not used in the determination of the average relative viscosity in Table 7.1, are evaluated next. This group of data is used to test if the fouling potential can be theoretically predicted for these diverse feed water conditions. The numerical predictions of the fouling potential are shown (lines) together with fouling potential obtained experimentally (symbols) in Fig. 7.9.

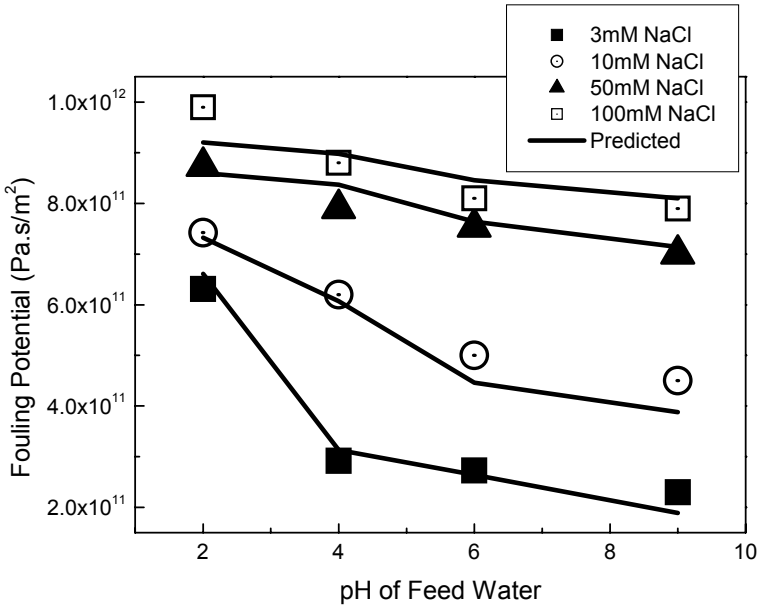

Fig. 7.9: Prediction of the fouling potential for feed waters containing ST20L colloids at different feed water pH and ionic strength (from Fig 5.5) (shown as solid lines) A good close fit is obtained with the average difference in fouling potential values less than 6%.

The graph indicates that the numerical predictions of the fouling potential fit the experimentally determined ones very well with an average difference of less than 6%. To further demonstrate the excellent fit, the predicted fouling potentials are plotted against the experimental fouling potentials in Fig. 7.10. The close fit of the data along the line of equality confirms that an average relative viscosity value of 7.32 is suitable to predict the fouling potential for the colloidal particles used in this study under the different membrane operating conditions and feed water chemistries.

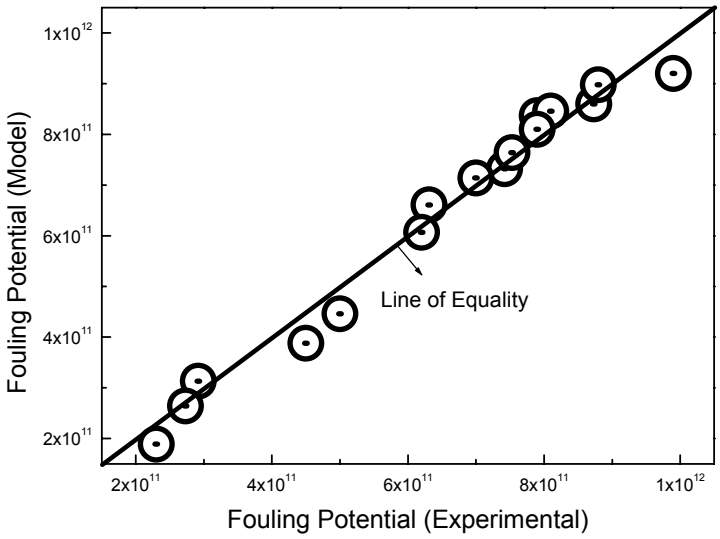

Fig. 7.10: Plot of theoretical fouling potentials (from the numerical model) against experimental ones. The data falls closely along the line of equality.

7.4 Simulation Study

The colloidal fouling potential is investigated theoretically for the effect of common feed water chemistry parameters in this section. A relative viscosity of 7.32 is used in all the simulations and the effects of feed water ionic strength, pH, colloidal concentration and operating pressure on the fouling potential are elucidated. This simulation study will serve to both validate previous experimental findings and also provide useful insights on colloidal fouling, beyond what has been discussed in the previous chapters. Unless otherwise stated, the simulation conditions used in this section are colloid radius =40 nm, colloidal concentration = 3.0×10^{-4} v/v, zeta-potential = -40mV, driving pressure = 280kPa, and membrane resistance = 2.0×10^{9} Pa.s/m.

7.4.1 Effect of Ionic Strength on Fouling Potential

The simulated fouling potentials determined for different ionic strengths and colloidal concentrations are plotted in Fig 7.11a and Fig. 7.11b for the same data.

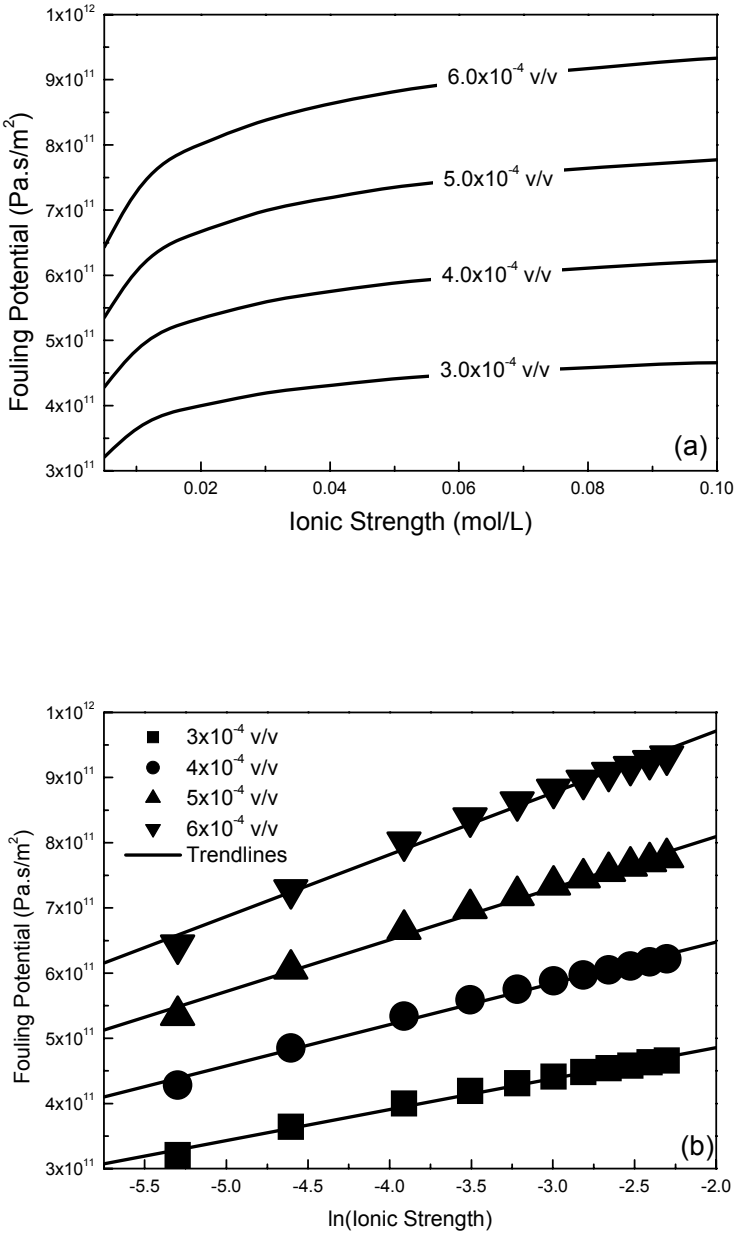

Fig. 7.11: (a) Fouling potentials at different feed water ionic strength for various colloidal concentrations. (b) Relationship between fouling potential and natural logarithmic of ionic strength for the simulated data. All trendlines have regression coefficients greater than 0.99.

As seen from Fig. 7.11a, the fouling potential increases with ionic strength at a decreasing rate for all colloid concentrations. The fouling potential can be related to ionic strength by a natural logarithmic relationship as supported from Fig 7.11b, where all trendlines have regression coefficients greater than 0.99. This confirms the findings in Chapter 4, where it was concluded empirically that the fouling potential could be related to ionic strength by a

natural logarithmic relationship. The fouling potential increases with colloid concentration in the feed water at all ionic strengths tested. This is better illustrated in Fig. 7.12.

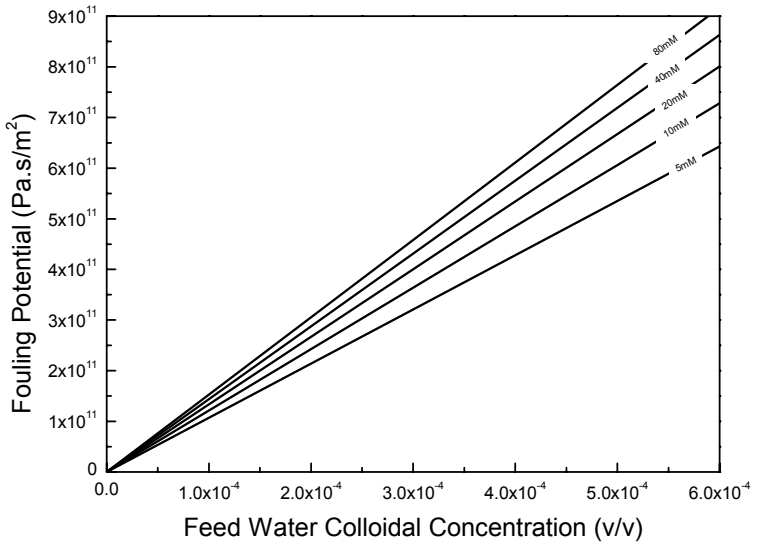

Fig. 7.12: Plot of fouling potential against feed water colloidal concentration for different feed water ionic strength.

The figure clearly indicates that the fouling potential is linearly related to colloidal concentration under constant feed water ionic strength. The slope of the lines which represent the specific fouling potential ($k_S = \frac{dk}{d\phi_b}$) increases proportionately as feed water ionic strength increases, thus verifying the bilinear model in Chapter 4.

7.4.2 Effect of Colloid Zeta-Potential on Fouling Potential

The effect of particle zeta potential on the colloidal fouling potential is investigated theoretically and the simulated results are plotted in Fig 7.13. The lines in the figure show that the colloidal fouling potential values converge to a single value (5.2×10^{11} Pa.s/m^2) as the zeta potential approaches zero. This represents the fouling potential of 'hard-sphere' colloidal particles. Similar trends were also inferred from the experimental data as highlighted in Fig. 5.7 in Chapter 5.

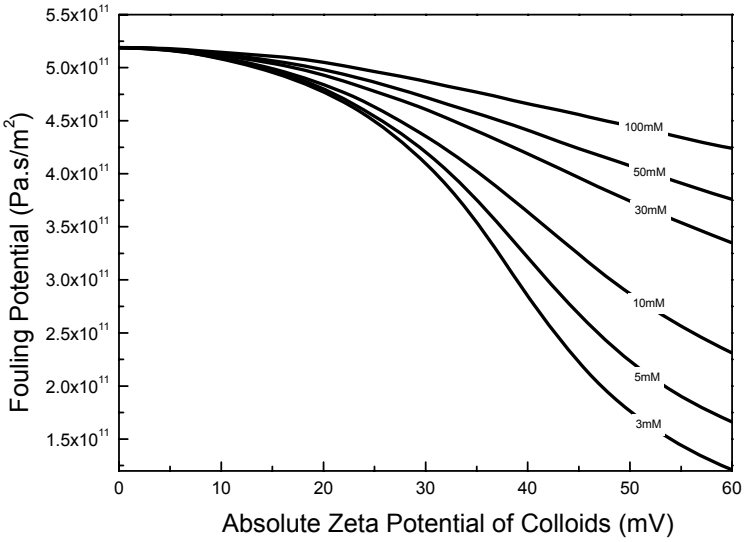

Fig 7.13: Effect of absolute zeta potential of colloidal particles on the fouling potential at different feed water ionic strengths. Colloidal concentration used in the simulation = 3.0×10^{-4} v/v, particle radius = 40 nm, membrane resistance = 2.0×10^{9} Pa.s/m and applied pressure = 280kPa.

Therefore near the isoelectric point of the colloidal particles, changes to feed water ionic strength have negligible effect on their fouling potential. According to the simulation results, at low ionic strengths (<10mM), the relationship between fouling potential and zeta potential of the colloidal particles conforms to an inverted 'S' shape. However, at higher ionic strengths (>10mM) the relationship between fouling potential and zeta potential appears to be linear for absolute zeta potential values greater than 20mV. In Chapter 5, the empirical relationship between the fouling potential and particle zeta potential was suggested to be linear from the high regression coefficients between the two parameters for the range of ionic strengths and zeta potentials tested. This corresponds with the predictions of the simulation study between the absolute zeta potential values of 25-40 mV, where the fouling potential appears to be linearly related to the zeta potential.

7.4.3 Effect of Solution Chemistry on Cake Compressibility

The compressibility of the cake layer, as defined in Chapter 6, is the slope of the plot between the specific fouling potential (k/ϕ_b) and applied pressure when plotted in logarithmic scales. Simulated data for colloidal particles with zeta potential = -56mV at different feed water ionic strengths are plotted in Fig. 7.14a in the form proposed to determine compressibility. Similarly, simulated data for constant ionic strength of 30mM and at different particle zeta potentials with all other conditions kept constant as above are plotted in Fig. 7.14b.

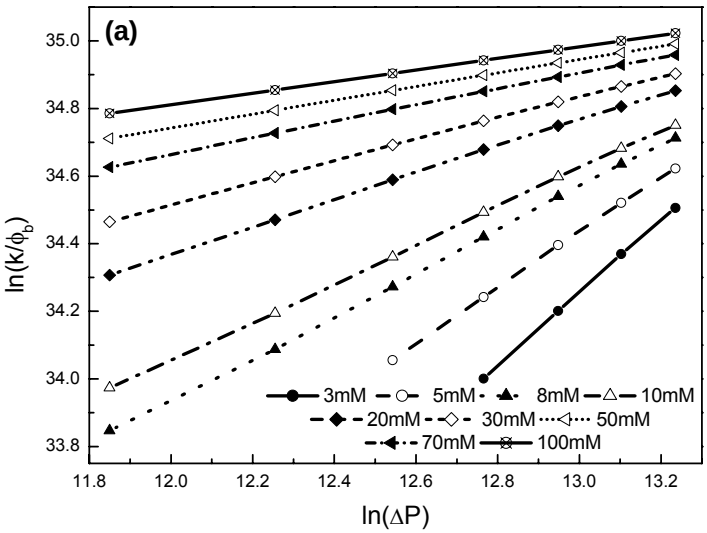

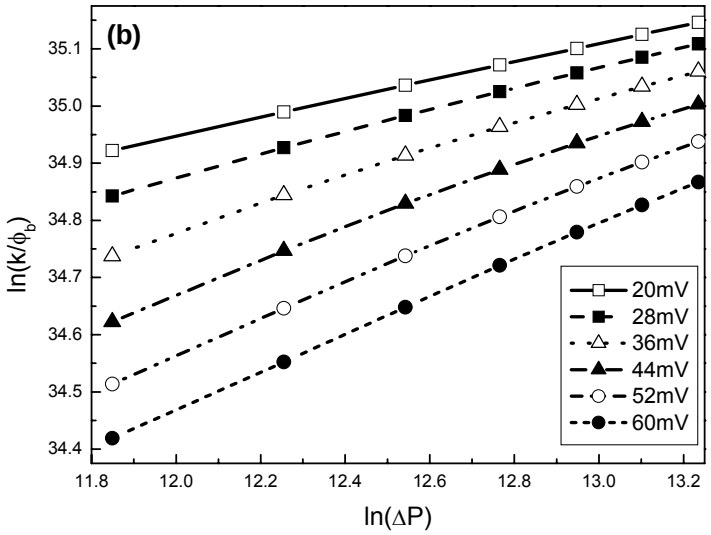

Fig. 7.14: Linear relationship between specific fouling potential (k/ϕ_b) and applied pressure (ΔP) in natural logarithmic scales at (a) different ionic strength and constant absolute zeta potential =56mV and (b) different absolute zeta potentials and constant ionic strength = 30mM. Particle radius = 40 nm and membrane of resistance = 2.0×10^9 Pa.s/m were used in the simulations.

Both figures validate the linear relationship between the specific fouling potential and applied pressure in natural logarithmic scales, derived in Chapter 6. The slopes of the lines represent the compressibility of the cake layer which is observed to be strongly influenced by the solution chemistry. A plot of the compressibility values against the ionic strength in Fig 7.15 for different particle zeta potentials provides a clearer illustration of the effects of ionic strength on compressibility of colloidal cakes. In chapter 6, it was concluded that compressibility of the cake decreased when ionic strength of the feed water increased and that compressibility and ionic strength could be well correlated either by a power law function or by a natural logarithmic relationship. The simulated compressibilities in Fig. 7.15 depict the same general trend of compressibility for different feed water ionic strengths at all zeta potential values. From Fig. 7.15 it can be further shown that the simulated relationship between compressibility and ionic strength follows a power law function for all zeta potential values. This verifies theoretically the linear relationship proposed in Eq. (6.7).

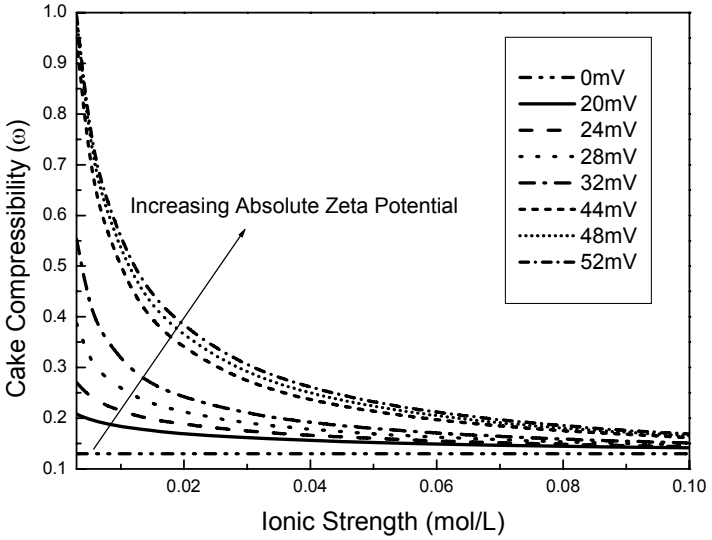

Fig. 7.15 Compressibility of the colloidal cake for feed water at different absolute colloidal zeta potentials and ionic strengths.

At the absolute zeta potential of zero, i.e. the isoelectric point of the colloids, the compressibility is independent of ionic strength and constant at approximately 0.13. Under constant feed water ionic strength, the cake compressibility increases with increasing zeta potential of the colloidal particles. This is more clearly depicted in Fig 7.16, where the compressibility is plotted against the absolute colloid zeta potential for different feed water ionic strengths. At constant feed water ionic strength, cake compressibility decreases as the zeta potential of the colloids approaches the isoelectric point (zeta potential = 0). This trend was also observed experimentally for decreasing feed water pH values in Fig. 6.9.

The predicted compressibility of the cake layer is the highest (≈ 1) at low feed water ionic strength and high particle zeta potential. This is the situation where electrokinetic phenomena (high surface potential and thick double layer) dominate the structure of the colloidal cake layer and the cake porosity is higher. By applying the same incremental driving pressure i.e. hydrodynamic drag force to a more porous cake, there is greater tendency for the porosity to

decrease significantly as compared to a tighter cake, therefore resulting in higher compressibility.

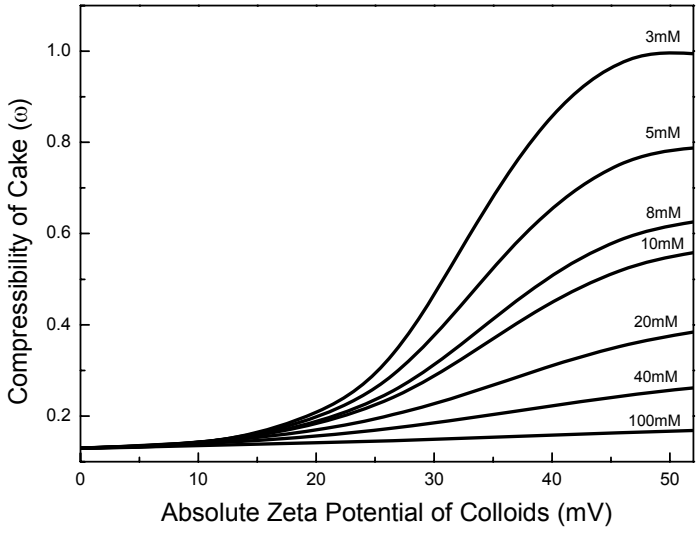

Fig 7.16: Data from Fig 7.15 plotted in terms of cake compressibility and zeta potential of the particles. As zeta potential approaches zero, the compressibility of the colloidal cake converges to a single value.

At all zeta potential values it is observed that the compressibility of the colloidal cake decreases with increasing ionic strength. Cake compressibility is low for high ionic strength feed waters irregardless of the particle zeta potential. The cake compressibility for all ionic strengths approaches a single value of 0.13 at the isoelectric point. This represents the compressibility of hard-sphere colloidal particles

7.5 Summary

In this chapter, it is demonstrated that the feed water fouling potential can be well correlated to water chemistry and operating conditions with the use of fundamental theories of colloidal interactions. Utilizing the fact that particles in a cake layer are held immobile by the balance of the forces acting on them, the average interparticle distance between the particles and subsequently the colloidal volume fraction were determined. When calibrated with

experimental fouling potentials, the permeate flux and the relative viscosity within the pores of the colloidal cake could be determined with an iterative numerical procedure.

Interestingly, the analysis revealed that the average relative viscosity value was 7.32, indicating that the water viscosity within the nano-sized pores of the colloidal cake were significantly higher than in the bulk liquid. This average relative viscosity value was not found to vary significantly under different feed water ionic strength, pH, membrane resistance and driving pressure, suggesting it could be used as an approximation for the relative viscosity in colloidal cakes under a wide range of conditions. The numerical fouling potential calculated theoretically, using this relative viscosity, was found to match the experimental data well with errors smaller than 8% for all comparisons. Simulations of the fouling potential and cake compressibility for different feed water conditions (e.g., ionic strength, particle zeta potential, colloid concentration, etc) confirmed the experimental trends found in the previous chapters (Chapters 4-6).

In conclusion, the fouling behavior of colloidal particles in membrane processes is strongly controlled by the colloidal interactions, which is in turn are affected by the water chemistry. Therefore, the numerical procedure presented in this chapter built up from fundamental colloidal interaction theory served two important purposes (1) it could be used to predict the feed water fouling potential based simply on knowledge of the feed water properties, operating pressure and membrane resistance; and (2) it allowed the determination of viscosity within the pores of the colloidal cake layer, which has not been considered previously.

Chapter 8

Recommendations and Conclusions

The main focus of the work presented in this thesis is to determine quantitatively the effect of solution chemistry on colloidal fouling. This chapter summarizes the main findings from the work in this thesis and recommends possible expansion of scope for future research work.

8.1 Main Findings

The main findings of the thesis from Chapter 3 – 7 are presented below. All the findings here are original, from the work described in the thesis.

1. The fouling potential determination method, unlike the MFI and SDI, did not require the use of a specific membrane and setup. Any membrane system could be used for determination of the feed water fouling potential, and if operated under the same permeation drag conditions, would depend only on the feed water properties. This was an important finding which allowed the fouling potential to be representative of the foulant layer properties since membrane type did not play an important role.

2. It was determined both experimentally and from the mathematical model that the fouling potential for colloidal waters, increased with ionic strength of the feed water. Below the critical coagulation concentration, ionic strength was related to fouling potential by a natural logarithmic relationship ($k = f(\ln(I))$). Beyond the critical coagulation concentration, the fouling potential decreased due to higher porosity of the aggregated colloidal cake on the membrane surface. The highest fouling potential was therefore observed at the critical coagulation concentration. Using different salts to adjust ionic strength of the feed water, showed that counter-ion type and valence could both have significant influence on the fouling potential of the colloidal feed

waters. LiCl consistently induced a higher fouling potential compared to NaCl, KCl and CsCl, which were noted to have an equivalent effect for various feed water ionic strengths. The increase in fouling potential due to LiCl, which has an equivalent effect as increasing the colloid concentration by 50% - 100%, was attributed to the masking of the surface groups on the silica surface by adsorption, thus reducing the repulsive forces between the silica colloids. $CaCl_2$ resulted in a much higher fouling potential at smaller ionic strength compared to NaCl. This indicated that counter-ion valence could play a further role in influencing the fouling potential besides enhancing the feed water ionic strength. However, despite the difference in fouling potential between the salts, all exhibited the same trends in relationship between the fouling potential and ionic strength below the critical coagulation salt concentration.

3. Solution pH, which is another important water chemistry parameter, also affected the fouling potential of colloidal feed waters. Fouling potential increased as the feed water pH approached the isoelectric pH of the colloids. Zeta-potential of the colloids was found to be a useful indicator of colloidal fouling. The fouling potential was found to be linearly related to the colloid zeta-potential for the experiments conducted. The linear relationship between fouling potential and zeta-potential was also observed when the feed water ionic strength was adjusted. Extrapolation of the linear relationship between fouling potential and zeta potential at different solution ionic strengths converged to a single value at the isoelectric point (zeta-potential=0mV). This interesting point suggested that on approaching the colloidal isoelectric point, differences in solution ionic strength would play a less pivotal role in colloidal fouling. The effect of the type of acid used to adjust feed water pH on colloidal fouling was also investigated. Results revealed that pH adjustment using strong acids resulted in a 2.5 fold increase in fouling potential over the baseline conditions, while weak acids only increased fouling by 1.5-2.0 times of the baseline conditions at the same pH values. The difference was attributed to the adsorption of

weak acid anions to the silica surface, thereby increasing the repulsive forces between the colloids. However, at high feed water ionic strength, no difference between the fouling potential for feed waters adjusted by weak and strong acids was observed. This suggested that selection of weak acids for feed water acidification, to prevent scaling of sparingly soluble salts, may invoke less serious colloidal fouling compared to strong acids for low salinity waters.

4. Increasing permeation drag force on the colloidal feed waters, exert a strong influence on colloidal fouling. The extent of this influence on colloidal fouling was defined as the compressibility of the colloidal cake. Experimental results revealed that compressibility was strongly dependent on the solution chemistry of the feed water. Increasing feed water ionic strength and adjusting feed water pH to values nearer the isoelectric point of the colloids reduced cake compressibility from approximately 0.8 to 0.3. At these feed water conditions, the repulsive forces between the particles were considerably reduced and they exhibited hard sphere-like attributes. This change in colloidal behavior resulted in a reduced compressibility for the colloidal cake.

5. A model to predict the fouling potential from water properties such as concentration of colloids in the feed water, zeta potential of the colloids, ionic strength of the feed water, mean size of colloids and operating conditions such as driving pressure and membrane resistance was developed. Given the difficulty in determining the viscosity of the liquid in the cake layer, it was used as an optimizing parameter for comparison with experimentally determined fouling potential values. After comparison with over 40 fouling experiments under different conditions, it was found that the relative viscosity was approximately constant at 7.32. This implied the viscosity of the liquid in the colloidal cake layer was approximately constant at 6.5×10^{-3} Pa.s under different solution chemistries, membrane resistance and driving pressures. With the constant relative viscosity found above, the model could be completely described and the

fouling potential due to variations in feed water ionic strength, pH, colloid concentration, driving pressure and membrane resistance could be predicted. The effects of solution chemistry on the compressibility were also determined from the model. The predicted fouling potential values and trends observed correlated well with the experimentally determined ones, validating the model.

8.2 Future Work

In the course of writing this thesis, many new ideas and directions for future research have arisen. Like most research work, more questions than answers were found. Highlighted in this chapter are some of the possible directions for future research work to be undertaken.

1. In chapter 4, the effect of colloidal aggregation on the fouling potential was briefly discussed. Particle aggregation in membrane processes is an interesting area of study, because the particle structure and dynamics change considerably with aggregation. The effects of crossflow shear, which can be neglected for microscopic colloids, become important when the particle size increases due to aggregation and could affect the fouling potential values considerably. Furthermore based on preliminary work outside of this thesis it does seem that a relationship between fouling potential and fractal dimension of the aggregates is plausible.

2. The work in this thesis focused on monodispersed colloidal particles to reduce the number of variables so that the effect of solution chemistry on colloidal fouling could be measured accurately. However, polydispersity is a common feature of natural feed waters and could influence colloidal fouling greatly.

3. The relative viscosity value obtained from optimizing model predictions of fouling potential to match experimentally determined values revealed that it was constant.

Further work should be carried out to ascertain the reason for it being a constant. In addition the effects of crossflow velocity and different colloidal particles of wider size range should be tested to determine the relative viscosity under these conditions.

4. The fouling potential as a quantitative tool for fouling has been extensively used in this thesis. It was found to be extremely useful and sensitive to minor changes in feed water properties for the colloidal waters. However, it has not been extended to other feed waters and its usefulness not fully maximized. A database compiled from the simple determination of the fouling potential for different feed waters can provide a wealth of information for operators and researchers.

8.3 Conclusion

In this thesis, the influence of physicochemical factors on colloidal fouling was determined both experimentally and finally through a model prediction. This is a quantitative study which considered primarily the effect of ionic strength, pH, and hydrodynamic pressure on colloidal fouling in membrane processes. No previous attempts have been made to link directly colloidal fouling to the interfacial interaction forces between the colloids. The fouling potential used to quantify colloidal fouling was the primary tool employed to measure the effects of the physicochemical factors on fouling. It was observed to be a useful method and several correlations were noted between the fouling potential and the physicochemical factors. These trends and fouling potential values found empirically were well matched with the trends and fouling potential values determined from a model developed based on fundamental colloidal interaction equations. The findings from this thesis would allow for better understanding and prediction of full scale membrane performance. It also shows the relevance of fundamental colloidal theories to colloidal fouling which could subsequently provide a framework to tackle the issue of membrane fouling.

References

Abendroth, R.P. (1970) Behavior of pyrogenic silica in simple electrolytes. *J. Colloid and Interface Sci.* 34, 591-596.

Aimar, P. (2003) Recent progress in understanding particle fouling of filtration membranes. IMSTEC, 10-14 November 2003, Sydney, Australia, Keynote Paper.

Allen, L.H., Matijevic, E. (1969) Stability of colloidal silica: I Effect of simple electrolytes. *J. Colloid Interface Sci.* 31, 287-296.

Allen, L.H., Matijevic, E. (1970) Stability of colloidal silica: II Ion exchange. *J. Colloid Interface Sci.* 33, 420-429.

Allen, L.H., Matijevic, E. (1971) Stability of colloidal silica: III Effect of hydrolyzable cations. *J. Colloid Interface Sci*. 35, 66-76.

Almy, C., Lewis, W.K. (1912) Factors determining the capacity of a filter press. J. *Ind. Eng. Chem.* 4, 528-532.

Al-Shammiri, M., Salman, A., Al-Shammiri, S., Ahmad, M. (2005) Simple program for the estimation of scaling potential in RO systems. *Desalination* 184, 139-147.

Antelmi, D., Cabane, B., Meireles, M., Aimar, P. (2001) Cake collapse in pressure filtration. *Langmuir* 17, 7137-7144.

ASTM E 2456-06, "Terminology for Nanotechnology," ASTM International

Atkins, D.T., Ninham, B.W. (1997) Surface and structural forces measured between silica surfaces in 1,2-ethanediol. *Colloid surf., A Physicochem. Eng. Asp.* 129, 23-32.

Atteia, O., Perret, D., Adatte, T., Kozel, R., Rossi, P. (1998) Characterization of natural colloids from a river and spring in a karstic basin. *Environ. Geol.* 34, 257-269.

Bacchin, P., Aimar, P., Sanchez, V. (1995) Model for colloidal fouling of membranes. *AIChE J*. 41, 368-376.

Bacchin, P., Si-Hassen, D., Starov, V., Clifton, M.J., Aimar, P. (2002) A unifying model for concentration polarization, gel layer formation and particle deposition in crossflow membrane filtration of colloidal suspension. *Chem. Eng. Sci.* 57, 77-91.

Baker, R.W. (2000) *Membrane technology and applications*, McGraw Hill, NY.

Barker, J.A., Henderson, D. (1967) Perturbation theory and equation of state for fluids II. A successful theory of liquids. *J. Chem. Phys.* 47, 4714-4721.

Belfer, S., Fainshtain, R., Purinson, Y., Gilron, Y., Nyström, M., & Mänttäri, M. (2004) Modification of NF membrane properties by in situ redox initiated graft polymerization with hydrophilic monomers, *J. Membr. Sci.*, 239, 55-64.

Belfort, G. (1989) Fluid mechanics in membrane filtration: Recent developments, J. Membr. Sci. 40, 123-147.

Belfort, G., Davis, R.H., Zydney, A.L. (1994) The behaviour of suspensions and macromolecular solutions in crossflow microfiltration. *J. Membr. Sci.* 96, 1-58.

Bergna, H.E., Roberts, W.O (Eds). *Colloids Silica, Fundamentals and Applications*, Surfactant science series vol 131, CRC Press/Taylor and Francis 2006.

Bergstrom, L. (1997) Hamaker constants of inorganic materials. *Adv. Colloid Interface Sci.* 70, 125-169.

Bhattacharjee, S., Kim, A.S., Elimelech, M. (1999) Concentration Polarization of Interacting Solute Particles in Crossflow Membrane Filtration. *J. Colloid Interface Sci.* 212, 81-99.

Biggs, S., Scales, P.J., Leong, Y-K., Healy, T.W. (1995) Effects of citrate adsorption on the interactions between zirconia surfaces. *J. Chem. Soc. Faraday Trans.* 91, 2921-2928.

Bikerman, J.J. (1940) Electrokinetic equations and surface conductance. A survey of the diffuse double layer theory of colloidal solutions. *Trans. Faraday. Soc.* 35, 154-160.

Birdi, K.S.(1997) *Handbook of Surface and Colloid Chemistry*, CRC Press, New York, Pg420.

Boerlage, S.F.E., Kennedy, M.D., Witkamp, G.J., vand der Hoek, J.T., Schippers, J.C. (1999) BaSO4 solubility prediction in reverse osmosis membrane system. *J. Membr. Sci*. 159, 47-59.

Boerlage, S.F.E., Kennedy, M., Aniye, M.P. and Schippers, J.C. (2003) Applications of the MFI-UF to measure and predict particulate fouling in RO systems, *J. Membr. Sci.*, 220, 97-116.

Bowen, W.R., Gan, Q. (1991) Properties of microfiltration membranes: flux loss during constant pressure permeation of bovien serum albumin. *Biotech. Bioeng.* 38, 688-696.

Bowen, W.R., Jenner, F. (1995a) Dynamic Ultrafiltration Model for Charged Colloidal Dispersions: A Wigner-Seitz Cell Approach. *Chem. Eng. Sci.* 50, 1707-1736.

Bowen, W.R., Jenner, F. (1995b) Electroviscous effects in charged capillaries. *J. Colloid Interface Sci.* 173, 388-395.

Bowen, W.R., Jenner, F. (1995c) Theoretical descriptions of membrane filtration of colloids and fine particles: an assessment and review. *Adv. Colloid Interface Sci.* 56, 141-200.

Bowen, W.R., Mongruel, A., Williams, P.M. (1996) Prediction of the rate of crossflow membrane ultrafiltration: a colloidal interaction approach. *Chem. Eng. Sci.* 51, 4321-4333.

Bowen, W.R., Williams, P.M. (2001) Obtaining the osmotic pressure of electrostatically stabilized colloidal dispersions from frontal filtration experiments, *J. Colloid Interface Sci.* 233, 159-163.

Bowen, W.R., Williams, P.M., Wilson, J. (2003) Quantifying extra interaction forces in charged colloidal dispersions from frontal ultrafiltration experiments *Colloids surf., A*

Physicochem. Eng. Asp. 231, 67-83.

Brandrup, J., Immergut, E.H. (1975) Polymer Handbook; Wiley Interscience: New York, pp IV-89.

Carman, P.C. (1939) Permeability of saturated sands soils and clays. *J. Agric. Sci.* 29, 262-273.

Casimir, H.B.G., and Polder, D. (1948) The influence of retardation on London-van der Waals Forces. *Phys. Rev.* 73, 360-372.

Chan, F.S., Blachford, J., Goring, D.A.I. (1966) The secondary electroviscous effect in a charged spherical colloid. *J. Colloid Interface Sci*. 22, 378-385.

Chan, D., Perram, J.W., White, L.R., Healy, T.W. (1975) Regulation of surface potential at amphoteric surfaces during particle-particle interaction. *J. Chem. Soc., Faraday Trans. 1.* 71, 1046-1057.

Chang, D.J., Hsu, F.C., Hwang, S.J. (1995) Steady-state permeate flux of crossflow microfiltration, *J. Membr. Sci.* 98, 97-106.

Chapel, J.-P. (1994) Electrolyte species dependent hydration forces between silica surfaces, *Langmuir* 10, 4237-4243.

Chapman D.L. (1913) A contribution to the theory of electrocapillarity. *Phil. Mag.* 25, 475-481.

Chellam, S., Wiesner, M.R. (1998) Evaluation of crossflow filtration models based on shear-induced diffusion and particle adhesion: complications induced by feed suspension polydispersivity. *J. Membr. Sci.* 138, 83-97.

Chen, V., Fane, A.G., Madaeni, S., Wenten, I.G. (1997) Particle deposition during membrane filtration of colloids: transition between concentration polarization and cake formation. *J. Membr. Sci.* 125, 109-122.

Chen B., Penwell D., Benedetti L. R., Jeanloz R., Kruger M. B. (2002) Particle-size effect on the compressibility of nanocrystalline alumina. *Phys. Rev. B* 66, 144101-144105.

Chen, J.C., Li, Q., & Elimelech, M. (2004) In situ monitoring techniques for concentration polarization and fouling phenomena in membrane filtration, *Adv. in Colloid Interface Sci.* 107, 83-109.

Chen, K.L., Song, L., Ong, S.L., Ng, W.J. (2004) The development of membrane fouling in full-scale RO processes, J. Membr. Sci. 232, 63-72.

Cheryan, M. (1986) *Ultrafiltration Handbook*, Technomic Publishing Company Inc, Lancaster, Pennsylvania.

Chin, C-J., Yiacoumi, S., Tsouris, C. (2002) Influence of metal ion sorption on colloidal surface forces measured by atomic force microscopy. Environ. Sci. Technol. 36, 343-348.

Cho, G.C., Dodds, J., Santamarina, J.C. (2006) Particle shape effects on packing density, stiffness and strength: Natural and crushed sands. *J. Geotech. & Geoenviron. Eng. 132, 591-602.*

Choi, K.Y.J., Dempsey, B.A. (2004) In-line coagulation with low-pressure membrane filtration. *Water Res.* 38, 4271-4281.

Chun, M.S., Chung, G.Y., Kim, J.J. (2001) On the behaviour of the electrostatic colloidal interaction in the membrane filtration of latex suspensions. *J. Membr. Sci.* 193, 97-109.

Churaev, N.V. (2000) *Liquid and vapor flows in porous bodies: surface phenomena. In:* Topics in chemical engineering, vol 13. Gordon and Breach Science Publishers, The Netherlands.

Cohen, R.D., Probstein, R.F. (1986) Colloidal fouling of reverse osmosis membranes, *J. Colloid Interface Sci.* 114, 194-207.

Collins, C.L., Ideker, J.H., Willis, G.S., Kurtis, K.E. (2004) Examination of the effects of LiOH, LiCl and $LiNO_3$ on alkali-silica reaction, *Cement & Concrete Res*. 34, 1403-1415.

Darton, E.G., Fazell, M. (2001) A statistical review of 150 membrane autopsies. *Presented at the 62nd Annual International Water Conference, Pittsburgh, October 2001.*

Darton, T., Annunziata, U., del Vigo Pisano, F., Gallego, S. (2004) Membrane autopsy helps to provide solutions to operational problems. *Desalination* 167, 239-245.

de Boer, J.H., Linsen, B.G. (1970) *Physical and Chemical Aspects of Adsorbents and Catalysts*, Academic Press, London, New York.

Debye, P. (1920) Van der Waals cohesion forces. *Physikalische Zeitschrift* 21, 178-187.

Debye, P. (1921) Molecular forces and their electrical interpretation. *Physikalische Zeitschrift* 22, 302-308.

Depasse, J. (1999) Simple experiments to emphasize the main characteristics of the coagulation of silica hydrosols by alkaline cations: applications to the analysis of the model of Colic et al. *J. Colloid Interface Sci.* 220, 174-176.

Derjaguin, B.V. (1934) Friction and adhesion IV, *Physikalische Zeitschrift* 69, 155-164.

Derjaguin, B.V., Landau, L. Theory of the stability of strongly charged lyophobic sols and of the adhesion of strongly charged particles in solutions of electrolytes, *Acta Physicochim URSS* 14 (1941) 633-662

Derjaguin, B.V., Titiyevskova, A.S., Abrikossova I.I., Malkina, A.D. (1954) Investigations of the forces of interaction of surfaces in different media and their application to the problem of colloid stability. *Discuss. Faraday. Soc.* 18, 24-41.

Ducker, W.A., Senden, T.J., Pashley, R.P. (1993) Direct measurement of colloidal forces using an atomic force microscope, *Nature* 353, 239-241.

Dzyaloshinskii, I.E., Lifshitz, E.M., Pitaevskii, L.P. (1960) Van der Waals forces in liquid films. *Soviet Phys. JETP* 10, 161-165.

Elimelech, M., Gregory, J., Jia, X., & Williams W. (1995). *Particle Deposition and Aggregation: Measurement, Modeling, and Simulation*. Oxford: Butterworth Heinemann.

Elimelech, M., and Bhattacharjee, S. (1998) A novel approach for modeling concentration polarization in cross membrane filtration based on equivalence of osmotic pressure model

and filtration theory. *J. Membr. Sci.* 145, 223-241.

Eliseev, A.A., Kolesnik, I.V., Lukashin, A.V., Vasiliev, R.B., Tretyakov, Y.D. (2004) Nanoparticle separation by mesoporous molecular sieves, *Mendeleev Commun.* 14, 173-174.

Elzo, D., Huisman, I., Middelink, E., Gekas, V. (1998) Charge effects on inorganic membrane performance in a crossflow microfiltration process. *Colloids and surf., A Physicochem. Eng. Asp.* 138, 145-159.

Eve, A.S., Creasey, C.H. (1945). *Life and Work of John Tyndall.* London: Macmillan

Faibish, R.S., Cohen, Y., Elimelech, M. (1998) Effect of interparticle electrostatic double layer interactions on permeate flux decline in crossflow membrane filtration of colloidal suspensions: an experimental investigation. *J. Colloid Interface Sci.* 204, 77-86.

Faibish, R.S., Cohen, Y. (2001) Fouling and rejection behavior of ceramic and polymer-modified ceramic membranes for ultrafiltration of oil-in-water emulsions and microemulsions, Colloids surf., A Physicochem. Eng. Asp. 191, 27-40.

Fane, A.G., Kim, K.J., Hodgson, P.H., Leslie, G., Fell, C.J.D., Franken, A.C.M., Chen, V. and Liew, K.H. (1992) Strategies to minimize fouling in membrane processing of biofluids. *Amer. Chem. Soc.*, 2, 304-319.

Feder, J. (1988) *Fractals*, Plenum Press, N.Y. 1988

Fowkes, F.M. (1967). In: *Surfaces and Interfaces*, J.J. Burke, Ed., Am. Chem. Soc. Publ., Washington, DC, p. 1.

Fratila-Apachitei, L.E., Kennedy, M.D., Linton, J.D., Blume, I. and Schippers, J.C. (2001) Influence of membrane morphology on the flux decline during dead-end ultrafiltration of refinery and petrochemical waste water. *J. Membr. Sci.* 182, 151-159.

Freundlich, H., Neumann, W. (1908) Zur Systematic der Farbstofflosungen. *Kolloid Zeitschrift & Zeitschrift* 3, 80-83.

Fu, L.F., Dempsey, B.A. (1998) Modeling the effect of particle size and charge on the structure of the filter cake in ultrafiltration, *J. Membr. Sci.* 149, 221-240.

Grabbe, A., Horn, R.G. (1993) Double layer and hydration forces measured between silica sheets subjected to various surface treatments. *J. Colloid Interface Sci.* 157, 375-383.

Grahame, D.C. (1947). The electrical double layer and the theory of electrocapillarity. *Chem. Rev.* 41, 441-501.

Gregory, J. (1969) The calculation of Hamaker constants. *Adv. Colloid Interface Sci.* 2, 396-417.

Gregory, J. (1981) Approximate expressions for retarded van der Waals interaction. *J. Colloid Interface Sci.* 83, 138-145.

Guihen, E., Glennon, J.D. (2003) Nanoparticles in separation science- recent developments, *Anal. Letters* 36, 3309-3336.

Guoy, G. (1910) Sur la constitution de la electrique a la surface d'un electrolyte *J. Phys.*

Radium 9, 457-468.

Hachisu, S., Kobayashi, Y. (1974) Kirkwood-Alder transition in monodisperse latexes. II Aqueous latexes at high electrolyte concentration. *J. Colloid Interface Sci.,* 46, 470-476.

Hamachi, M., Mietton-Peuchot, M. (1999) Experimental investigations of cake characteristics in crossflow microfiltration. *Chem. Eng. Sci.* 54, 4023-4030.

Hamaker, H.C. (1937) The London-van der Waals attraction between spherical particles. *Physica* 4, 1058-1072.

Happel, J. (1958) Viscous flow in multiparticle systems: slow motion of fluids relative to beds of spherical particles. *AIChE, J.* 4, 197-201.

Happel, J. Brenner, H. (1991) *Low Reynolds number hydrodynamics,* Kluwer, Dordrecht.

Harding, R.D. (1971) Stability of silica dispersions. *J. Colloid Interface Sci.* 35, 172-174.

Hermans, P.H., Bredee, H.L. (1936) Principles of the mathematical treatment of constant pressure filtration. *J. Soc. Chem. Ind*. 1-4.

Hermia, J. (1982) Constant pressure blocking filtration laws-application to power – law non-newtonian fluids. *Trans. I. Chem. Eng.* 60, 183-187.

Hiemenz, P.C., Rajagopalan, R. (1997) *Principles of Colloid and Surface Chemistry*, Marcel Dekker, New York.

Hlavacek, M., Bouchet, F. (1993) Constant flowrate blocking laws and an example of their application to dead-end microfiltration of protein solutions. *J. Membr. Sci*. 82, 285-295.

Ho, C-C. and Zydney, A.L. (2000) A combined pore blockage and cake filtration model for protein fouling during microfiltration. *J. Colloid Interface Sci.* 232, 389-399.

Hoek, E.M.V., Elimelech, M. (2003) Cake-enhanced concentration polarization: A new fouling mechanism for salt rejecting membranes. *Environ. Sci. Technol.* 37, 5581-5588.

Hogg, R., Healy, T.W., and Fuerstenau, D.W. (1966) Mutual coagulation of colloidal dispersion. *Trans. Faraday Soc.* 62, 1638-1651.

Hong, S., Faibish, R.S., Elimelech, M. (1997) Kinetics of permeate flux decline in crossflow membrane filtration of colloidal suspensions. *J. Colloid Interface Sci.* 196, 267-277.

Hong, Y.K., Eom, D.H. Lee, S.H., Kim, T.G., Park, J.G., Busnaina, A.A. (2004) The effect of additives in post-Cu CMP cleaning on particle adhesion and removal. *J. Electrochemical Society* 151, G765-G761.

Horn, R.G. (1990) *Abstracts of Papers*, *200th ACS National Meeting*: American Chemical Society: Washington, DC, Division of Colloids and Surfaces, paper no. 41.

Howe, K. J.; Clark, M. M. (2002) Fouling of microfiltration and ultrafiltration membranes by natural waters. *Environ. Sci. Technol.* 36, 3571-3576.

Howell, J.A. (2004) Future of membranes and membrane reactors in green technologies and for water reuse. *Desalination* 162, 1-11.

Hunter, R.J. (2000) *Foundations of Colloid Science,* 2nd Edition, Oxford University Press, UK.

Hwang, K.J., Liu, H.C., Lu, W.M. (1998) Local properties of cake in crossflow microfiltration and submicron particles. *J. Membr. Sci.* 138, 181-192.

Icopini, G.A., Brantley, S.L., Heaney, P.J. (2005) Kinetics of silica oligomerization and nanocolloid formation as a function of pH and ionic strength at 25deg C. *Geochim. Cosmochim. Acta* 69, 293-303.

Iler, R.K. (1955) *The Colloid Chemistry of Silica and Silicates,* Cornell University Press, Ithica, NY.

Iler, R.K. (1975) Coagulation of colloidal silica by calcium ions, mechanism, and effect of particle size. *J. Colloid Interface Sci.* 53, 476-488.

Iler R.K. (1977) *Hydrogen-bonded complexes of silica with organic compounds.* In Biochemistry of Silicon and related problems (Bendz G. and Lindquist I. eds) Plenum, New York, 53-76.

Iler, R.K. (1979) *The Chemistry of Silica: Solubility, Polymerization. Colloid and Surface Properties and Biochemistry*, Wiley: New York.

Iritani, E., Mukai, Y., Tanaka, Y. and Murase, T. (1995) Flux behaviour in dead-end microfiltration of protein solutions. *J. Membr. Sci.* 103, 181-191.

Israelachvili, J. N. (1992) Intermolecular and Surface Forces., Academic Press, London.

Israelachvili, J., Wennerstrom, H. (1996) Role of hydration and water structure in biological and colloidal interactions. *Nature* 379, 219-225.

IUPAC (1972) Compendium of Chemical Terminology. 31, 618

IUPAC (1996) Terminology for membranes and membrane processes. *J. Membr. Sci.* 120, 149-159.

Jonsson, A.S., Jonsson, B. (1996) Ultrafiltration of colloidal dispersions – a theoretical model of the concentration polarization phenomena. *J. Colloid Inteface Sci.* 180, 504-518.

Keesom, W.H. (1920) Quadrupole moments of the oxygen, and nitrogen and nitrogen molecules. *Proc. Roy. Neth. Acad. Sci. Amsterdam* 23, 939-942.

Keesom, W.H. (1921) On Waal's cohesion forces. *Physikalische Zeitschrift* 22, 129-141.

Kelly, S.T. and Zydney, A.L. (1995) Mechanisms for BSA fouling during microfiltration. *J. Membr. Sci.* 107, 115-127.

Khirani, S., Aim, R.B. and Manero, M.H. (2006) Improving the measurement of the Modified Fouling Index using nanofiltraiton membranes (NF-MFI), *Desalination* 191, 1-7.

Kilduff, J.E., Mattaraj, S., Zhou, M.Y., Belfort G. (2005) Kinetics of membrane flux decline: The role of natural colloids and mitigation via membrane surface modification, *J. Nanoparticle Research* 7, 525-544.

Kim, A.S., Hoek, E.M.V. (2002) Cake structure in dead-end membrane filtration: Monte

Carlo simulations. *Env. Eng. Sci.* 19, 373-385.

Kim, A.S., Yuan, R. (2005) A new model for calculating specific resistance of aggregated colloidal cake layers in membrane filtration processes, *J. Membr. Sci.* 249, 89-101.

Kim, S., Marion, M., Jeong, B.H., Hoek, E.M.V. (2006) Crossflow membrane filtration of interacting nanoparticle suspensions. *J. Membr. Sci*. 284, 361-372.

Kobayashi, M., Juillerat, F., Galletto, P., Bowen, P., Borkovec, M. (2005) Aggregation and charging of colloidal silica particles: effect of particle size. *Langmuir* 21, 5761-5769.

Kosmulski, M. (2003) A literature survey of the differences between the reported isoelectric points and their discussion. *Colloids Surfaces A: Phys. Eng. Asp.* 222, 113-118.

Kozeny, J. (1927) About capillaries conducting water in the earth. *Committee Report of the Viennese Academy* 136(2a), 271-306.

Kremen, S.S. and Tanner, M. (1998) Silt density indices (SDI), percent plugging factor (%PF); their relation to actual foulant deposition. *Desalination*, 119, 259-262.

Lecoanet, H.F., Bottero, J.Y., Wiesner, M.R. (2004) Laboratory assessment of the mobility of nanomaterials in porous media. *Environ. Sci. Technol.*38, 5164-5169.

Lee, Y., Clark, M.M. (1998) Modeling of flux decline during crossflow ultrafiltration of colloidal suspensions. *J. Membr. Sci.* 149, 181-202.

Lee, H.J., Moon, S.H. (2004) Influences of colloidal stability and electrokinetic property on electrodialysis performance in the presence of silica sol. *J. Colloid Interface Sci.* 270, 406-412.

Leu, M., Lee, M.H., Tiller, F.M. (1993) Cake compactability- a rigorous definition. *In Sixth world filtration congress*. Nagoya, Japan 148-153.

Li, J.X., Sanderson, R.D., Chai, G.Y., Hallbauer, D.K. (2005) Development of an ultrasonic technique for in situ investigating the properties of deposited protein during crossflow ultrafiltration. *J. Colloid Interface Sci.* 284, 228-238.

Lifshitz, E.M. (1956) Theory of molecular attractive forces. *Soviet Phys.* JETP 2, 73-83.

London, F. (1930) Theory and systematic of molecular forces. *Physikalische Zeitschrift* 63, 245-279.

Lonsdale, H.K. (1982) The growth of membrane technology. *J. Membr. Sci.*, 10, 81-181.

Lu, S., Pugh, R.J., Forssberg, E. (2005). *Interfacial Separation of Particles in Mobius*, D., Miller, R. Studies in Interface Science. Elsevier, Amsterdam.

Lyklema, J. (1991) *Fundamentals of Interface and Colloid Science*, Vol 1: *Fundamentals*, Academic Press Limited, London.

Matsumoto, Y., Kawakatsu, T., Nakajima, M., Kikuchi, Y. (1999) Visualization of filtration phenomena of a suspended solution including o/w emulsion or a solid particle and membrane separation properties of the solution. *Water Res.* 33, 929-936.

Mavredaki, E.; Neofotistou, E.; Demadis, K. D. (2005) Inhibition and dissolution as dual mitigation approaches for colloidal silica fouling and deposition in process water systems:

functional synergies. *Ind. Eng. Chem. Res.* 44, 7019-7026.

McDonogh R.M., Welsch K., Fane A.G., Fell C.J.D. (1992) Incorporation of the cake pressure profile in the calculation of the effect of particles charges on the permeability of filter cakes obtained in the filtration of colloids and particulates. *J. Membr. Sci.* 72, 197-204.

Meeten, G.H. (2000) Septum and filtration properties of rigid and deformable particle suspensions. *Chem. Eng. Sci.* 55, 1755-1767.

Michaels, A.S. (1968) New separation technique for the CPI. *Chem. Eng. Prog*. 64, 31-40.

Mitchell, L.D., Beaudoin, J.J., Grattan-Bellew, P. (2004) The effects of lithium hydroxide solution on alkalie silica reaction gels creasted with opal, *Cement & Concrete Res*. 34, 641-659.

Mulder, M. (1996) Basic Principles of Membrane Technology, 2nd ed., Kluwer Academic, Dordrecht, The Netherlands.

Murashov, V.V.; Leszczynski, J. (1999) Adsorption of the phosphate groups on silica hydroxyls: An ab initio study. *J. Phys. Chem. A* 103, 1228-1238.

Neumann, A.W., Omenyi, S.N., and van Oss, C.J. (1979) Negative Hamaker coefficients I. Particle engulfment or rejection at solidification fronts. *Colloid Polymer Sci.* 257, 413-419.

Niemi, H., Bulsari, A., Palosaari, S. (1995) Simulation of membrane separation by neural networks. *J. Membr. Sci.* 102, 185-197

Nirschl, H., Schafer, B. (2005) Distinction between electrostatic and electroviscous effects on the permeability of colloidal packed beds. *Chem. Eng. & Technol.* 28, 862-866

O'Brien, R.W., White, L.R. (1978) Electrophoretic mobility of a spherical colloidal particle. *J. Chem. Soc., Faraday Trans. 2* 74, 1607-1626.

Park, P.K., Lee, C.H., Lee, S. (2006) Permeability of collapsed cakes formed by deposition of fractal aggregates upon membrane filtration. *Environ. Sci. Technol.* 40, 2699-2705.

Pashley, R.M., Israelachvili, J.N. (1984) DLVO and hydration forces between mica surfaces in Mg2+, Ca2+, Sr2+ and Ba2+ chloride solutions. *J. Colloid Interface Sci.* 97, 446-455.

Peavy, H., Rowe, D.R., Tchobanoglous, G. (1985) *Environmental Engineering,* McGraw Hill Inc, NY.

Perrin, J. (1905) Mecanisme de l'electrisation de contact et solutions colloidales. *J. Chim. Phys.* 3, 50-110.

Persello, J. (2000) Surface and interface structure of silicas in Adsorption on silica surfaces Papirer, E. eds. Surfactant science series Vol 90 Marcel Dekker Inc. New York, pp 322.

Peschel, G., Belouscheck, P., Muller, M.M., Muller, R., Konig, R. (1982) The interaction of solid surfaces in aqueous systems. *Colloid Polymer Sci.* 260, 444-451.

Petsev, D.N., Starov, V.M., Ivanov, I.B. (1993) Concentrated dispersions of charged colloidal particles: sedimentation, ultrafiltration and diffusion, *Colloids surf., A*

Physicochem. Eng. Asp. 81, 65-81.

Puls, R.W., Powell, R.M. (1992) Transport of inorganic colloids through natural aquifer material: Implications for contaminant transport. *Environ. Sci. Technol.* 26, 614-621.

Rabinovich, Ya.I., Derjaguin, B.V., Churaev, N.V. (1982) Direct measurements of long-range surface forces in gas and liquid media. *Adv. Colloid Interface Sci.* 16, 63-78.

Raghavan, S.R., Walls, H.J., Khan, S.A. (2000) Rheology for silica dispersion in organic liquids: new evidence for solvation forces dictated by hydrogen bonding. *Langmuir* 16, 7920-7930.

Romero, C.A., Davis, R.H. (1990) Transient model of crossflow microfiltration. *Chem. Eng. Sci.* 45, 13-25.

Russel, W.B., Saville, D.A., Schowalter, W.R. (1989) *Colloidal Dispersions*, Cambridge University Press, Cambridge.

Ruth, B.F., Montillon, G.H., Montonna, R.E. (1933) Studies in filtration I critical analysis of filtration theory. Ind. Eng. Chem. Res. 1933, 25, 76-82.

Salam, G.P., Zannella, S., Jansak, L., Abdel-Jawad, M., Ebrahim, S., Al-Atram, F. and Al-Shammari, S. (1997) Pretreatment of the municipal wastewater feed for reverse osmosis plants, *Desalination* 109, 211-223.

Schippers, J.C. and Verdouw, J. (1980) The modified fouling index, a method of determining the fouling characteristics of water, *Desalination*, 32, 137-148.

Schufle, J.A., Huang, C.-T., Hansen, W.D. (1976) Temperature dependence of surface conductance and a model of vicinal (interfacial) water. *J. Colloid Interface Sci.*54, 184-202.

Sharma, M.M., Lei, Z.M. (1991) A model for clay filter cake properties. *Colloids surf., A Physicochem. Eng. Asp.* 56, 357-381.

Singh, G., Song, L. (2004) Quantifying the effect of ionic strength on colloidal fouling potential in membrane filtration. *J. Colloid Interface Sci.* 284, 630-638.

Singh, G., Song, L. (2006) Influence of sodium dodecyl sulfate on colloidal fouling potential during ultrafiltration. *Colloids surf., A Physichochem. Eng. Asp.* 281, 138-146.

Sjoberg, S. (1996) Silica in aqueous environments. *J. Non-Crystalline Solids* 196, 51-57.

Snoeyink, V.L. and Jenkins, D. (1980) *Water Chemistry*, Wiley: New York.

Song, L., Elimelech, M. (1995) Theory of concentration polarization in crossflow filtration. *J. Chem. Soc., Faraday Trans.* 91, 3389-3398.

Song, L. (1998a) Flux decline in crossflow microfiltration and ultrafiltration: mechanisms and modeling of membrane fouling, *J. Membr. Sci*. 139, 183-200.

Song, L. (1998b) A new model for the calculation of the limiting flux in ultrafiltration. *J. Membr. Sci.* 144, 173-185.

Song, L., Chen, K.L., Ong, S.L., Ng, W.J. (2004) A new normalization method for determination of colloidal fouling potential in membrane processes, *J. Colloid Interface*

Sci. 271, 426-433.

Sonnefeld, J. (1995) Surface charge density on spherical silica particles in aqueous alkali chloride solutions. *Colloid & Polymer Sci.* 273, 932-938.

Sourirajan, S. (1970) *Reverse Osmosis*, Academic Press, New York.

Sourirajan, S. and Matsuura, T. (1985) *Reverse Osmosis/Ultrafiltration Process Principles,* National Research Council of Canada, Ottawa.

Szymczyk, A., Fievet, P., Reggiani, J.C., Pagetti, J. (1998) Characterisation of surface properties of ceramic membranes by streaming and membrane potentials. *J. Membr. Sci.* 146, 277-284.

Tadros, Th. F., Lyklema, J. (1969) Adsorption of potential determining ions at the silica water interface, *J. Electroanal. Chem.* 22, 1-7.

Tadros, M.E. & Mayes, I. (1980) *Effects of particle properties on filtration of aqueous suspensions* in: R. Sanasundaram (Ed.), Fine Particles Processing, vol 2, American Institute of Mining, Metallurgical and Petroleum Engineers, New York, 1583-1593.

Taniguchi, M., Kilduff, J.E., & Belfort, G. (2003) Low fouling synthetic membranes by UV-assisted graft polymerization: monomer selection to mitigate fouling by natural organic matter, *J. Membr. Sci.* 222, 59-70.

Tarabara, V.V., Koyuncu, I., Wiesner, M.R. (2004) Effect of hydrodynamic and solution ionic strength on permeate flux in crossflow filtration: direct experimental observation of filter cake cross-sections. *J. Membr. Sci.* 241, 65-78.

Tay, K.G., Song, L. (2005) A more effective method for fouling characterization in a full-scale reverse osmosis process, *Desalination* 177, 95-107.

Teixeira, M.R., Rosa, M.J. (2003) pH adjustment for seasonal control of UF fouling by natural waters, *Desalination* 151, 166-175.

Tiller, F.M., Tsai, C.D. (1986) Theory of filtration of ceramics: I slip casting. *J. Am. Ceramic Soc.* 69, 882-887.

Tiller, F.M., Yeh, C.S., Leu, W.F. (1987) Compressibility of particulate structures in relation to thickening, filtration and expression – A review. *Sep. Sci. & Technol.* 22, 1037-1063.

Tosun, I. (1986) Formulation of cake filtration, *Chem. Eng. Sci.* 41, 2563-2568.

Van der Meeren, P., Saveyn, H., Kassa, S.B., Doyen, W., Leysen, R. (2004) Colloid-membrane interaction effects on flux decline during crossflow ultrafiltration of colloidal silica on semi-ceramic membranes, *Phys. Chem. Chem. Phys.* 6(7), 1408-1412.

van der Waals, J.H. (1873). P.h.D. Thesis, University of Leiden

Van Hoof, S.C.J.M., Minnery, J.G., Mack, B. (2002) Performing a membrane autopsy, *Desalination Water Reuse* 11, 40-46.

van Oss, C.J., Good, R.J., and Chaudhury, M.K. (1986) The role of van der Waals forces and hydrogen bonds in "hydrophobic interactions" between biopolymers and low energy

surfaces. *J. Colloid Interface Sci.* 111, 378-390.

van Oss, C.J., Chaudhury, M.K., Good, R.J. (1987) Monopolar surfaces. *Adv. Colloid Interface Sci.* 28, 35-64.

van Oss, C.J., Chaudhury, M.K., Good, R.J. (1988) Interfacial Lifshitz-van der Waals and polar interactions in macroscopic systems, *Chem. Rev.* 88, 927.

van Oss, C.J. (1990) In: Biophysics of the Cell Surface, R. Glaser and D. Gingell Eds., Springer-Verlag, New York, pp 131-152

van Oss, C.J. (1994) *Interfacial Forces in Aqueous Media*, Marcel Dekker, New York

Verwey, E.J.W. and Overbeek, J. Th.G. (1948). *Theory of stability of lyophobic colloids.* Elsevier, Amsterdam

Vigil, G., Xu, Z.H., Steinberg, S., Israelachvili, J.N. (1994) Interactions of silica surface. *J. Colloid Interface Sci.* 166, 367-385.

Visser, J. (1972) On Hamaker constants:a comparison between Hamaker constants and Lifshitz-van der Waals constants. *Adv. Colloid Interface Sci*. 3, 331-363.

Vivian, H.E. (1961) The reactions of various alkalis with silica, *Aust. J. Appl. Sci*. 12, 96-103.

Vrijenhoek, E.M., Hong, S., Elimelech, M. (2001) Influence of membrane surface properties on initial rate of colloidal fouling of reverse osmosis and nanofiltration membranes. *J. Membr. Sci*. 188, 115-128.

Waite, T.D., Schafer, A.I., Fane, A.G., Heuer, A. (1999) Colloidal fouling of ultrafiltration membranes: Impact of aggregate structure and size. *J. Colloid Interface Sci.* 212, 264-274.

Walker, W.H., Lewis, W.K. McAdams, W.H. (1927) *Principles of Chemical Engineering*; McGraw-Hill: New York.

Wienser, M.R., Clark, M.M., Mallevialle, J. (1989) Membrane filtration of coagulated suspensions. *J. Environ. Eng. ASCE* 115, 20-40.

Wiesner, M.R., Chellam, S. (1999) The promise of membrane technology. *Environ. Sci. Technol.* 33, 360-366.

Wiesner, M.R., Lowry, G.V., Alvarez, P., Dionysiou, D., Biswas, P. (2006) Assessing the risks of manufactured nanomaterials, *Environ. Sci. Technol.*40, 4336-4345.

Wiese, G. and Healy, T.W. (1970) Effect of particle size on colloid stability. *Trans. Faraday Soc.* 66, 490-500.

Wijmans, J.G., Nakao, S., Smolders, C.A. (1984) Flux limitation in Ultrafiltration. Osmotic pressure model and gel layer model. *J. Membr. Sci.* 20, 115-124.

Winfield, B.A. (1979) The treatment of sewage effluents by reverse osmosis – pH based studies of the fouling layer and its removal, *Water Research* 13, 561-564.

Yiantsios, S.G., Karabelas, A.J. (1998) The effect of colloid stability on membrane fouling. *Desalination* 118, 143-152.

Yiantsios, S.G., Sioutopoulos, D. and Karabelas, A.J. (2005) Colloidal fouling of RO membranes: an overview of key issues and efforts to develop improved prediction techniques, *Desalination* 183, 257-272.

Yoon, R., Vivek, S. (1998) Effects of short-chain alcohols and pyridine on the hydration forces between silica surfaces. *J. Colloid Interface Sci.* 204, 179-186.

Yuan, W., Kocic, A. and Zydney, A.L. (2002) Analysis of humic acid fouling during microfiltration using a pore blockage-cake filtration model. *J. Membr. Sci.* 198, 51-62.

Zerrouk, R., Foissy, A., Mercier, R., Chevallier, Y., Morawski, J.C. (1990) Study of Ca^{2+} induced silica coagulation by small angle scattering. *J. Colloid Interface Sci.* 139, 20-29.

Zhang, M., Li, C., Benjamin, M. M., Chang, Y. (2003) Fouling and natural organic matter removal in adsorbent/membrane systems for drinking water treatment, *Environ. Sci. Technol.* 37, 1663-1669.

Zhu, X., Elimelech, M. (1997) Colloidal fouling of reverse osmosis membranes: measurements and fouling mechanisms, *Environ. Sci. Technol.* 31, 3654–3662.

Zidouri, H. (2000) Desalination of Morocco and presentation of design and operation of the Laayonne seawater reverse osmosis plant. *Desalination*, 131, 137-145.